On the Viability of Year-round Magnetotelluric Measurements at ELF/VLF and their Application to Groundwater Exploration

A Thesis

Submitted to the College of
Graduate Studies and Research

in Partial Fulfilment of the Requirements
for the Degree of

Master of Science

in the Department of Physics and Engineering Physics
University of Saskatchewan
Saskatoon

By
David K. Goldak

November, 1997

GSR 302

College of Graduate Studies and Research
University of Saskatchewan
Room 50 Murray Building, Telephone (306) 966-5751, Facsimile: (306) 966-5756

Permission to use Postgraduate Thesis

TITLE OF THESIS On the Viability of Year-round Magnetotelluric Measurements at ELF/VLF and their Application to Groundwater Exploration

NAME OF AUTHOR David Kelsey Goldak

DEPARTMENT OR COLLEGE Physics and Engineering Physics/Graduate Studies and Research

DEGREE Master of Science

In presenting this thesis in partial fulfillment of the requirements for a postgraduate degree from the University of Saskatchewan, I agree that the libraries of this University may make it freely available for inspection. I further agree that permission for copying of this thesis in any manner, in whole or in part, for scholarly purposes may be granted by the professor or professors who supervised my thesis work or, in their absence, by the department Head of the Department or the Dean of the College in which my thesis work was done. It is understood that any copy or publication or use of this thesis or parts thereof for financial gain shall not be allowed without my written permission. It is also understood that due recognition shall be given to me and to the University of Saskatchewan in any use which may be made of any material in my thesis.

SIGNATURE

ADDRESS

DATE November 6, 1997

Abstract

Magnetotelluric (MT) measurements in the Extremely-Low-Frequency (ELF) and Very-Low-Frequency (VLF) bandwidth have been largely regarded as impractical during the winter months, even at relatively low latitude. The economic impact of being able to make valid MT measurements at ELF/VLF during the winter months at mid-high latitude could be significant as many northern areas conducive to mineral exploration are accessed easiest, sometimes solely, during the winter. In the specific case of mineral exploration on fresh water lakes, electrical and electromagnetic methods are best implemented during the winter when the lake surface is frozen. MT surveys at ELF/VLF may prove to be very effective in such an environment due to fewer problems, compared to controlled-source surveys, in penetrating through the thick conductive overburden formed by the mud water-bottom of the lake. Furthermore, at lower latitudes, such as the mineral areas of south-western U.S.A. and northern Mexico, geophysical exploration is best accomplished during the winter when cooler temperatures are prevalent.

It is shown in the present study that magnetotelluric measurements at ELF/VLF are viable on a year-round basis at mid-high latitude, providing the correct recording method is used. Specifically, a recording method which exploits the time localized, transient nature of the largest signals in the ELF/VLF bands of the geoelectromagnetic field is required in order to conduct MT surveys at ELF/VLF in all seasons. Such signals originate in electromagnetic radiation from *individual*, particularly strong or equivalently, relatively nearby lightning discharges. The contradicting statements made in many previous studies is mainly a consequence of the use of a recording technique which implicitly assumes that the MT source field at ELF/VLF is of a continuing nature, or equivalently, one which requires a high level of natural-source activity in order to be successful, a condition not generally seen in the winter months,

especially at mid-high latitude.

Previous groundwater exploration studies employing MT measurements at ELF/-VLF have taken place dominantly in volcanic environments where aquifers are conductive targets, as opposed to relatively thin, resistive targets, which is the case in sedimentary environments. It is shown in the present study that MT measurements at ELF/VLF are of use for groundwater exploration in the sedimentary environment of southern Saskatchewan, both for shallow and deep exploration. The benefit of using MT for groundwater exploration in sedimentary environments is its ability to more cost-effectively image both as shallow as, and much deeper than, time-domain electromagnetic (TEM) soundings. This allows the geophysicist to obtain not only electrical information about shallow glacial deposits but also structural information regarding pre-glacial deposits, the youngest of which is termed Quaternary bedrock. The latter is more difficult to obtain with DC resistivity or TEM methods and has traditionally been the task of refraction seismology. Therefore, of all the geophysical methods, MT measurements at ELF/VLF are somewhat uniquely positioned in being able to cost-effectively provide not only the shallow electrical information normally obtained with DC resistivity or TEM surveys but also deeper structural information usually obtained with the more expensive refraction seismology technique.

Acknowledgements

Much credit for the quality of the present study is owed to my research supervisor, Dr. K. V. Paulson, who introduced me to the exciting field of magnetotellurics. His abundant assistance and academic guidance throughout the course of the present research were essential to the success of the present study. In particular, his help with the field work, data processing and hardware issues are especially acknowledged.

Also, the importance of Peter Kosteniuk in the present study cannot be overstated. His wealth of knowledge in computer programming, hardware, and general MT knowledge was invaluable. The present study would not have been possible without the help of Peter Kosteniuk. I would also like to thank Y. Zhang for his many insights. Similarly, many fruitful discussions were had with Dr. W.H. Pelton throughout the author's stay at Barringer GeoSystems.

I wish to thank my fiance Sheila for her unending patience and moral support throughout this project. Also, her help with some of the field work was greatly appreciated. Lastly, this work is dedicated to the memory of my father whose marine exploration work was the inspiration behind the winter MT research contained herein.

Contents

List of Figures

Chapter 1

Introduction

1.1 Objectives

A magnetotelluric (MT) survey in the ELF/VLF [1] bands of the geoelectromagnetic field was performed with the following objectives.

i. Assessment of the applicability of MT to groundwater exploration in a sedimentary environment.

ii. Assessment of the viability of performing MT surveys in winter with respect to natural signal levels, natural source field activity and operations on frozen ground.

1.2 Geological Targets

The geology of the project area is that of a sedimentary basin with near-surface glacial deposits and deeper pre-glacial deposits. Glacial drift varies in thickness from 6 m at structural highs to over 160 m in glacial valleys (Christiansen et al., 1970) and consists of three main groups; these being from oldest to youngest, the Empress, Sutherland and Saskatoon groups. Regional stratigraphy in this area is shown in Figure 1.1, taken with permission from Fortin et al. (1990).

[1] ELF:Extremely-Low Frequency, 3 Hz - 3 kHz; VLF:Very-Low Frequency, 3 kHz - 30 kHz.

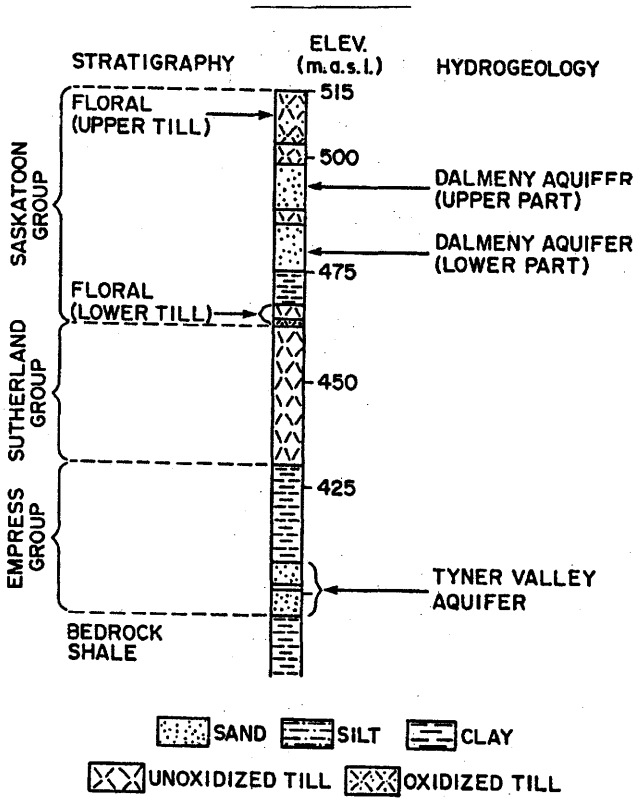

Figure 1.1: Stratigraphy of glacial deposits typical in the study area.

The Empress group is composed of up to 30 m of gravel, sand, silt and clay, the Sutherland group consists of up to 60 m of till and stratified drift. Lastly, the Saskatoon group consists of all sediments lying between the Sutherland group and the surface, also comprised of till and stratified drift but reaching 115 m in thickness in some areas. The sub-surface electrical properties in this area have been studied extensively with well logs. A typical single point resistance and self-potential log, along with lithologic information is shown in Figure 1.2, taken with permission from Christiansen et al. (1970). Note that the first non-glacial deposit is termed bedrock, quaternary in age in this case.

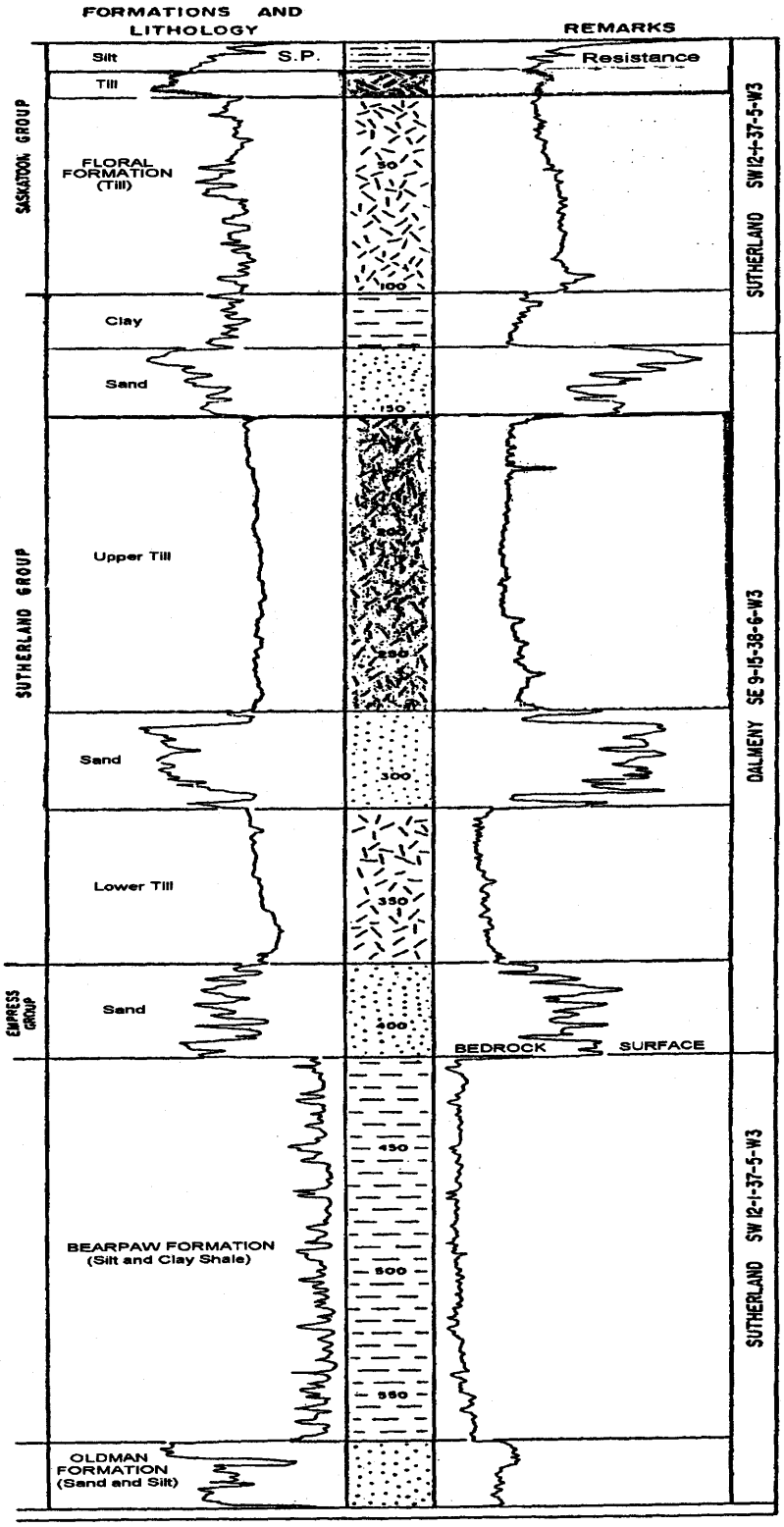

Figure 1.2: Shallow Self-Potential (S.P.) and Resistance log

Shown in Figure 1.3 is a similar well log but one which additionally displays the electrical properties of deeper geologic horizons in the study area.

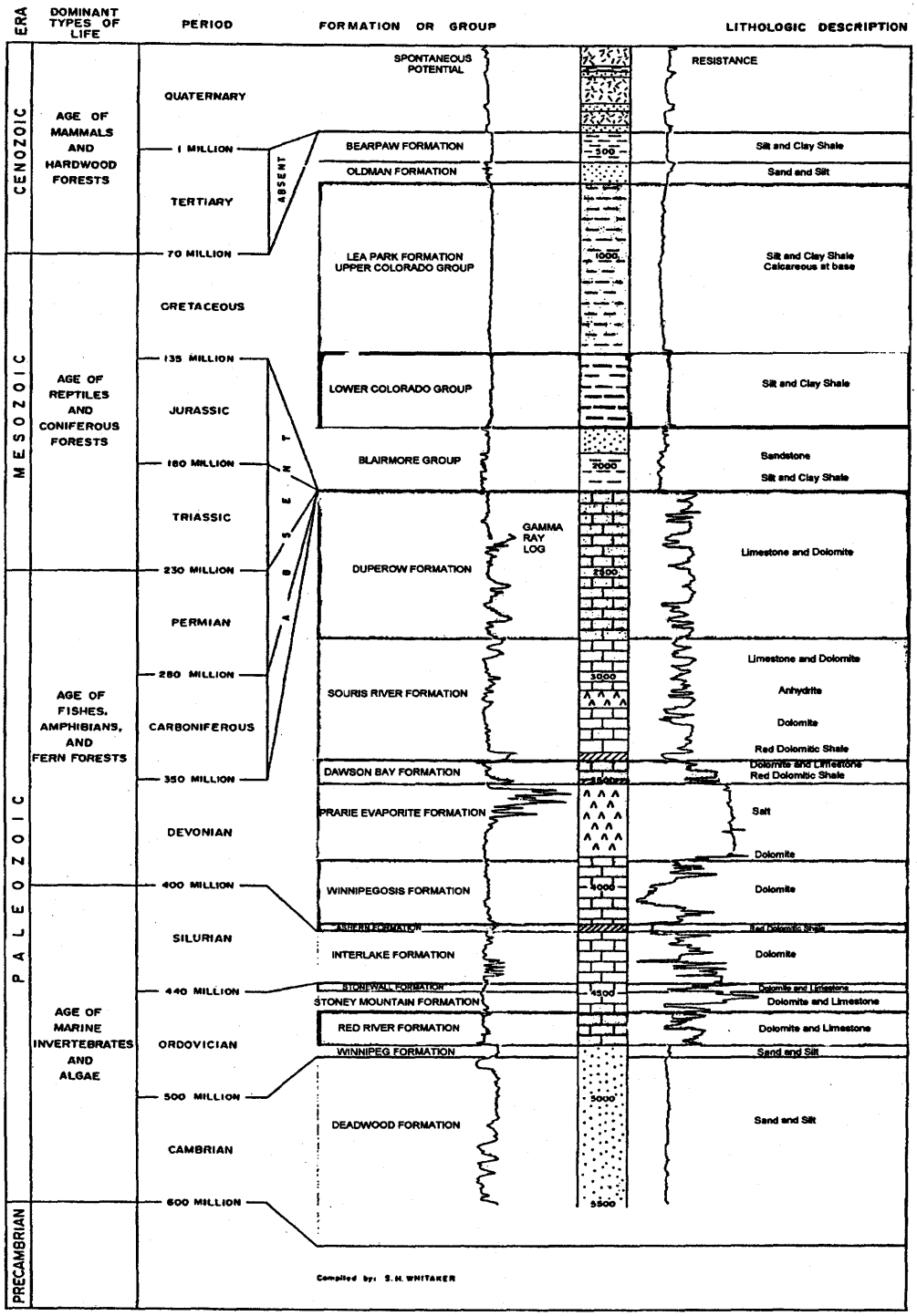

Figure 1.3: Typical Resistance and Self-Potential logs of non-glacial deposits

As is seen on the stratigraphic column of Figure 1.1 and the well log of Figure 1.2, there are at least three sand/gravel layers at various depths within, and themselves partly comprising, the glacial deposits in this area. These sand/gravel layers are extensive and form the two predominant aquifer systems, these being the Dalmeny and Tyner Valley aquifers. The Dalmeny aquifer occurs within the Saskatoon group and consists of two sand/gravel layers with an inter-till layer as shown in Figure 1.1. The deeper Tyner Valley aquifer occurs within the Empress group and is also a sand/gravel aquifer. These two aquifer systems are the geologic targets of the present investigation. Note that resistivity contrasts between layers is about three to five and that the targets are resistive, both of these factors are less than optimum for imaging with diffusive electromagnetic wavefields.

1.3 MT Energy Source

Having identified the geologic targets, it is now useful to estimate the source parameters needed to image these targets. If we assume a near surface resistivity of $10\ \Omega - m$, then with the usual definition of the skin depth we have

$$\delta = \sqrt{\frac{2\rho}{\mu_o \omega}} \tag{1.1}$$

where ρ is the resistivity of an assumed homogeneous half space, μ_o is the permeability of free space and ω is the angular frequency. At frequencies of 10 Hz and 10 kHz we obtain skin depths of 503 m and 16 m respectively. This frequency range is appropriate for identification of both aquifer systems as the Dalmeny aquifer consists of two sand/gravel layers at approximately 20 m and 40 m depth, the Tyner valley aquifer occurs at a depth of about 100 m. Therefore, frequency domain information from 10 Hz to 10 kHz should permit one to obtain resistivity information from about 20 to 500 m depth.

With the magnetotelluric (MT) method we rely on naturally occurring fluctuations in the geomagnetic field which induce sub-surface currents to flow, the size of which are determined by the earth's local electrical structure. The chief source of energy in the ELF/VLF bands from 10 Hz to 10 kHz and above is almost exclusively due to thunderstorm activity at near and great distance. At lower frequencies, approximately

less than 1 Hz, the interaction of the solar wind with the earth's magnetosphere is the dominant energy source. The division between the two sources is not rigid and changes with location among other factors, but for the purposes of this study the electromagnetic energy radiated by lightning strikes is used exclusively to probe the sub-surface, local electrical structure of the earth.

The simplest model for electromagnetic radiation from lightning channels is that of an oscillating vertical electric dipole. The structure of the radiation fields are that of a vertical electric field E_z and an azimuthal magnetic flux density B_ϕ. The electric field is tilted slightly forward in the direction of propagation to account for a small but finite horizontal electric field which exists at the air-earth interface. The presence of the horizontal electric field is due to the finite conductivity of the earth giving rise to energy flow into the earth upon reflection-transmission at the air-earth interface. Of course if the earth were perfectly conducting then complete reflection would occur and the horizontal electric field at the surface of the earth would vanish. Therefore, the electromagnetic radiation from lightning channels is propagated to the far field as a plane wave with the magnetic field vector oscillating perpendicular to the direction of propagation.

The electromagnetic radiation from lightning strokes (called atmospherics, or sferics for short) can be propagated to great distances because they are trapped within the global waveguide formed by the conducting earth and its ionosphere. The global waveguide has preferred frequencies of transmission with regions of relatively low attenuation less than 200 Hz and above 7 kHz. Between 200 Hz and 7 kHz attenuation rises to a maximum at roughly 2 kHz. Theoretical calculations made by Barr (1970) predict an attenuation maximum on the order of 60 dB/Mm while experimental measurements (Chapman et al. , 1956. Challinor,1967) obtained an attenuation maximum on the order of 35 dB/Mm. Regardless, the attenuation maximum depends on location, season and time of day among other factors (Dinger et al., 1980), the result being that sferics usually have very little energy at or around 2 kHz, the most notable exception being when sferics are received from a nearby thunderstorm, perhaps 200 to 500 km distant. Consequently, most MT surveys at ELF/VLF have a "dead band" in the data where there is effectively no signal. The width of the dead band is dominantly a function of distance to the source, since thunderstorms are on average

closer to a measurement site in the summer months, the summer dead band is usually quite narrow, typically 1 kHz to 3 kHz for mid to northern Saskatchewan (pers.comm., P.R. Kosteniuk), in winter when thunderstorms are farther away, the width of the dead band was found to increase to 500 Hz to 5 kHz at 52°N. There are are four main storm centers where 100-150 thunderstorms occur each year, these being Central America and the equatorial regions of Brazil, Africa and the east Asian archipelago (World Meteorological Organization, 1956). Therefore, there exists a high probability that at any given time a thunderstorm is in progress somewhere on the earth. Global lightning flash frequency has been a point of debate for many years in lightning research circles. Brooks (1925) arrived at the commonly stated number of 100 lightning flashes per second, in part due to observations made by Marriot (1908) over a twenty eight minute period (Orville et. al, 1979, Dennis, 1965). Satellite observations have amazingly confirmed this number to be approximately correct with global flash frequency estimates between 96 (northern winter) to 123 (northern summer) flashes per second (Orville et.al, 1979). However, it must be stated that for MT at ELF/VLF, global lightning flash frequency is only relevant to MT measurements at lower ELF (10 - 200 Hz) as this is the only frequency range where global waveguide attenuation is low enough that we can truly receive sferics on a global scale. Throughout much of the ELF/VLF spectrum, global waveguide attenuation is such that we are usually limited in receiving signals from thunderstorms within approximately 5000 km of the measurement site (under daytime conditions).

1.4 Survey Locations

Having identified the geologic targets of interest and the corresponding MT energy source, it was decided that it would be desirable to collect MT data over the edge of both the Dalmeny and Tyner valley aquifer systems if possible. Figure 1.4a, taken with permission from Fortin et al. (1990), shows the areal extent of both the Dalmeny and Tyner valley aquifers, with the study area circled. Shown in Figure 1.4b is the study area in detailed form, referred to as the Hepburn site. Filled circles indicate sites where MT data was collected, open circles show sites that were surveyed in but not occupied and filled squares indicate the location of logged wells. The northern-

most MT site is denoted as Site 102, the southern-most site, nearest the logged well, Site 110.

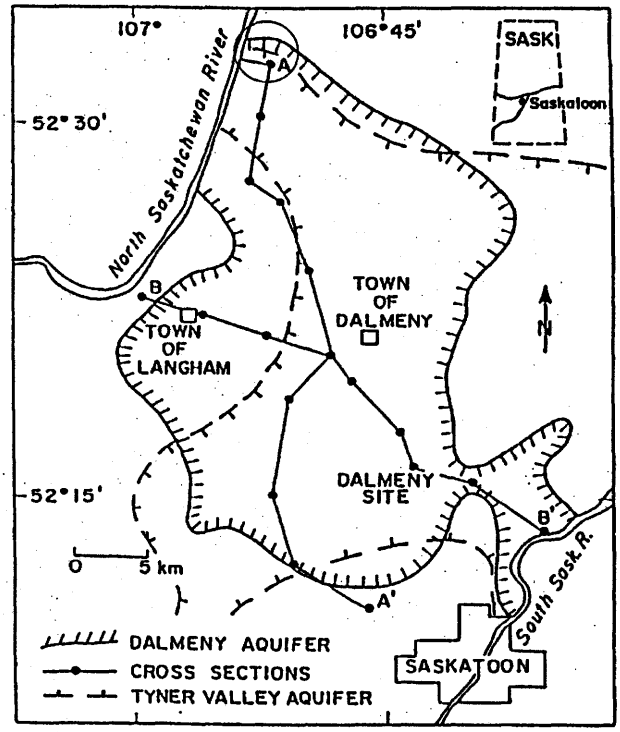

Figure 1.4a: Areal Extent of Aquifer System

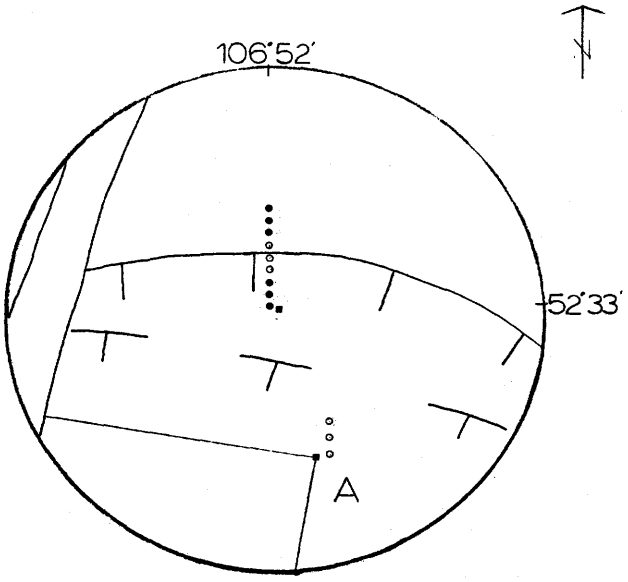

Figure 1.4b: Study Area in Detailed Form

Note that the location of the edge of the two aquifers is based on well log information with a small volume of investigation (Chapter 6). Furthermore, due to pinch out of sand layers near the boundaries, the location of the edge of the two aquifer systems is not exact (Fortin et al., 1990).

For the winter research it was decided to conduct the sounding on a lake as the waterbottom of the lake remains perenially unfrozen. Rabbit Lake was chosen due to it's close proximity to the author's residence and it's relatively easy access. Shown in Figure 1.5 is the Rabbit Lake site, circled and located with the cross-hair; the Hepburn site is similarly shown for reference.

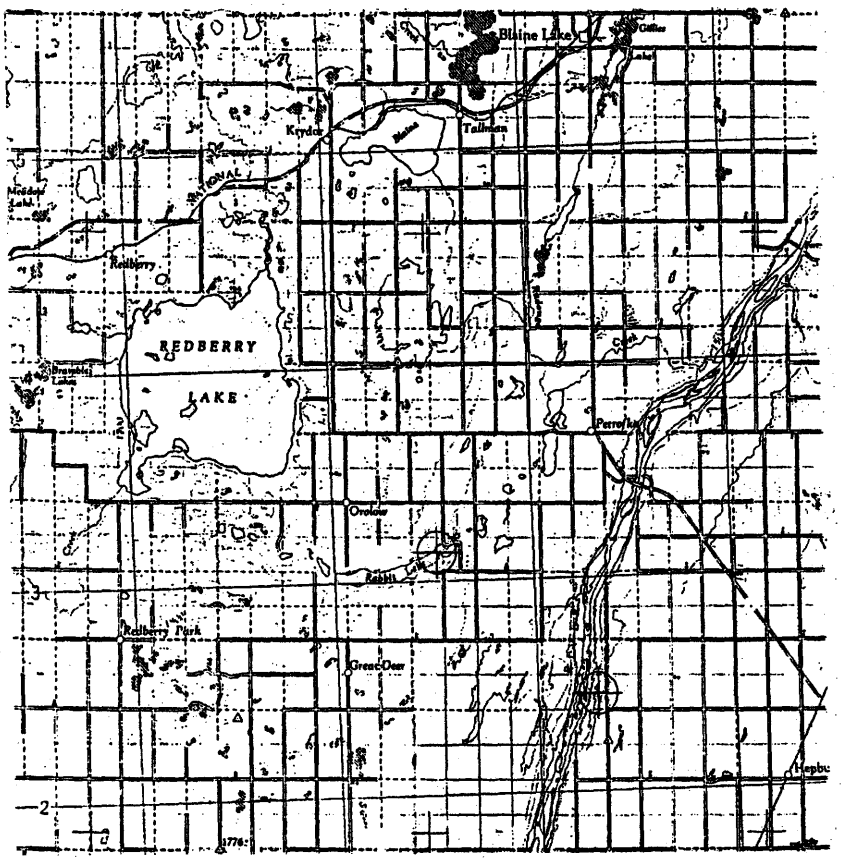

Figure 1.5: Location of the Rabbit Lake and Hepburn sites

1.5 Previous Geophysical Work

1.5.1 MT in Groundwater Exploration

Previous natural source MT work in groundwater exploration has been mainly limited to structural studies, ironically employing scalar instruments!. Perhaps the first example is an M.Sc. thesis by Robin (1984), from the University of Paris although no detailed information is known about this project.

More recent work includes a structural study in South America by Padilha et al. (1989) whose objective was to map the depth to resistive basement in an area where little well control existed and find any contacts between conductive overlying sedimentary formations and more resistive volcanic groups. They collected 31 sites of scalar MT data and concluded that while MT was able to successfully map contacts between sedimentary and volcanic formations, it was not useful in identifying sand/gravel layers (aquifers) within the sedimentary sequence, presumably due to the low resistivity contrasts involved. Of course this limitation is applicable to any EM method where conductive layers are imaged more effectively than resistive layers. Specifically, conductive layers are imaged according to their conductivity-thickness product whereas resistive layers are imaged by thickness alone (Wannamaker, 1983). Resistive sand/gravel layers are often times the target for groundwater studies but aquifers can also be a conductive target if they are the type due to fracturing within resistive, volcanic host rock.

Bernard et al. (1990) of the BRGM (Bureau de Recherches Geologiques et Minieres) carried out a scalar MT survey on La Reunion Island, located 700 km east of Madagascar in the Indian Ocean, relatively close to the storm center of equatorial Africa and less so Indonesia. Local geology is volcanic (resistive) and the goal of the survey was to map the possible location of a sinkhole in which water bearing structures might be present. They verified the location of the sinkhole with MT but no further results are known.

Perhaps the most comprehensive example of MT applied to groundwater exploration is the extensive project of Bourgeois et al. (1994), also of the BRGM. In 1990-91 they collected a total of 303 scalar MT sites (with the same instrument as used by Bernard et al., 1990) in an effort to map basement topography for groundwater pur-

poses in the Kalahari desert, Botswana. I quote:"Basement topography has a major influence on lithology; in particular, the sandstone forming the aquifer is more porous at the bases of grabens where the deposits are coarse grained". They successfully mapped the depth to resistive basement over their project area and 6 out of 20 wells drilled partially as a result of the MT study yielded producing water wells. This was an integrated geophysical study with total field magnetics, gravity, time domain EM and DC resistivity surveys performed also. The MT data was used to map large scale structural features of their project area and horizontal loop EM was used to find conductive zones associated with water collected in faults at the edges of grabens, although MT would have arguably provided the same information.

The most recent example of MT applied to groundwater exploration, and the only one to the author's knowledge employing a tensor system is that of Nichols et al. (1994). They developed a "hybrid" tensor MT system named STRAGEM which uses natural frequencies up to 500 Hz and a controlled source (vertical loops) for frequencies from 1 kHz to 100 kHz. The objective of their study was to not only image sand/gravel aquifers but also identify which ones contain fresh water (more resistive) and which ones have been invaded by salt water (less resistive). They showed results from such a survey in the Salinas Valley, California where a fresh water aquifer beneath an invaded aquifer was mapped. Good correlation with well-logs was obtained.

To summarize, past MT work related to groundwater studies has been mainly limited to structural studies with scalar instruments, excluding the study of Nichols et al. (1994).

1.5.2 Natural Source ELF/VLF Signals in Winter

Conventional wisdom is that thunderstorm-source MT surveys are impossible in winter because the natural signal level is too weak, a statement often exploited by controlled-source contractors. Performing MT surveys in winter is potentially valuable as in many cases certain areas can only be accessed in winter when surfaces are frozen (muskeg, swamps, lakes). In February of 1982 a magnetotelluric winter test survey was carried out by Geoconsult of Denver, Colorado for AGIP Canada in Northern Saskatchewan. Geoconsult was the American arm of the world famous French geophysical company, CGG, and hence was a high quality contractor. Their test survey

was for the most part unsuccessful. Specifically, they stated problems with signal strengths above 100 - 200 Hz. I quote:"There was a total lack of coherent signal at high frequencies. In general the soundings do not go above 100 - 200 Hz.", (Herisson, 1982). Other studies at lower latitudes have been carried out by Ward (1959) related to his AFMAG (Audio Frequency MAGnetic) method, which is a tilt angle method, but one in which thunderstorms are used as an energy source. Ward (1959) concluded that, "Variations in field strength limit the annual applicability of the method. Up until the last six months, the use of ground AFMAG has been limited to April 1 to November 1 and airborne AFMAG from May 1 to October 1 in Northern Canada". Hoover et al. (1978) collected large amounts of scalar MT data for geothermal studies in the U.S.A.. They state: "Above 200 Hz and centered near 2 kHz, an absorptive band limits the signal strength making data acquisition difficult if not impossible in the mid-band region, particularly during the winter months". They show examples of spectra from measurements taken in February in Nevada, at about 37°N. They go on to state:"As winter approaches, the signal strength decreases in the AMT [2] mid-frequency range and the no-signal band widens. This absorption makes data acquisition very difficult from about 250 to 5000 Hz". They also state, "This is consistent with our experience with the AMT system, field work can be conducted at all seasons if one is not concerned about losing data above 200 Hz". Labson et al. (1985) state with reference to the AFMAG method, "An equally serious problem with AFMAG is the fact that the signal strength is inadequate in high latitudes in the winter. The inherent noise level of the coils and and their electronics is higher than the level of the weak signals originating in storms at the equator and southern temperate zones". Lakanen (1986) also states, "This cutoff explains the lack of intensity in winter at frequencies from 100 to 5000 Hz, an unfortunate fact for AMT observations. Lower frequencies, however, behave well in winter". These references show a common misconception throughout the literature that thunderstorm-source MT surveys are not viable in winter.

In the area of lightning research (source studies), notable work has been carried out by Lugeon et al. (1959), where count rates and direction of arrival of sferics were

[2]Strangway et al. (1973) coined the term AMT or Audio Frequency Magnetotellurics for MT in the frequency range 10 Hz - 10 kHz or more generally at ELF/VLF.

analyzed for almost three years continuously. Data was collected simultaneously at a mid-high latitude location at Zurich (47 deg N, 8 deg E) and at a polar station (80 deg N, 18 deg E) on the island of Kinnvika, in the archipelago of Svalbard near the island of West Spitsbergen, in the Arctic Circle. Count rates were found to have a maximum at night during the winter months, both at Zurich and the polar station. J.M. Wallace (1974) analyzed diurnal variations in thunderstorm frequency over the U.S.A.. He too found that thunderstorm frequency of occurrence was highest at night during the winter. Dinger et al. (1980) carried out an extensive study for the U.S. Navy with respect to communications research. He also found the highest levels of thunderstorm signals in the band 1 to 4 kHz occured at night throughout the winter months, both at a mid latitude site in Italy and a polar site in Norway. The night time maxima mainly reflect enhanced propagation of signal at night due to the disappearance of the absorptive D-layer at approximately 60 km height. At night the upper surface of the global waveguide is formed by the more conductive E-layer at approximately 90 km height giving enhanced propagation throughout much of frequency band, mainly above 100 Hz and extending to at least 30 kHz.

1.5.3 Electric Field measurements in Winter

There is a dramatic difference in the resistivity of frozen and unfrozen earth materials. Conduction in the earth is accomplished mainly through the motion of ions contained in groundwater present in the pore spaces of earth materials. When the ground freezes, the mobility of ions in solution is dramatically reduced and the resistivity of the material increases markedly. The increase in resistivity upon freezing depends on the material, temperature and water content but increases by a factor of 10 to 1000 are common (Hoekstra et .al, 1975. Hessler and Franzke, 1958). This increase in resistivity lowers the quality of electric field measurements as large contact resistances can be likened to a thermal noise source, which is well known in electronic circles to be $\propto \sqrt{R}$ (Netzer, 1981), where R is the resistance.

High frequency signal distortion caused by large contact resistances has been noticed previously by Zonge et al. (1980) in their controlled-source magnetotelluric studies. They show the need for an "active pot" when working on ground with high resistivity. The active pot design involves the placement of an op-amp right at the

electrode which allows the wire running back to the recording instrument to be driven at the output impedance of the op-amp, perhaps a few tens of ohms. This eliminates the high frequency signal distortion and was arguably implemented first by Collett and Becker (1968) in the design of the Geonics VLF resistivity instrument, the EM16-R. Such instruments essentially perform a controlled source magnetotelluric sounding at one or two frequencies by making use of powerful VLF transmitters used mainly by the U.S.A. and European countries for naval communications. Case histories detailing the use of this instrument on frozen ground for mapping permafrost are extensive and include Hoekstra et al. (1975) and Powell et al. (1981).

Besides using an active pot, another possibility for electric field measurements on highly resistive ground is to use a non-contacting electrode. Thiel et al. (1989) recommend the use of a dipole antenna (non contacting) for electric field measurements with MT and VLF instruments. Another option is to use a capacitive electrode, the modifier "capacitive" indicating that the electrode is coupled to the earth capacitively and as such is non-contacting. The only published paper detailing the use of capacitive electrodes is that of Macnae et al. (1991) of Lamontagne Geophysics, however the possibility of their use was apparently shown by Scott also (Powell et al., 1981). In Macnae's study a survey is done over the same area in summer and winter with conventional and capacitive electrodes respectively, giving very similar electric field data showing that capacitive electrodes can be used to give repeatable electric field data year round. Yves Lamontagne designed the capacitive electrodes for his UTEM, time domain EM system (5 Hz - 50 kHz). According to Lamontagne, they function identically to conventional electrodes in that they measure the potential difference between two points, dividing by the separation distance between electrodes yielding the electric field in V/m. The main difference is that capacitive electrodes are coupled to the earth capacitively (no DC contact) as opposed to resistively with conventional electrodes. Lamontagne states that the biggest problem in their use is that everything must be kept dry to maintain the high impedance of the measuring circuit. Scintrex Ltd. also markets their Omni VLF resistivity unit as having the option of using capacitive electrodes. Similar devices in use by lightning researchers are used to measure the intense vertical electric field associated with lightning transients. In such cases a flat metal plate is suspended in the air, perhaps a meter above ground and

the charge induced on the plate is measured with a high impedance charge amplifier and related to the vertical electric field. The frequency response of the antenna is determined by the RC time constant of the measuring circuit. The first use of such a device appears to be due to Kitagawa et.al (1960). The similarities between capacitive electrodes for geophysical measurement of the horizontal electric field and the antennae used by lightning researchers for measuring the vertical electric field seems evident.

1.6 Thesis Outline

A mostly non-mathematical introduction to the magnetotelluric method is presented in Chapter 2. Maxwell's equations in the inductive limit are found and a discussion of the magnetotelluric impedance tensor follows. Finally the Bostick transform is presented.

The instrumentation aspects of this project including a description of the recording instrument and all sensors used (electric and magnetic field) is given in Chapter 3.

Data processing issues are discussed in Chapter 4 where a time localized Fourier transform data processing method is introduced.

A source field analysis with the data collected in the fall, winter and spring of 1995/96 is the subject of Chapter 5. Signal amplitudes, signal-to-noise ratios, activity variations and approximate source locating methods are analyzed in an attempt to characterize the ELF/VLF MT signal source at mid-high latitude throughout the fall, winter and spring of 1995/96.

Chapter 6 contains a presentation of all the processed results of the MT soundings and an interpretation of the results. Lastly, conclusions and recommendations for future work is found in Chapter 7.

Chapter 2

Theory of the Magnetotelluric Method

2.1 Introduction

The magnetotelluric (MT) method is a geophysical exploration technique in which the earth's electrical structure at depth may be determined from surface measurements of naturally occurring fluctuations in the earth's geoelectromagnetic field along with corresponding electric field fluctuations induced within the earth by the former.

With MT we are able to obtain resistivity information as a function of depth by making frequency dependent measurements, with lower frequencies reflecting deeper electrical features and higher frequencies shallower ones. Profiling information is obtained through a series of soundings at sites placed as little as 25 m or as large as 5 km apart.

The fathers of the MT method are Tikhonov (1950) and Caignard (1953) who made the simplifying assumption of plane wave source fields. This assumption has been carefully scrutinized by many and was found in almost all but the most exceptional cases to be correct (Wait, 1954. Price, 1962. Madden and Nelson, 1964). In the context of MT measurements at ELF/VLF, which dominantly use thunderstorms as an energy source, it has been found that the plane wave or far field criterion can be satisfied if we are on the order of 200 km or more from the nearest thunderstorm. At this distance, the radiation field components dominate over the near field electrostatic

and inductive field components (Volland, 1982). Considering only the higher frequencies, $\geq$ 1 kHz, the far field criterion is satisfied as long as we are more than 50 km removed from the nearest thunderstorm (Pierce, 1977).

The fundamental quantity of interest for MT surveys is the impedance tensor which is the transfer function between mutually orthogonal, horizontal components of $\vec{H}$ and $\vec{E}$ fields. The impedance tensor is most easily estimated in the frequency domain by averaging the results from many calculations, each calculation involving estimation of auto powers of, and cross powers between various components of $\vec{E}$ and $\vec{H}$. The original formula was solved by Madden and Nelson (1964) and is presented in Vozoff (1972) among others. Biasing of the impedance tensor due to noise on the field channels was soon noticed and prompted the development of the remote reference method (Gamble et al., 1979). The remote reference method was an improvement as it allowed the impedance tensor to be estimated with cross powers only, removing the bias present when the impedance tensor is calculated with the auto powers of the field channels. Vozoff (1991) states:"The present situation is that the remote reference method is deemed cost effective under average conditions, but is unnecessary in quiet locations and is no help in very noisy locations". The present study employs the conventional, single site estimation of the impedance tensor.

A routine step in MT surveys is correcting data for topography variations. Subsurface current paths are affected by topographic changes, subsequently the electric field is also distorted by topographic changes. Finite element programs have been written by P.R. Kosteniuk, Cybernetics Laboratory, University of Saskatchewan to correct MT data for topography changes, however, no topographic correction was needed in the present study.

Another routine step in MT surveys is that of strike determination. For the one-dimensional case strike is not defined. For the case of an idealized two-dimensional structure, the formula of Swift (1967) resolves the correct strike angle. However, in two-dimensional cases when current chanelling occurs, the Swift (1967) analysis fails to give the correct strike angle (Groom and Bailey, 1989), this is also the situation in three-dimensional cases. The most powerful and general method to date is due to the work of Yee and Paulson (1987), who introduced the canonical decomposition. The canonical decomposition makes no assumptions about earth models, as does the

widely used Groom-Bailey decomposition (1989), and is applicable in the general three-dimensional case. In the present study no means of strike determination was necessary as the data at the Hepburn site was found to be one dimensional to a very good approximation.

Lastly, apparent resistivity information as a function of frequency must be inverted to, ideally, give true earth resistivity as a function of depth. A very simple one-dimensional inversion algorithm was derived by Bostick (1977). In one-dimensional cases, the Bostick transform can be used directly for interpretation purposes and is also used in many systems for in-field inversion purposes. For in office processing with two-dimensional inversions, the Bostick transform is often times used as a starting point for these iterative inversion programs.

2.2 Maxwell's Equations

The general form of Maxwell's equations, expressed in the time domain, are

$$\nabla\times\mathbf{E} = -\frac{\partial\mathbf{B}}{\partial t} \quad \text{(Faraday's Law)}, \tag{2.1}$$

$$\nabla\times\mathbf{H} = \mathbf{J} + \frac{\partial\mathbf{D}}{\partial t} \quad \text{(Ampère's Law)},$$

$$\nabla\cdot\mathbf{B} = 0 \quad \text{(no magnetic monopoles)},$$

$$\nabla\cdot\mathbf{D} = \rho' = 0 \quad \text{(Gauss's Law)},$$

where $\mathbf{E}$ is the electric field intensity in (V/m), $\mathbf{B}$ is the magnetic flux density in (T), $\mathbf{H}$ is the magnetic field intensity in (A/m), $\mathbf{D}$ is the electric displacement in (C/m^2), $\mathbf{J}$ is the current density in (A/m^2), ρ' is the charge density in (C/m^3), assumed to be negligible, all within a medium of magnetic permeability μ, electric permittivity ϵ and conductivity σ where

$$\mathbf{B} = \mu\mathbf{H}, \quad \mathbf{D} = \epsilon\mathbf{E}, \text{ and } \mathbf{J} = \sigma\mathbf{E}.$$

After one-dimensional Fourier transformation of 2.1, and using the relations above, we obtain Maxwell's equations in the frequency domain, for a homogeneous, isotropic medium

$$\nabla\times\tilde{\mathbf{E}} = -\imath\omega\mu\tilde{\mathbf{H}}, \tag{2.2}$$

$$\nabla \times \tilde{\mathbf{H}} = (\sigma + \imath\omega\epsilon)\tilde{\mathbf{E}},$$

$$\nabla \cdot \tilde{\mathbf{B}} = 0, \text{ and}$$

$$\nabla \cdot \tilde{\mathbf{D}} = 0.$$

By taking the curl of Ampère's law and using the vector identity

$$\nabla \times \nabla \times \tilde{\mathbf{H}} = \nabla(\nabla \cdot \tilde{\mathbf{H}}) - \nabla^2 \tilde{\mathbf{H}},$$

we get

$$\nabla(\nabla \cdot \tilde{\mathbf{H}}) - \nabla^2 \tilde{\mathbf{H}} = (\sigma + \imath\omega\epsilon)\nabla \times \tilde{\mathbf{E}}.$$

Since $\nabla \times \tilde{\mathbf{E}} = -\imath\omega\mu\tilde{\mathbf{H}}$ and $\nabla \cdot \tilde{\mathbf{H}} = 0$,

$$\nabla^2 \tilde{\mathbf{H}} = (\sigma + \imath\omega\epsilon)\imath\omega\mu\tilde{\mathbf{H}}.$$

Equivalently,

$$\nabla^2 \tilde{\mathbf{H}} + k^2 \tilde{\mathbf{H}} = 0 \tag{2.3}$$

with complex wave number k given by

$$k = (\omega^2 \mu\epsilon - \imath\omega\mu\sigma)^{1/2}. \tag{2.4}$$

Similarly, for the electric field we obtain

$$\nabla^2 \tilde{\mathbf{E}} + k^2 \tilde{\mathbf{E}} = 0. \tag{2.5}$$

Equations 2.3 and 2.5 are Helmholtz equations for $\tilde{\mathbf{H}}$ and $\tilde{\mathbf{E}}$ respectively, with complex wave number k, which includes the contribution of both displacement currents and conduction currents. Displacement currents are easily shown to be negligible for electromagnetic methods operating at relatively low frequencies. The ratio of conduction to displacement currents is

$$\frac{\mu\sigma\omega}{\epsilon\mu\omega^2} = \frac{1}{\rho\epsilon\omega}, \tag{2.6}$$

where $\rho = 1/\sigma$ is the resistivity of the material in question. For constant permittivity, we see that displacement currents become comparable to conduction currents only

when the resistivity-frequency product becomes large. Consider resistive granite with $\rho = 1 \times 10^5\ \Omega - m$, $\epsilon = 8.854 \times 10^{-12}\ F/m$ (Keller and Frischknecht, 1966) at a frequency of 10 kHz. With these parameters we find that conduction currents are still over 17.9 times as large as displacement currents. In fact, most earth materials encountered in field work have resistivities less than $1000\ \Omega - m$ so that conduction currents are often more than a factor of 1000 larger than displacement currents for frequencies less than 10 kHz. Therefore, in all but the most exceptional circumstances we can neglect displacement currents. When displacement currents are negligible, we are said to be in the inductive limit where we are now dealing with a diffusion process with

$$k = \sqrt{-\imath\mu\sigma\omega} \tag{2.7}$$

That is, the induced field strengths within the earth are governed by the diffusion equation and can be likened to a smoke ring which expands outward with increasing depth into the earth (Nabighian et al., 1991). Therefore, we also note that as frequency decreases, depth of exploration increases but so too does the lateral extent of exploration(Hoover et al., 1976). This readily shows the lack of resolution of electromagnetic methods operating in the inductive limit (Ward et al., 1988).

Finally, Maxwell's equations in the inductive limit become

$$\begin{aligned} \nabla \times \tilde{\mathbf{E}} &= -\imath\omega\mu\tilde{\mathbf{H}}, \\ \nabla \times \tilde{\mathbf{H}} &= \sigma\tilde{\mathbf{E}}, \\ \nabla \cdot \tilde{\mathbf{B}} &= 0, \\ \text{and } \nabla \cdot \tilde{\mathbf{D}} &= 0. \end{aligned} \tag{2.8}$$

2.3 The Magnetotelluric Impedance Tensor

2.3.1 The Impedance Tensor for a One-Dimensional Earth

For magnetotelluric measurements, we define a right handed co-ordinate system with ^+x to the north, ^+y to the east and ^+z down into the earth. For a homogeneous half

space, with conductivity σ and magnetic permeability μ, equations 2.3 and 2.5 admit plane wave solutions of the form (Griffiths, 1989)

$$\tilde{\mathbf{E}} = E_o e^{-\imath(kz-\omega t)}, \tag{2.9}$$

$$\text{and } \tilde{\mathbf{H}} = H_o e^{-\imath(kz-\omega t)}. \tag{2.10}$$

The complex wavenumber k, shown in the inductive limit in equation 2.7, can be rewritten as

$$k = \sqrt{\frac{\sigma\omega\mu}{2}} - \imath\sqrt{\frac{\sigma\omega\mu}{2}}. \tag{2.11}$$

Rewriting equations 2.9 and 2.10 with k defined above we obtain

$$\tilde{\mathbf{E}} = E_o e^{\imath\omega t} e^{-\imath\alpha z} e^{-\alpha z}, \tag{2.12}$$

$$\tilde{\mathbf{H}} = H_o e^{\imath\omega t} e^{-\imath\alpha z} e^{-\alpha z}, \tag{2.13}$$

where

$$\alpha = \sqrt{\frac{\sigma\omega\mu}{2}}. \tag{2.14}$$

This serves to show that the field strengths diffusing downward into the earth have a harmonic time dependence ($e^{\imath\omega t}$), harmonic depth variation ($e^{-\imath\alpha z}$) and are exponentially damped or attenuated with increasing depth z ($e^{-\alpha z}$).

With Faraday's law it can be shown that (Griffiths, 1989)

$$\tilde{\mathbf{H}} = \frac{k}{\mu\omega}\tilde{\mathbf{E}}, \tag{2.15}$$

and therefore, with the ratio of $\tilde{\mathbf{E}}$ over $\tilde{\mathbf{H}}$ we obtain

$$\frac{\tilde{\mathbf{E}}}{\tilde{\mathbf{H}}} = \frac{\omega\mu}{k} = \tilde{Z}, \tag{2.16}$$

where $\tilde{Z}$ is the wave impedance, for an assumed homogeneous half space of conductivity σ and magnetic permeability μ. However, for magnetotelluric measurements, the wave impedance is not necessarily a scalar quantity, independent of measurement axes as indicated in equation 2.14. More generally, the magnetotelluric wave impedance is defined by a rank two tensor and therefore involves at surface measurements of orthogonal, horizontal components of $\vec{E}$ and $\vec{H}$, which after Fourier transformation are related via the impedance tensor as

$$\begin{bmatrix} \tilde{E}_x \\ \tilde{E}_y \end{bmatrix} = \begin{bmatrix} \tilde{Z}_{xx} & \tilde{Z}_{xy} \\ \tilde{Z}_{yx} & \tilde{Z}_{yy} \end{bmatrix} \cdot \begin{bmatrix} \tilde{H}_x \\ \tilde{H}_y \end{bmatrix} \tag{2.17}$$

or simply

$$\tilde{\mathbf{E}} = \tilde{\mathbf{Z}}\tilde{\mathbf{H}}$$

where $\tilde{\mathbf{Z}}$ is the magnetotelluric impedance tensor, a complex quantity which thus contains amplitude and phase information as a function of frequency.

With the co-ordinate system defined previously, E_x then refers to the north-south electric field component; similarly, E_y is the electric field component in the east-west direction. The off-diagonal elements of the impedance tensor, $\tilde{Z}_{xy}$ and $\tilde{Z}_{yx}$, are the elements from which the apparent resistivity and phase in the x and y directions, respectively, are found. However, the diagonal elements $\tilde{Z}_{xx}$ and $\tilde{Z}_{yy}$ are equally as important as they reflect earth structure. Generally speaking, if $|\tilde{Z}_{xx}|$ and $|\tilde{Z}_{yy}|$ are negligible compared to $|\tilde{Z}_{xy}|$ and $|\tilde{Z}_{yx}|$ (less than ten percent) then we either have a one-dimensional, isotropic earth or a two-dimensional case with measurement axes aligned parallel and orthogonal to strike. Theoretically, for a one-dimensional, isotropic earth, or a 2D case with measurement axes aligned parallel and orthogonal to strike, $|\tilde{Z}_{xx}| = |\tilde{Z}_{yy}| = 0$. For field work noise is inevitably present and hence the diagonal elements are never seen to be zero. In addition to the previous criteria, if $|\tilde{Z}_{xy}| = |\tilde{Z}_{yx}|$ then we have a one-dimensional, isotropic earth. Once again, for field work the equality only approximately holds as noise is always present in the recordings. If $|\tilde{Z}_{xx}|$ and $|\tilde{Z}_{yy}|$ are initially not negligible but can be made so by rotating the co-ordinate system through some angle and $|\tilde{Z}_{xy}| \neq |\tilde{Z}_{yx}|$, then we have a two-dimensional case with the rotation angle defining the direction of geologic strike relative to the measurement co-ordinate system. If none of the above cases can be met, we have a three dimensional case. The above discussion is largely qualitative as real data usually displays a mixed dimensional behaviour so that most times we can only say that we have an approximately 1D or an approximately 2D case. It should also be noted that the only way to differentiate between a two-dimensional earth and a one-dimensional anisotropic earth is through measurement of $\tilde{H}_z$ (Telford et al., 1990), the present instrument does not incorporate this measurement and hence this distinction cannot be clarified if present.

If we consider equation 2.16 (noise free case) written in full we get

$$\tilde{E}_x = \tilde{Z}_{xx}\tilde{H}_x + \tilde{Z}_{xy}\tilde{H}_y, \tag{2.18}$$
$$\text{and } \tilde{E}_y = \tilde{Z}_{yy}\tilde{H}_y + \tilde{Z}_{yx}\tilde{H}_x.$$

Consider the one-dimensional, isotropic, noise free case with $|\tilde{Z}_{xx}| = |\tilde{Z}_{yy}| = 0$, then equation 2.18 becomes

$$\tilde{E}_x = \tilde{Z}_{xy}\tilde{H}_y, \tag{2.19}$$
$$\text{and } \tilde{E}_y = \tilde{Z}_{yx}\tilde{H}_x.$$

In this case the impedance is a scalar quantity independent of the orientation of the measurement co-ordinate system. Considering amplitudes only we get

$$|\tilde{Z}_{xy}| = \frac{|\tilde{E}_x|}{|\tilde{H}_y|} = |\tilde{Z}_{yx}| = \frac{|\tilde{E}_y|}{|\tilde{H}_x|}. \tag{2.20}$$

Having discussed the amplitude behaviour of the impedance tensor in the 1D, isotropic case, a discussion of the phase behaviour is also needed. For this purpose, consider the simplest case of all, that of a homogeneous half space with conductivity σ and permeability μ, as previously considered with the derivation of the wave impedance. The expression for $\tilde{Z}_{xy}$ becomes

$$\tilde{Z}_{xy} = \frac{\tilde{E}_x}{\tilde{H}_y} = \frac{\omega\mu}{k} = \sqrt{\frac{\omega\mu}{\sigma}}e^{i\frac{\pi}{4}} \tag{2.21}$$

where the complex exponential reflects the phase properties of $\tilde{Z}_{xy}$. In this case we see that $\tilde{Z}_{xy}$ has a positive phase angle of $\pi/4$ radians or 45 degrees. This means that the electric field $\tilde{E}_x$ leads the magnetic field intensity $\tilde{H}_y$ by 45 degrees over a homogeneous half space. For $\tilde{Z}_{yx}$ we find that

$$\tilde{Z}_{yx} = \frac{\tilde{E}_y}{\tilde{H}_x} = -\frac{\omega\mu}{k} = \sqrt{\frac{\omega\mu}{\sigma}}e^{i\frac{5\pi}{4}} \tag{2.22}$$

as expected, $|\tilde{Z}_{yx}| = |\tilde{Z}_{xy}|$ but the phase difference between $\tilde{E}_y$ and $\tilde{H}_x$ is $5\pi/4$ radians or 225 degrees, it should be noted that for field measurements it is customary to remove the extra 180 degree offset in the yx phase so that both phase curves oscillate about 45 degrees and are therefore bounded between 0 and 90 degrees (Vozoff, 1991).

To summarize, in the one-dimensional, isotropic, noise free case, the diagonal elements of the impedance tensor are zero and the amplitude of the off-diagonal elements are equal with phase angles of 45 and 225 degrees for $\tilde{Z}_{xy}$ and $\tilde{Z}_{yx}$ respectively. In matrix form we have

$$\begin{bmatrix} \tilde{E}_x \\ \tilde{E}_y \end{bmatrix} = \begin{bmatrix} 0 & \tilde{Z}_o \\ -\tilde{Z}_o & 0 \end{bmatrix} \cdot \begin{bmatrix} \tilde{H}_x \\ \tilde{H}_y \end{bmatrix} \tag{2.23}$$

where $\tilde{Z}_o = \sqrt{\omega\mu/\sigma} \cdot e^{i\pi/4}$. The interested reader is referred to Yee and Paulson (1987) for a more rigorous discussion of the impedance tensor.

2.3.2 Estimation of the Impedance Tensor

Obtaining the impedance tensor requires measurement of at least four quantities. These being two orthogonal components of the horizontal $\vec{E}$ field and two orthogonal components of the horizontal $\vec{H}$ field. Occasionally the vertical component of $\vec{H}$ is also measured as a determinant of departure from one-dimensionality. As shown in the previous section, the frequency domain, noise free relationship between the horizontal components of $\tilde{\mathbf{E}}$ and $\tilde{\mathbf{H}}$ is given by

$$\tilde{E}_x = \tilde{Z}_{xx}\tilde{H}_x + \tilde{Z}_{xy}\tilde{H}_y,$$

$$\text{and } \tilde{E}_y = \tilde{Z}_{yy}\tilde{H}_y + \tilde{Z}_{yx}\tilde{H}_x,$$

where all quantities above are complex. Because the quantities are complex, we see that we have eight unknowns (real and imaginary parts) and only four equations. Therefore, to solve the equations for the impedance tensor requires at least two independent measurements of the $\vec{E}$ and $\vec{H}$ fields. For MT measurements at ELF/VLF, the largest signal energies are well localized in time, therefore, a recording with GEOCOM-MT (Chapter 3) consists of a sequence of individual "events". If we record N events in the time domain, the impedance tensor may be found in the following manner, where $\tilde{E}_{xi}$, $\tilde{E}_{yi}$, $\tilde{H}_{xi}$, $\tilde{H}_{yi}$ denotes the i^{th} recorded event subjected to Fourier transformation, facilitating a frequency domain analysis.

$$\begin{bmatrix} \tilde{E}_{x1} & \tilde{E}_{x2} & \dots & \tilde{E}_{xN} \\ \tilde{E}_{y1} & \tilde{E}_{y2} & \dots & \tilde{E}_{yN} \end{bmatrix} = \begin{bmatrix} \tilde{Z}_{xx} & \tilde{Z}_{xy} \\ \tilde{Z}_{yx} & \tilde{Z}_{yy} \end{bmatrix} \begin{bmatrix} \tilde{H}_{x1} & \tilde{H}_{x2} & \dots & \tilde{H}_{xN} \\ \tilde{H}_{y1} & \tilde{H}_{y2} & \dots & \tilde{H}_{yN} \end{bmatrix} \tag{2.24}$$

Post multiplying both sides of equation 2.24 by the Nx2 matrix formed from complex conjugates of the magnetic field elements, we get

$$\begin{bmatrix} \tilde{E}_{x1} & \tilde{E}_{x2} & \dots & \tilde{E}_{xN} \\ \tilde{E}_{y1} & \tilde{E}_{y2} & \dots & \tilde{E}_{yN} \end{bmatrix} \begin{bmatrix} \tilde{H}^*_{x1} & \tilde{H}^*_{y1} \\ \tilde{H}^*_{x2} & \tilde{H}^*_{y2} \\ \vdots & \vdots \\ \tilde{H}^*_{xN} & \tilde{H}^*_{yN} \end{bmatrix} = \begin{bmatrix} \tilde{Z}_{xx} & \tilde{Z}_{xy} \\ \tilde{Z}_{yx} & \tilde{Z}_{yy} \end{bmatrix} \begin{bmatrix} \tilde{H}_{x1} & \tilde{H}_{x2} & \dots & \tilde{H}_{xN} \\ \tilde{H}_{y1} & \tilde{H}_{y2} & \dots & \tilde{H}_{yN} \end{bmatrix} \begin{bmatrix} \tilde{H}^*_{x1} & \tilde{H}^*_{y1} \\ \tilde{H}^*_{x2} & \tilde{H}^*_{y2} \\ \vdots & \vdots \\ \tilde{H}^*_{xN} & \tilde{H}^*_{yN} \end{bmatrix}.$$

Or, equivalently,

$$\begin{bmatrix} \sum_{i=1}^{N} \tilde{E}_{xi}\tilde{H}^*_{xi} & \sum_{i=1}^{N} \tilde{E}_{xi}\tilde{H}^*_{yi} \\ \sum_{i=1}^{N} \tilde{E}_{yi}\tilde{H}^*_{xi} & \sum_{i=1}^{N} \tilde{E}_{yi}\tilde{H}^*_{yi} \end{bmatrix} = \begin{bmatrix} \tilde{Z}_{xx} & \tilde{Z}_{xy} \\ \tilde{Z}_{yx} & \tilde{Z}_{yy} \end{bmatrix} \begin{bmatrix} \sum_{i=1}^{N} \tilde{H}_{xi}\tilde{H}^*_{xi} & \sum_{i=1}^{N} \tilde{H}_{xi}\tilde{H}^*_{yi} \\ \sum_{i=1}^{N} \tilde{H}_{yi}\tilde{H}^*_{xi} & \sum_{i=1}^{N} \tilde{H}_{yi}\tilde{H}^*_{yi} \end{bmatrix}.$$

The matrix elements are estimates of auto and cross spectral densities which we express as

$$\begin{bmatrix} < \tilde{E}_x\tilde{H}^*_x > & < \tilde{E}_x\tilde{H}^*_y > \\ < \tilde{E}_y\tilde{H}^*_x > & < \tilde{E}_y\tilde{H}^*_y > \end{bmatrix} = \begin{bmatrix} \tilde{Z}_{xx} & \tilde{Z}_{xy} \\ \tilde{Z}_{yx} & \tilde{Z}_{yy} \end{bmatrix} \begin{bmatrix} < \tilde{H}_x\tilde{H}^*_x > & < \tilde{H}_x\tilde{H}^*_y > \\ < \tilde{H}_y\tilde{H}^*_x > & < \tilde{H}_y\tilde{H}^*_y > \end{bmatrix}. \quad (2.25)$$

This yields four complex valued equations:

$$\begin{aligned} < \tilde{E}_x\tilde{H}^*_x > &= \tilde{Z}_{xx} < \tilde{H}_x\tilde{H}^*_x > + \tilde{Z}_{xy} < \tilde{H}_y\tilde{H}^*_x >, \quad (2.26) \\ < \tilde{E}_x\tilde{H}^*_y > &= \tilde{Z}_{xx} < \tilde{H}_x\tilde{H}^*_y > + \tilde{Z}_{xy} < \tilde{H}_y\tilde{H}^*_y >, \\ < \tilde{E}_y\tilde{H}^*_x > &= \tilde{Z}_{yx} < \tilde{H}_x\tilde{H}^*_x > + \tilde{Z}_{yy} < \tilde{H}_y\tilde{H}^*_x >, \\ \text{and } < \tilde{E}_y\tilde{H}^*_y > &= \tilde{Z}_{yx} < \tilde{H}_x\tilde{H}^*_y > + \tilde{Z}_{yy} < \tilde{H}_y\tilde{H}^*_y > . \end{aligned}$$

Therefore, we now have eight (real and imaginary parts) linear, simultaneous equations and eight unknowns which can be solved, among other ways, with Cramer's rule to give

$$\tilde{Z}_{xx} = \frac{\begin{vmatrix} < \tilde{E}_x\tilde{H}^*_x > & < \tilde{H}_y\tilde{H}^*_x > \\ < \tilde{E}_x\tilde{H}^*_y > & < \tilde{H}_y\tilde{H}^*_y > \end{vmatrix}}{\begin{vmatrix} < \tilde{H}_x\tilde{H}^*_x > & < \tilde{H}_y\tilde{H}^*_x > \\ < \tilde{H}_x\tilde{H}^*_y > & < \tilde{H}_y\tilde{H}^*_y > \end{vmatrix}}, \quad (2.27)$$

$$\tilde{Z}_{xy} = \frac{\begin{vmatrix} <\tilde{H}_x\tilde{H}_x^*> & <\tilde{E}_x\tilde{H}_x^*> \\ <\tilde{H}_x\tilde{H}_y^*> & <\tilde{E}_x\tilde{H}_y^*> \end{vmatrix}}{\begin{vmatrix} <\tilde{H}_x\tilde{H}_x^*> & <\tilde{H}_y\tilde{H}_x^*> \\ <\tilde{H}_x\tilde{H}_y^*> & <\tilde{H}_y\tilde{H}_y^*> \end{vmatrix}}, \tag{2.28}$$

$$\tilde{Z}_{yx} = \frac{\begin{vmatrix} <\tilde{E}_y\tilde{H}_x^*> & <\tilde{H}_y\tilde{H}_x^*> \\ <\tilde{E}_y\tilde{H}_y^*> & <\tilde{H}_y\tilde{H}_y^*> \end{vmatrix}}{\begin{vmatrix} <\tilde{H}_x\tilde{H}_x^*> & <\tilde{H}_y\tilde{H}_x^*> \\ <\tilde{H}_x\tilde{H}_y^*> & <\tilde{H}_y\tilde{H}_y^*> \end{vmatrix}}, \tag{2.29}$$

$$\text{and } \tilde{Z}_{yy} = \frac{\begin{vmatrix} <\tilde{H}_x\tilde{H}_x^*> & <\tilde{E}_y\tilde{H}_x^*> \\ <\tilde{H}_x\tilde{H}_y^*> & <\tilde{E}_y\tilde{H}_y^*> \end{vmatrix}}{\begin{vmatrix} <\tilde{H}_x\tilde{H}_x^*> & <\tilde{H}_y\tilde{H}_x^*> \\ <\tilde{H}_x\tilde{H}_y^*> & <\tilde{H}_y\tilde{H}_y^*> \end{vmatrix}}. \tag{2.30}$$

Solving the determinants for the individual elements of the impedance tensor we arrive at the final results.

$$\tilde{Z}_{xx} = \frac{<\tilde{E}_x\tilde{H}_x^*><\tilde{H}_y\tilde{H}_y^*> - <\tilde{E}_x\tilde{H}_y^*><\tilde{H}_y\tilde{H}_x^*>}{<\tilde{H}_x\tilde{H}_x^*><\tilde{H}_y\tilde{H}_y^*> - <\tilde{H}_x\tilde{H}_y^*><\tilde{H}_y\tilde{H}_x^*>}. \tag{2.31}$$

$$\tilde{Z}_{xy} = \frac{<\tilde{E}_x\tilde{H}_y^*><\tilde{H}_x\tilde{H}_x^*> - <\tilde{E}_x\tilde{H}_x^*><\tilde{H}_x\tilde{H}_y^*>}{<\tilde{H}_x\tilde{H}_x^*><\tilde{H}_y\tilde{H}_y^*> - <\tilde{H}_x\tilde{H}_y^*><\tilde{H}_y\tilde{H}_x^*>}. \tag{2.32}$$

$$\tilde{Z}_{yx} = \frac{<\tilde{E}_y\tilde{H}_x^*><\tilde{H}_y\tilde{H}_y^*> - <\tilde{E}_y\tilde{H}_y^*><\tilde{H}_y\tilde{H}_x^*>}{<\tilde{H}_x\tilde{H}_x^*><\tilde{H}_y\tilde{H}_y^*> - <\tilde{H}_x\tilde{H}_y^*><\tilde{H}_y\tilde{H}_x^*>}. \tag{2.33}$$

$$\tilde{Z}_{yy} = \frac{<\tilde{E}_y\tilde{H}_y^*><\tilde{H}_x\tilde{H}_x^*> - <\tilde{E}_y\tilde{H}_x^*><\tilde{H}_x\tilde{H}_y^*>}{<\tilde{H}_x\tilde{H}_x^*><\tilde{H}_y\tilde{H}_y^*> - <\tilde{H}_x\tilde{H}_y^*><\tilde{H}_y\tilde{H}_x^*>}. \tag{2.34}$$

It is here that we see that the solution of the magnetotelluric impedance tensor is essentially a spectral estimation problem.

It must be noted that there are actually six possible, but usually only four stable solutions to the impedance tensor obtained through choice of complex conjugates multiplied to equation 2.24 (Sims et al., 1971). The four stable solutions for $\tilde{\mathbf{Z}}$ are obtained with choices of $(\tilde{H}_x, \tilde{H}_y)$, $(\tilde{E}_y, \tilde{E}_x)$, $(\tilde{E}_x, \tilde{H}_x)$ or $(\tilde{E}_y, \tilde{H}_y)$. Sims et al. (1971)

found that the best results were obtained using the pair of channels with the lowest noise. Usually the magnetic field channels have better signal-to-noise ratio so it is common to use $(\tilde{H}_x, \tilde{H}_y)$ in the solution of the impedance tensor. In the present study, the solution of the impedance tensor was obtained using the pair $(\tilde{H}_x, \tilde{H}_y)$, as the magnetic field channels always had as good as or better signal-to-noise ratio than the electric field channels (Chapter 5).

It must also be noted that for field measurements we actually measure changes in the $\vec{B}$ field, *not* the $\vec{H}$ field. Therefore, every $\tilde{H}_x$ and $\tilde{H}_y$ term in equations 2.31 through 2.34 should be changed to $\tilde{B}_x$ and $\tilde{B}_y$ respectively. Solving the impedance tensor in this fashion allows us to obtain the apparent resistivity (units of $\Omega - m$) which may be considered a bulk average of some field absorbing volume. With $\vec{B}$ in units of nT and $\vec{E}$ in units of mV/km or, equivalently, $\mu V/m$, we can solve for the impedance elements as in equations 2.31 through 2.34 from which the apparent resistivity may be found as

$$\tilde{\rho}_{ij} = \frac{1}{5f}|\frac{\tilde{E}_i}{\tilde{B}_j}|^2 \tag{2.35}$$

where the subscripts ij refer to the combinations of xy and f is the frequency in Hz. The phase $\tilde{\phi}_{ij}$ is simply the phase of $\tilde{Z}_{ij}$ which can be found from

$$\tilde{\phi}_{ij} = \arctan\frac{\Im(\tilde{Z}_{ij})}{\Re(\tilde{Z}_{ij})}. \tag{2.36}$$

Although the impedance tensor is the fundamental quantity of interest in MT surveys, the apparent resistivity and phase defined above are almost always used for presentation purposes.

2.4 1D MT inversion with the Bostick transform

Bostick (1977) developed an approximate, one-dimensional MT inversion scheme based on the asymptotic nature of the apparent resistivity curves at low frequencies. Bostick begins his derivation by considering two simple earth models. The first model consists of a single layer of resistivity ρ overlying a perfectly conducting basement. With this

model, Bostick found that at low frequencies the apparent resistivity would be

$$\tilde{\rho_a} = \omega \mu_o D^2, \tag{2.37}$$

where ω is the angular frequency, μ_o is the permeability of free space and D is the depth to the perfectly conducting basement. At the other extreme, Bostick considered a single layer of resistivity ρ overlying a perfectly insulating basement. With this model the apparent resistivity at low frequencies was

$$\tilde{\rho_a} = \frac{1}{\omega \mu_o S^2}, \tag{2.38}$$

where S is the conductivity-thickness product of the single layer overlying the perfectly insulating basement at depth D. Therefore, with these two solutions Bostick showed that for a layered earth model the apparent resistivity is determined by the ratio of the depth D to the average conductivity-thickness product S above the depth D, where D depends on the apparent resistivity $\tilde{\rho_a}$ and angular frequency ω. Specifically,

$$\tilde{\rho_a} = \frac{D}{S}, \tag{2.39}$$

where

$$\tilde{\sigma_a} = \frac{1}{\tilde{\rho_a}} = \frac{1}{D} \int_0^D \sigma(z) dz. \tag{2.40}$$

Therefore, solving for σ we find

$$\sigma = \frac{dS}{dD} = \frac{dS}{d\omega} \Big/ \frac{dD}{d\omega}.$$

Using the relations above for $\tilde{\rho_a}$ in terms of D and S we get the Bostick transform

$$\rho_b = \tilde{\rho_a} \frac{1 - \frac{dlog\tilde{\rho_a}}{dlog\omega}}{1 + \frac{dlog\tilde{\rho_a}}{dlog\omega}}, \tag{2.41}$$

where ρ_b is the Bostick resistivity (approximate earth resistivity) at depth D defined as

$$D = \sqrt{\frac{\tilde{\rho_a}}{\omega \mu_o}}. \tag{2.42}$$

The derivative term in equation 2.41 causes the Bostick transform to be sensitive to noise (scatter) in the data. To reduce the sensitivity of the inversion to noise,

the phase can be used to estimate this derivative. This comes about because the magnetotelluric impedance tensor is a causal, minimum phase function and therefore the real and imaginary parts of $\tilde{\mathbf{Z}}$ are Hilbert transform pairs, even in the 3D case (Yee and Paulson, 1988). The zeroth order approximation to the Hilbert transform yields the required relation between the phase data and the logarithmic derivative of $\tilde{\rho_a}$ as

$$\tilde{\phi} = \frac{\pi}{4}(1 + \frac{dlog\tilde{\rho_a}}{dlog\omega}). \tag{2.43}$$

The dispersion relation, equation 2.43 was originally solved independently by Weidelt (1972) and Kunetz (1972). Equation 2.43 has been used to estimate phase data from amplitude data or vice-versa. Good quality amplitude data is usually easier to obtain so that the more difficult to measure phase may be estimated directly from amplitude data (Fischer and Schnegg, 1979). On the other hand, if good quality phase data can be obtained, unbiased estimates of the impedance tensor can, in principle, be obtained from single site measurements of phase data alone (Boehl et al.,1977, Satarno and Vozoff, 1991). Solving the dispersion relation of equation 2.43 for the logarithmic derivative of $\tilde{\rho_a}$ we get

$$\frac{dlog\tilde{\rho_a}}{dlog\omega} = \frac{4\tilde{\phi}}{\pi} - 1, \tag{2.44}$$

substitution of the above into equation 2.41, yields, after manipulation, the phase constrained Bostick transform at depth D

$$\rho_b(D) = \tilde{\rho_a}(\frac{\pi}{2\tilde{\phi}} - 1). \tag{2.45}$$

Chapter 3

Instrumentation

3.1 The Recording Instrument

Data acquisition was performed with GEOCOM-MT, a four channel, 12 bit, 100-kHz-throughput, tensor MT system, designed and built at the Cybernetics Laboratory, University of Saskatchewan, by P.R. Kosteniuk and Dr. K.V. Paulson (Kosteniuk and Paulson, 1988). The maximum throughput of 25 kHz per channel defines a theoretical Nyquist frequency of 12.5 kHz; therefore, for field use an upper limit of 10 kHz is used for data acquired with GEOCOM-MT. A lower limit of 10 Hz is enforced due to the rapid decline of the induction coil response at that frequency. Therefore, the effective bandwidth for GEOCOM-MT is 10 Hz to 10 kHz.

To lessen the dynamic range requirements of the instrument, the frequency range 10 Hz to 10 kHz is divided into three overlapping bands (Low-Band, Mid-Band and High-Band) allowing amplification according to signal levels in the frequency band of interest. The electric and magnetic field signals first pass through differential amplifiers with a gain of 20, and then through an analog, Twin-T notch filter network which removes either 50 or 60 Hz powerline noise (user set), although the notch filter network can be bypassed in cases when cultural noise is not prevalent. After notch filtering, the signals are further amplified with a user adjustable gain of 1, 10 or 100 prior to digitization. Low-Band is acquired at a sample rate of 1 kHz per channel and was band pass filtered by the author (after being recorded to floppy disk) from 10 Hz to 200 Hz. This for the most part eliminates aliasing or folding of data above

Nyquist down into the frequency range of interest and removes artifacts in the data below 10 Hz due to the diminished response of the induction coil magnetometer here. Mid-Band is acquired at a sample rate of 10 kHz per channel and was similarly band pass filtered from 100 Hz to 1000 Hz. Lastly, High-Band is acquired at a sample rate of 25 kHz per channel and was band pass filtered from 1 kHz to 10 kHz.

Perhaps the most notable feature of GEOCOM-MT is the manner in which the data is recorded. Magnetic field transients in the frequency range 1 Hz and above are caused almost exclusively by thunderstorm activity at near and great distance. Such an energy source is random in nature and accordingly we may have long intervals of time between transients when we effectively have no signal. This is the case in fall and winter when natural source activity is considerably lower than in summer (Chapter 5). To avoid recording the noise in the time interval between events, GEOCOM-MT "triggers" on magnetic field transients so that, ideally (see below), data is recorded only when valid source signal is present. This is accomplished by waiting for times at which the digitized output of the induction coil magnetometer exceeds a user specified threshold or trigger level. However, data is accepted only after ensuring commonality on all four channels within a narrow time window ($\leq 10\ ms$). GEOCOM-MT then windows the event on each channel, the length of the window depending on the frequency band. For Low-Band, a window $512\ ms$ long (512 samples) is used, for Mid-Band a $51.2\ ms$ window (512 samples) is used and for High-Band a $10.24\ ms$ window (256 samples) is used. In this manner we minimize as much as possible the amount of noise recorded, which is extremely important for rapid and accurate estimation of the impedance tensor. Of course it is up to the operator not to set the threshold so low that we trigger on noise. In this fashion, we ensure that every recorded event has a valid signal component. This differs from the conventional recording technique where data is acquired continuously (blindly) and as such many "events" with no valid signal components may be recorded giving rise to unusable, or at best poor results in times of low source field activity. Lastly, the user has the option of processing data in the field with the polarization stacking program (Kosteniuk and Paulson, 1988) or recording raw, multiplexed time domain data to floppy disk which can be processed at a later date.

3.2 Measurement of the Electric Field

3.2.1 Field Procedure

The horizontal electric field is obtained from measurement of the potential difference between earthed electrodes at known separation. Dividing the potential difference V between electrodes by their separation distance d, yields the electric field $\vec{E} = V/d$, averaged over the length of the separation distance between electrodes. The earthed electrodes are arranged parallel to the measurement co-ordinate system x and y axes to obtain E_x and E_y, the electric field components in the x and y directions respectively. The distance between electrodes is chosen large enough so that the signal measured, on the order of $\mu V/m$, is above the noise level of the electrodes and their associated electronics. For MT measurements at ELF/VLF, separation distances of 100 m are common although the author has used separation distances as small as 50 m in summer under high signal-to-noise conditions. Note that the separation distance required to achieve a given signal-to-noise ratio is also dependent on earth resistivity, for a given amplitude change in the $\vec{B}$ field, larger electric fields are necessarily induced in more resistive earth materials so that in general, the electric field signal-to-noise ratio is a function not only of distance between electrodes but also of earth resistivity and natural source signal amplitude.

The choice of separation distance between electrodes is also governed by other factors, namely that larger separation distances allow one to better average over any near surface, isolated anomalous bodies which would otherwise distort electric field measurements. As we decrease electrode separation, the risk of measuring a distorted electric field caused by anomalous near surface features is increased. This has led to the development of MT arrays where many electrodes are placed in various geometrical orientations to achieve the spatial averaging necessary to remove any near surface distortions. A "Diamond-Necklace" array was developed by Dr. K.V. Paulson (1987) and has been used extensively for MT data acquisition (Kalantzis, 1990. Chen, 1991). EMAP (Electro-Magnetic Array Profiling) developed by Bostick et al. (1985) is another example. However, increased spatial averaging is attained at the cost of survey resolution. A rule of thumb is that the separation distance should be no larger than the smallest target of interest (Zonge et al., 1991), however, even if a body is

small compared to the separation distance, it can still be detected if it is conductive enough. Generally though, the minimum separation is most often limited by noise considerations (Zonge et al., 1991).

3.2.2 Types of Electric Field Sensors

An electrochemical reaction is developed when a metal is placed in contact with an electrolyte. Such is the case when a metallic electrode is in contact with the earth, a mostly ionic conductor. A variable potential difference is established between the electrode and the electrolyte, the magnitude of which depends on temperature, type of material and other factors. This variable potential difference is a source of noise in electric field measurements and should be minimized if possible.

There are two kinds of electrodes that are usually employed for electric field measurements in MT surveys. The first is a simple metal electrode, usually lead, the second is a non-polarizing or porous pot electrode which consists of a metal immersed in one of its own salts. The latter have superior noise characteristics as compared to simple metal electrodes.

Many different kinds of porous pot electrodes exist but perhaps the most practical are lead-lead chloride ($Pb - PbCl_2$) electrodes. Practicality is assured through their low cost of manufacture and their performance with respect to noise levels are as good as or better than the much more expensive and less robust silver-silver chloride ($Ag - AgCl$) electrodes. Petiau and Dupis (1980) compared the noise spectrum, temperature coefficient and polarization characteristics of various electrodes. They found that the best overall performance was attained with $Pb - PbCl_2$ electrodes.

Construction of $Pb - PbCl_2$ electrodes is easily accomplished with a tubular design, a lead wire is immersed in a plaster of paris mud, saturated with lead chloride ($PbCl_2$, 15 g/L) and common table salt (360 g/L), all contained within PVC (poly-vinyl-chloride) tubing, with one end left open. Porous pot electrodes make electrical contact with the earth in two steps. Metal-electrolyte contact is made between the lead wire and the conducting plaster of paris where significant electrochemical potentials of .1 to 1 V are generated (Petiau and Dupis, 1980). Fortunately this large electrochemical potential remains constant as long as the chemical concentrations inside the electrode and its temperature is held constant. The latter variable is more difficult to control

in the field and is one of the reasons why the electrodes are usually buried. Contact with the earth is made in the second step when the electrolyte diffuses through the plaster of paris, exposed at the bottom. Potentials generated in the second step are quite small, on the order of mV (Petiau and Dupis, 1980), and in this fashion a stable, low noise contact with the earth is attained.

Alternatively, a simple metal electrode offers ease of use. At one time, simple lead electrodes were the electrode of choice for MT surveys (Keller and Frischknecht, 1966). Petiau and Dupis (1980) recommend the use of simple metal electrodes for MT surveys above 10 Hz as they state that amplifier noise dominates over electrode generated noise at these frequencies, although this would also depend on earth resistivity (Vozoff, 1991). Instrumentation improvements would also alter this statement. Generally speaking, unless their use is precluded, as is the case on frozen ground, the best quality electric field data at ELF/VLF will be attained with porous pot electrodes, although at VLF a simple metal electrode may perform nearly as well (Chapter 5).

3.3 Measurement of dB/dt

Orthogonal, horizontal components of the time rate of change of the magnetic flux density $\vec{B}$ were measured with a ferrite-core, induction coil magnetometer. The design of the induction coil magnetometer used in the present study was based on that of Hoover et al. (1978), in his studies for the United States Geological Survey.

The basic principle of operation with induction coil magnetometers is the generation of a voltage V in a conductive loop with cross-sectional area A, when a magnetic flux density $\vec{B}$ cutting through the loop changes with time. The voltage generated is proportional to the area of the loop multiplied by the time derivative of $\vec{B}$ cutting the loop (Vozoff, 1991). To provide a measurable voltage many turns of wire are employed, as such, the weight of a coil can be large and its capacitance, inductance and resistance appreciable. The equivalent circuit of an induction coil magnetometer is very approximately that of a resonant RLC circuit, therefore induction coil magnetometers operated in the classical voltage mode have resonant frequencies where the response is a maximum. At ELF/VLF, fewer turns of wire need be employed to achieve a given sensitivity, thus induction coils designed to operate at these higher

frequencies can be made considerably smaller and thus more portable than induction coils used in low frequency MT surveys ($\leq 1Hz$).

For a given number of turns, the sensitivity of an induction coil magnetometer can be increased by winding the coil on a core of highly permeable material which increases the magnetic flux density through the coil (Keller and Frischknecht, 1966). Conversely, with a permeable core the number of turns of wire needed to achieve a given sensitivity is reduced, thus decreasing the weight of the induction coil magnetometer. For lower frequency applications ($\leq$ 200 Hz) mu-metal is the permeable core of choice, for high frequency applications ferrite cores are preferred (pers. comm., Dr. W.H. Pelton). Several papers have been published detailing the design of induction coil magnetometers, perhaps the most recent and detailed being that of Lukoschus (1979). It was found that the weight of the device is the most prevalent design criterion. The tolerable weight of an induction coil magnetometer for a given core length (assumed cylindrical) and high frequency cutoff, along with pre-amplifier characteristics, yields a unique configuration which results in the best noise characteristics, i.e., noise inherent to the induction coil/amplifier combination itself. Similarly, the design of single frequency air-core loops is detailed in Becker (1967) where it is also found that the signal-to-noise ratio is determined by the geometry and weight of the device. Thermal noise generated in the windings of the coil due to random, "thermal" motion of electrons is the most prevalent source of noise inherent to induction coils themselves, which limits the smallest amplitude signal that can be detected. Conversely the largest amplitude signal that can be detected is limited by the Tesla level required to saturate the core (Vozoff, 1991). For measurements at ELF/VLF, the largest natural source signals encountered are approximately tens of nT at most, therefore, the signal amplitudes over which a particular induction coil magnetomter can operate is mainly limited by thermal noise in the windings of the coil, which increases with the resistance of the coil windings (pers. comm, P.R. Kosteniuk). Other sources of noise which arise due to changes in core permeability with temperature and with mechanical stress (Barkhausen noise) are usually minor compared with thermal noise.

The induction coil magnetometer employed in the present study has a .36 m square, high permeability ferrite core (MN-60), .038 m high and .019 m thick. Each of the four legs has 200 turns of no. 14 copper, armored polythermalized wire wound in

two layers. Each pair of opposite legs is connected in series to a step up transformer with an 80:1 ratio. An op-amp is used for further amplification to drive the signal down the ten metre cable connecting the coil to the recording instrument. Lastly, the entire assembly is housed in an electrostatic shield or Faraday Cage to prevent the induction coil from responding to low frequency electric field changes. This induction coil magnetometer weighs about 13 kg and is hence quite portable. The interested reader is referred to Labson et al. (1985) for a good description of this induction coil also. The amplitude response of the induction coil magnetometer is shown in Figure 3.1, measured by P.R. Kosteniuk at Dawn Lake, Saskatchewan in July, 1984. Note the resonant frequency of approximately 1.3 kHz where a maximum sensitivity of approximately 50 mV/nT is obtained. It should be remarked that the resonant peak is also partly due to the fact that this coil operates in the "voltage" mode. It is now commonplace for coils to operate in the "current" mode where the current in the induction coil is sensed. Induction coils operated in the current mode have a very flat amplitude and therefore also a very slowly varying phase response across a wide band of frequencies (Labson et al., 1985). In some cases a flat response is desired due to ease of amplitude/phase compensation during data processing, in other cases a response with a sharp peak can be desirable, as is the case with MT at ELF/VLF where the increased attenuation between 200 Hz and 7 kHz can be at least partly counteracted with a coil response as shown below.

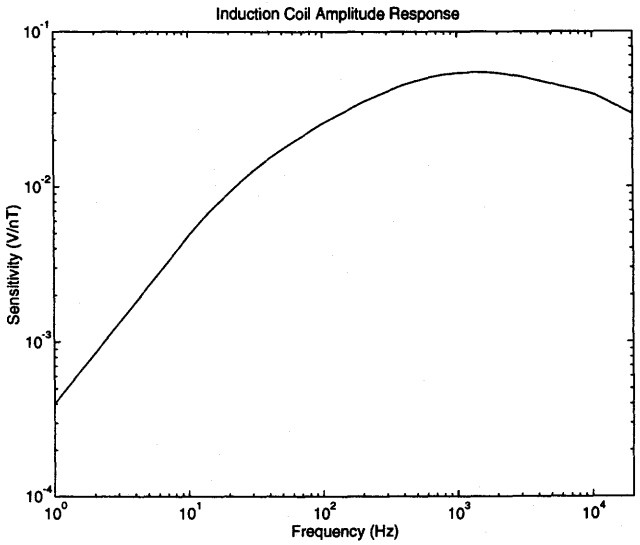

Figure 3.1: Amplitude Response of Induction Coil Magnetometer

Chapter 4

Data Processing

4.1 Introduction

Data processing with GEOCOM-MT can be accomplished in two ways. One option is to employ the polarization stacking program of Kosteniuk and Paulson (1988) which enables one to get in-field results. The second approach is to record raw data in the field and process later. The latter method was enforced upon the present study due to a faulty 60 Hz notch filter in the E_x channel which made the polarization stacking scheme ineffective with the E_x channel.

Raw data is recorded multiplexed, in units of A/D bits and is convolved with the frequency dependent responses of the recording instrument and the induction coil magnetometer. Therefore, a Matlab program was written to demultiplex the recorded data and correct (deconvolve) the raw data for the amplitude response of the instrument and the amplitude and phase response of the induction coil magnetometer.

After the data has been deconvolved and converted to fundamental MT units, each frequency band was band passed filtered in order to remove any artifacts that may have been generated by the compensation program and to lower noise levels if possible. After band pass filtering, manual editing of the times sequences were performed to remove any bad events that may have been recorded.

Each event on all four channels was then windowed by forming a modified boxcar window with smoothly tapered ends. To maintain the original frequency resolution in the FFT, the data segment outside the window was zero-padded to the original

record length of either 512 samples for Low and Mid-Band or 256 samples for High-Band. The windowing in this fashion decreased the amount of noise going into the frequency domain analysis and thus yielded much smoother impedance estimates with significantly fewer events.

Impedance estimation was carried out with the classical method as outlined in Chapter 2. For smoothing and presentation purposes the raw curves were averaged over a range of frequencies to give 10-14 points per decade, equispaced on a log-log scale. However, with the windowing and zero-padding procedure, the raw curves were already smooth enough that no averaging was needed other than to give the customary 10-14 points per decade for presentation purposes.

Lastly, a graphical editor was used to interpolate over the dead band in the data, approximately from 500 Hz to 5 kHz (late fall and winter). The final edited curves were then used as input to a one-dimensional Bostick transform to give approximate earth resistivity as a function of depth.

It should be noted that in most cases it is necessary to apply a topographic correction to MT data as topography changes distort the sub-surface $\vec{E}$ field. At the Hepburn site this was unnecessary as all the sites were at the same elevation to within 70 cm.

Also, since the Hepburn site was approximately one-dimensional, no strike exists and therefore no tensor decomposition or rotation to some principal co-ordinate system was required. Furthermore, the use of a one-dimensional inversion is thus justified.

4.2 Implementation of the Data Processing Algorithm

4.2.1 Instrument and Magnetometer Compensation

GEOCOM-MT operates under the CPM/86 operating system, therefore the first step in processing recorded data is to convert the data files from CPM/86 format to MS-DOS. This was accomplished with a program called 22Disk with the NEC3 NEC PC 8801/8831A DSDD 48 tpi format.

Since the time domain data files were multiplexed as B_{xi}, B_{yi}, E_{xi}, E_{yi}, B_{xi+1} etc, where the subscript i denotes the event number, the second step was to demultiplex

the recorded data file yielding four individual data files, one for each channel of B_x, B_y, E_x and E_y.

The third step was to correct all the channels for the amplitude response of the instrument and additionally the $\vec{B}$ channels for the amplitude and phase response of the induction coil magnetometer. It should be noted that for solely calculating apparent resistivity and phase curves it is not necessary to correct the data for the amplitude response of the instrument because we essentially calculate the ratio of $\vec{E}/\vec{B}$, and as long as the amplitude response of the instrument is the same on both channels, the effect is negated. This was found to be true by the author during calibration of GEOCOM-MT. The amplitude response was identical on corresponding $\vec{E}$ and $\vec{B}$ channels to within two percent for all three frequency bands. However, in order to save $\vec{E}$ and $\vec{B}$ data in fundamental units, the amplitude response of the instrument has to be accounted for. Towards this end, GEOCOM-MT was calibrated on all four channels so that the instrument amplitude response could be accurately known and therefore $\vec{E}$ and $\vec{B}$ data saved in fundamental units. Magnetometer calibration data collected by P.R. Kosteniuk in July of 1984 was used to correct the $\vec{B}$ field channels for the response of the magnetometer.

Additionally, 60 Hz noise was removed from the E_x channel with a digital approximation of the analog 60 Hz notch filters used by GEOCOM-MT. This allowed all four channels to be used permitting a full tensor calculation. (Note, the faulty notch filter was fixed in Dec, 1995 by P.R. Kosteniuk.) The compensation program also corrects the phase of the four channels for A/D skew error, arising from the fact that all four channels aren't sampled simultaneously. The phase error introduced by A/D skew is large at high frequencies and quite small at low frequencies. Lastly, the data files were band pass filtered and saved in fundamental units of mV/km, or equivalently, $\mu V/m$, for the electric field and nT for the magnetic field. The following list summarizes the operations performed by the compensation program.

- Demultiplex the recorded time sequences to yield the four channels of data for E_x, E_y, B_x and B_y.
- Apply a 60 Hz notch filter on the E_x channel.
- Apply an instrument gain correction as a function of frequency.

- Apply a magnetometer amplitude and phase correction to the $\vec{B}$ channels.
- Apply an A/D skew error correction.
- Apply a band pass filter, 10 Hz - 200 Hz for Low-Band, 100 Hz - 1 kHz for Mid-Band and 1 kHz - 10 kHz for High-Band.
- Save the corrected data in fundamental MT units. $\mu V/m$, or equivalently, mV/km, for the electric field and nT for the magnetic field.

4.2.2 Estimating the Impedance Tensor

Calculation of the impedance tensor was accomplished with the classical approach presented in Chapter 2. Before data was input to the impedance estimation program, the corrected data files were edited to remove any bad events that may have been recorded. Next, the windowing and zero padding procedure was carried out.

Specifically, a modified boxcar window, consisting of the unity amplitude portion of a boxcar window with one half of a Hanning window on each end, was formed around each event. This window was used as the Hanning window portion forces the ends of the windowed event smoothly to zero, thereby satisfying the circular assumption in the FFT and avoiding any transient effects at the edges of the windowed event. The unity amplitude, central portion of the modified boxcar window was used to preserve the original character of the time domain data without affecting phase relationships between channels (pers. comm., P.R. Kosteniuk). The windowed event was subsequently zero-padded to its original length of 256 points for High-Band and 512 points for Mid and Low-Band. The length of the modified boxcar window was chosen so as to "zoom-in" on the signal as much as possible while using a wide enough window to permit impedance calculations to a sufficiently low frequency. For High-Band, a 32 point window was used, the lowest frequency signal that would fit into this window is $f_o = 781$ Hz, for Mid-Band a 128 point window was used ($f_o = 78$ Hz) and for Low-Band a 128 point window was used ($f_o = 7.8$ Hz). A typical Low-Band event, before and after windowing and zero-padding is shown in Figure 4.1.

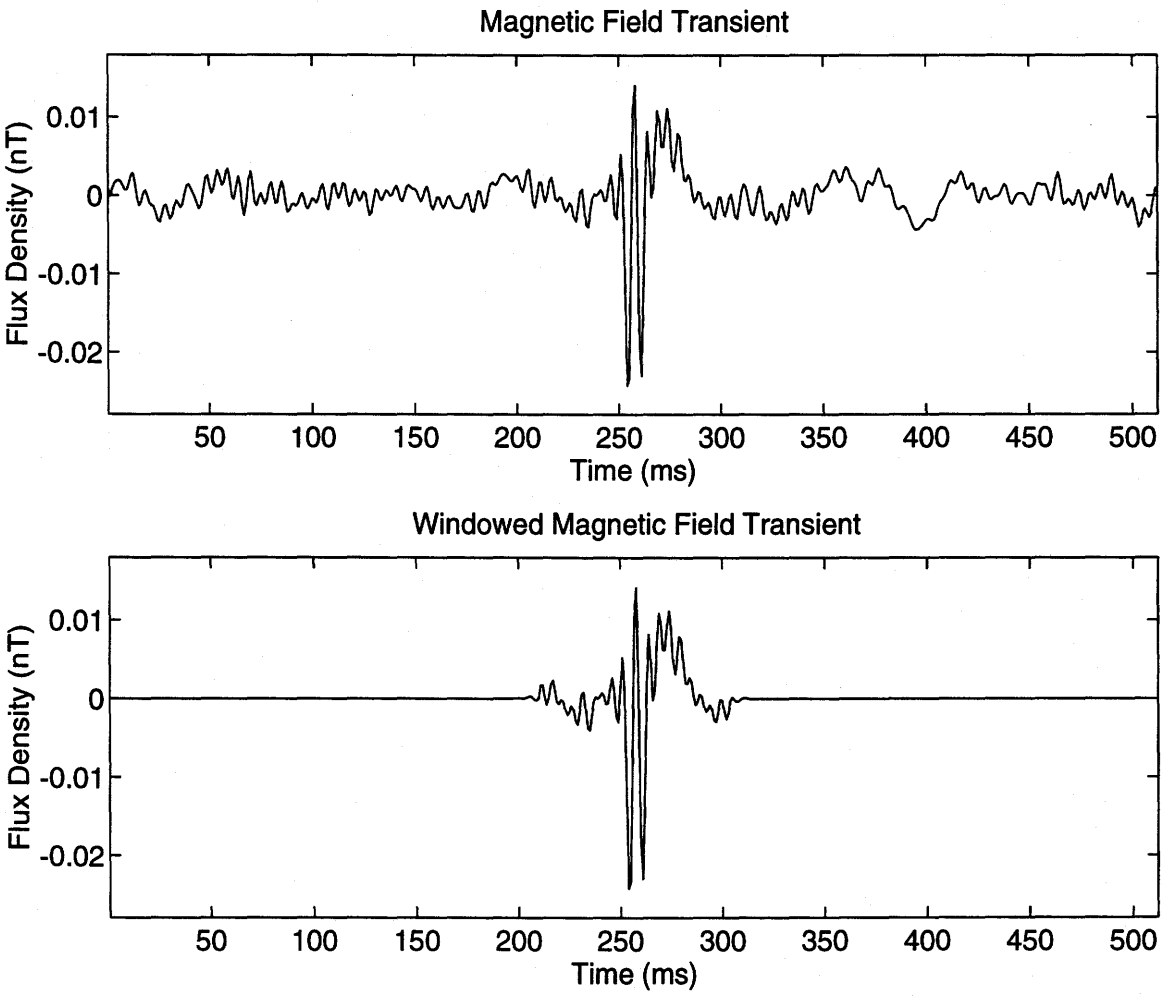

Figure 4.1: A typical ELF (Low-Band, 10-200 Hz) B_x event, before and after event windowing

Windowing and zero-padding was found to be an important step in the processing flow as it decreased the amount of noise in the spectral analysis and thereby reduced the scatter in the calculated curves. In some cases, this procedure allowed the "pulling out" of events from noisy time sequences that would have been otherwise unusable. An example of this is shown in Figure 4.2, where an unwindowed and windowed High-Band E_x, B_y transient pair is shown. This data was collected at the University of Saskatchewan, geophysical field school site on August 27, 1996. This site is characterized by very high noise levels due to buried powerlines and by four nearby microwave transmitters ($\leq$ 3 km) used for television broadcasts. Note the presence of noise

spikes on the order of or higher than signal levels on the E_x channel. The noise is absent on the B_y channel, a fortunate situation as we trigger off the $\vec{B}$ channels with GEOCOM-MT. The reason for the large noise spikes on the E_x channel, and their absence on B_y, is most likely due to enhanced coupling of noise from buried powerlines with the electric field.

It is noteworthy that the author's data processing method gave $\tilde{\rho}_{yx}$ and $\tilde{\phi}_{yx}$ (east-west) values at 10 kHz which are almost identical with those obtained with a VLF-R (Chapter 1) instrument at approximately 25 kHz. The $\tilde{\rho}_{yx}$ and $\tilde{\phi}_{yx}$ MT derived quantities are comparable to the VLF-R measurements because the VLF-R instrument at the field school locked in on transmitters NAA (Cutler, Maine 24 kHz) and NLK (Seattle, Washington 24.8 kHz). The signals from these transmitters propagate with the magnetic field vector oscillating perpendicular to the direction of propagation (TM mode) and therefore induce currents to flow perpendicular to magnetic field vector oscillation, or parallel to the bearing of the transmitter (in the 1D case) which is roughly east for Cutler, Maine and west for Seattle, Washington. Therefore, VLF-R measurements made with these transmitters would be expected to correlate most closely with the $\tilde{\rho}_{yx}$, $\tilde{\phi}_{yx}$ quantities recorded with GEOCOM-MT and processed by the author. This was found to be the case as $\tilde{\rho}_{yx}$ and $\tilde{\phi}_{yx}$ at 10 kHz, processed by the author, were less than ten percent different than VLF-R derived $\tilde{\rho}$ and $\tilde{\phi}$ quantities at roughly 25 kHz. This helped verify the author's data processing method and programs.

Also note the monstrous size of the recorded signal shown in Figure 4.2, the High-Band B_y transient is on the order of 5 nT peak to peak. The author has recorded High-Band transients as large as 10 nT peak to peak in August, 1996 at 52°N. Such large signals most likely arise from relatively near thunderstorms ($\leq$ 500 km), as such $\vec{B}$ field transients of this magnitude were not seen in winter as thunderstorms were found to be on average, approximately 3000 km distant (Chapter 5) at 52°N throughout the winter months.

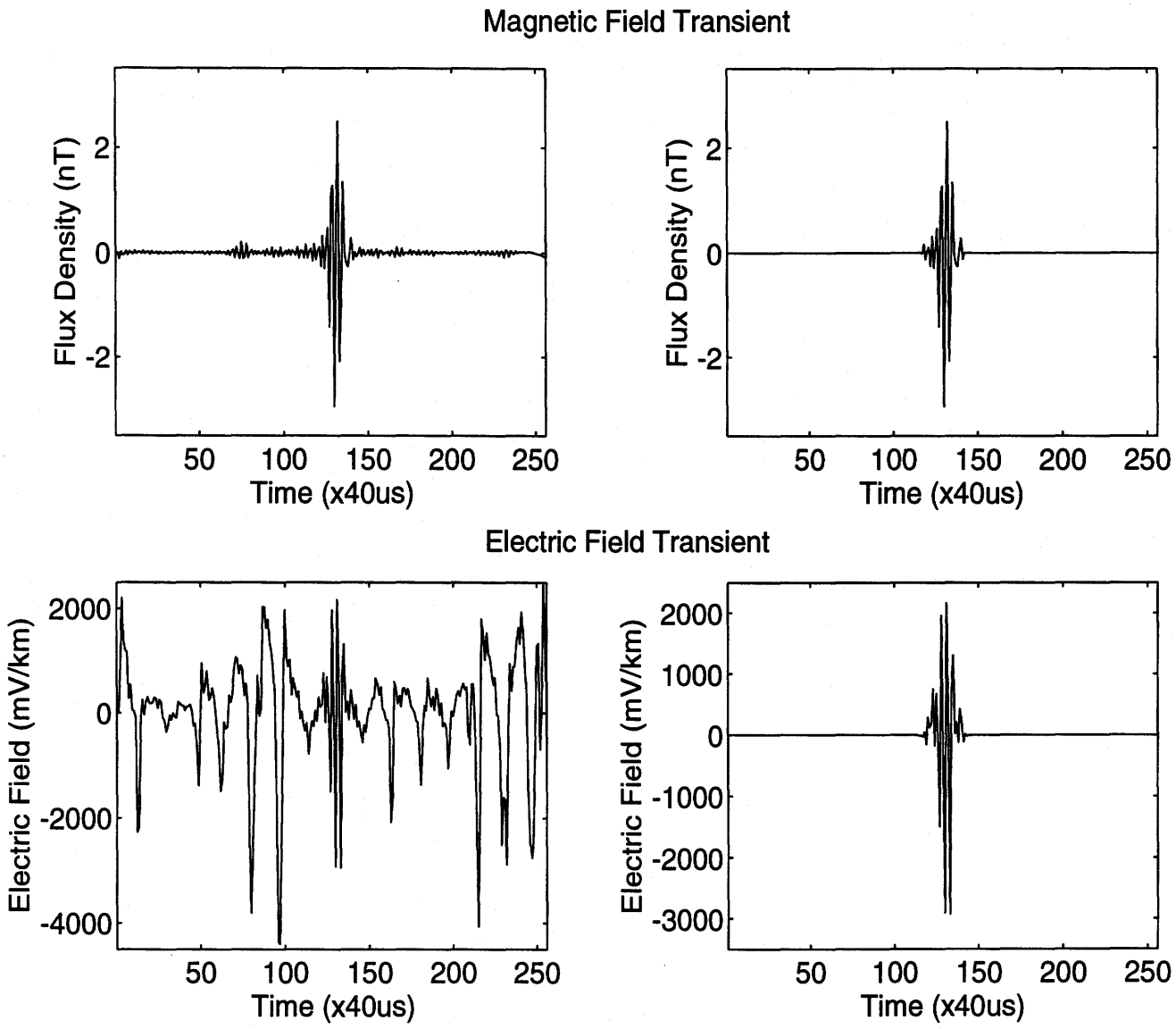

Figure 4.2: A large VLF, B_y, E_x transient pair, before and after event windowing

With this procedure as few as 20 events per frequency band (Low, Mid and High-Band) were needed to get repeatable and smooth earth response curves. This is especially important in times of low source field activity and low signal-to-noise ratio, such as fall and more so winter, as fewer recorded events means reduced recording times which leads to better productivity.

The improvement to be had with the author's data processing method depends on the signal-to-noise ratio of the recorded data. By triggering on $\vec{B}$ field transients, GEOCOM-MT already achieves a high degree of signal localization. Localizing the

signal further doesn't make much of a difference in cases of high signal-to-noise ratio. Substantial improvements were found, though, in cases of low signal-to-noise ratio, as was generally seen throughout the winter months in the present study (Chapter 5). For the winter data collections, or times of low signal-to-noise ratio, the author's data processing method was found to be essential.

It should be noted that the above procedure was made possible only because the recording method used by GEOCOM-MT is such that we have precise knowledge about the location in time of the transient signal of interest. Therefore, we can localize our transient signal of interest even further, and in some cases achieve a significant signal-to-noise enhancement. Specifically, the signal-to-noise enhancement (SNE) in dB can be found to be (Kosteniuk and Paulson, 1988)

$$SNE = 10 \log_{10} \frac{N}{M}, \tag{4.1}$$

where N is the original record length, and M is the length of the window used to localize the signal. It is assumed that the noise is uniform over the length of the recording window and the signal is located entirely at the center of the window. With this, we find a SNE of approximately 9 dB in High-Band and approximately 6 dB in Mid and Low-Band.

Conversely, it should be realized that in cases when multiple events occur in a single record, the author's processing method negates these events as we retain the triggered event at the center of each record only. Although it was never done, the processing program could be modified to to pull out multiple events that may have occurred in a single record length. However, even though in some instances we are destroying valid signal, the advantages of the above procedure were found to outweigh any disadvantages, although as stated above, in cases of high signal-to-noise ratio, one might as well use the entire record length, automatically including multiple events if present.

With all the preliminary work now completed, a Matlab program was written for estimation of the impedance tensor using spectral analysis functions incorporated in Matlab. Matlab uses Welch's averaged periodogram method to estimate auto and cross spectral density functions. Specifically, Fourier transforms are used to obtain the required frequency domain quantities, the appropriate multiplications between all

four channels yields the required spectral density estimates which are are subsequently averaged over all events (usually 100 events for High-Band, 50 events for Mid and Low-Band) forming the averaged periodogram estimate. The user additionally has the option of overlapping subsequent events to achieve more averaging and thus, more heavily smooth the spectral density estimate. Strictly speaking, Welch's method with no overlap between records is called Bartlett's method (Press et al., 1988), which is what was used in the present study. This was found to be advantageous in that it allowed the author to easily see the transition between signal and no-signal portions of the data (i.e., the dead band in the data could be easily identified). In this fashion, one of each required auto and cross spectral density estimate for the impedance tensor element in question ($\tilde{Z}_{xx}$, $\tilde{Z}_{xy}$, $\tilde{Z}_{yx}$ or $\tilde{Z}_{yy}$) was obtained. With the required auto and cross spectral density estimates, one element of the impedance tensor could be calculated after which calculation of the Fourier transforms for the next element can begin. This procedure continues until all four elements of the impedance tensor have been estimated.

From the four elements of the impedance tensor, the apparent resistivity and phase were calculated, yielding the raw apparent resistivity and phase curves. From the raw apparent resistivity and phase curves, smoothed or averaged curves were obtained by averaging over expanding frequency windows, to end up with 12 points per decade, equi-spaced on a log-log scale. For the purposes of smoothing, this last step was found to be superfluous as the so called raw curves were already very smooth due to the omission of noise with the event windowing procedure. Therefore, in the present study the author preferred to view data which has been smoothed as little as possible (i.e., the raw curves) and rely on personal judgement to distinguish between valid data points and noise.

Next, a graphical editor in Matlab was employed to interpolate through the dead band in the data, approximately from 500 Hz to 5 kHz (late fall and winter), thus yielding the edited apparent resistivity and phase curves. This was accomplished by plotting the raw apparent resistivity and phase curves in Matlab and invoking the Matlab graphical editor "ginput", at which time a crosshair appears on the screen of the monitor. Clicking the mouse button at the location specified by the crosshair causes Matlab to store the location of this data point. In this manner we can interpol-

ate through the dead band in the data. One hundred points were used with ginput, these one hundred points were subsequently decimated to fifty points and then interpolated to the thirty nine points in a pre-determined frequency vector for the edited curves. The graphical editing step is justified by noting that the apparent resistivity, or more fundamentally the impedance tensor, must be a smoothly varying function of frequency.

Shown in Figure 4.3 are the raw and edited $\tilde{\rho}_{xy}$, $\tilde{\phi}_{xy}$ curves from SITE 104 (Chapter 1), recorded on October 28, 1995. For the sake of comparison, the results of processing the data from SITE 104 without windowing and zero padding is shown in Figure 4.4, with the edited curves from Figure 4.3 for reference. We see the increased scatter in the curves caused by the higher noise content in the spectral analysis. Note the large low in the $\tilde{\rho}_{xy}$ and $\tilde{\phi}_{xy}$ curves at 60 Hz. This is due to mis-balancing of the depth of the notch between the digital 60 Hz notch filter applied to E_x and the analog 60 Hz notch applied to B_y. Also, note the dead band in the data, most evident in the phase curve, indicated by the scatter in the data from approximately 500 Hz to 5 kHz.

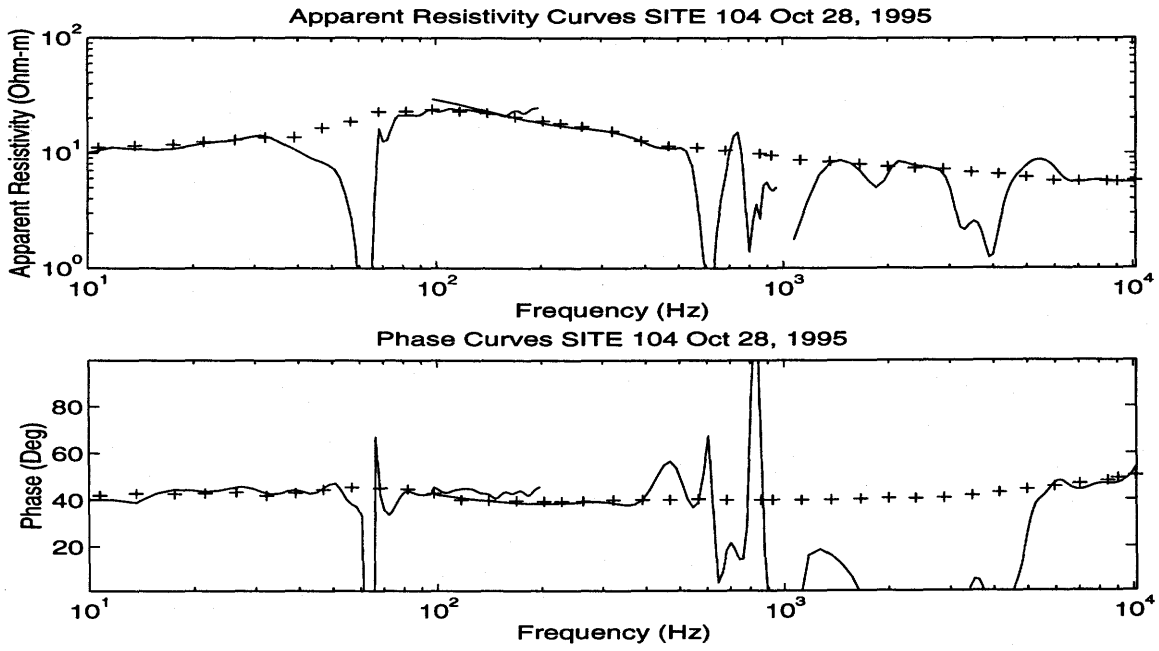

Figure 4.3: Raw (Solid) and Edited (+) $\tilde{\rho}_{xy}$, $\tilde{\phi}_{xy}$ curves

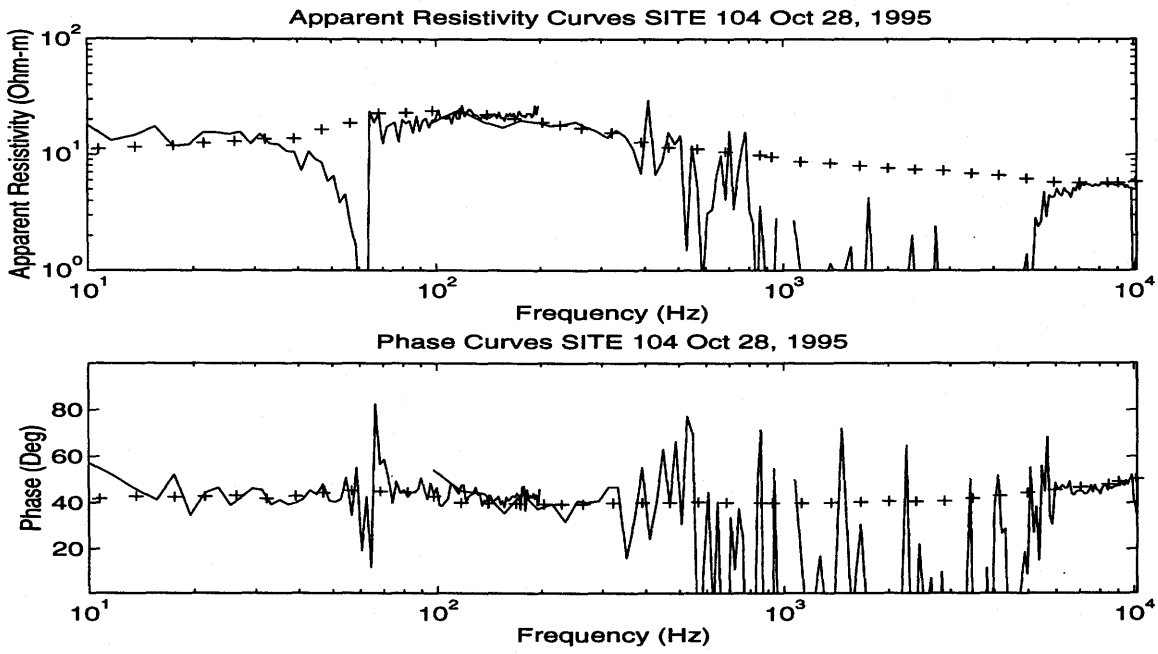

Figure 4.4: Raw (Solid) $\tilde{\rho}_{xy}$, $\tilde{\phi}_{xy}$ curves obtained without event windowing and zero padding and edited (+) $\tilde{\rho}_{xy}$, $\tilde{\phi}_{xy}$ curves

4.3 Correcting MT data for Topography Variations

Topographic features alter the path of sub-surface currents, they can be thought of as reflecting "current streamlines" in the ground (Grant and West, 1965) so that in valleys current streamlines may be squeezed together and conversely spread apart on topographic highs. This affects both the magnetic field and the electric field although the effect on the electric field is more intense.

The general principle of correcting MT data for topography is to forward model the response of a flat earth model with given resistivity structure, then forward model that same resistivity structure with topographic relief. Dividing the impedance tensor from the topographic model by the flat earth model impedance tensor allows one to obtain the so called distortion tensor which distorts the true sub-surface response. In some cases it is possible to eliminate this distortion without knowing the sub-surface conductivity structure (Kosteniuk, 1990). This is the case when the distortion mainly depends on the topographic relief, not the sub-surface conductivity structure. Finite-element programs are usually used for modeling topography since surface features of

arbitrary shape and complexity can be accurately modeled (Kosteniuk, 1990).

4.4 Canonical Decomposition of the Impedance Tensor

The problem of strike determination has been a subject of active research in the MT community. The canonical decomposition of Yee and Paulson (1987) is "the most general and elegant" (Vozoff, 1991) of all methods proposed thus far. The canonical decomposition is based on the complex singular value decomposition (CSVD) of the impedance tensor $\tilde{\mathbf{Z}}$. From the canonical decomposition of $\tilde{\mathbf{Z}}$ we obtain the the directions of minimum and maximum resistivity with associated phases and polarization states of the electric and magnetic fields.

A canonical decomposition program was written in Matlab and applied to the Hepburn data and it was found that no additional information was gained with the canonical decomposition. This provided further evidence that we have an approximately one-dimensional case at the Hepburn site. This can be seen firsthand in the edited resistivity curves from SITE 104 in Figure 4.5. We see that $\tilde{\rho}_{xx}$ and $\tilde{\rho}_{yy}$ are negligible compared to $\tilde{\rho}_{xy}$ and $\tilde{\rho}_{yx}$ (less than ten percent). Furthermore, we see that $\tilde{\rho}_{xy}$ is approximately equal to $\tilde{\rho}_{yx}$. These are the criteria for a one-dimensional, isotropic earth. As stated previously, in the one- dimensional, isotropic, noise free case, $\tilde{\rho}_{xx} = \tilde{\rho}_{yy} = 0$ and $\tilde{\rho}_{xy} = \tilde{\rho}_{yx}$. In reality the equality doesn't hold because noise is inevitably present in field recordings. Because the Hepburn data are one-dimensional to a good approximation, no method of strike determination is needed.

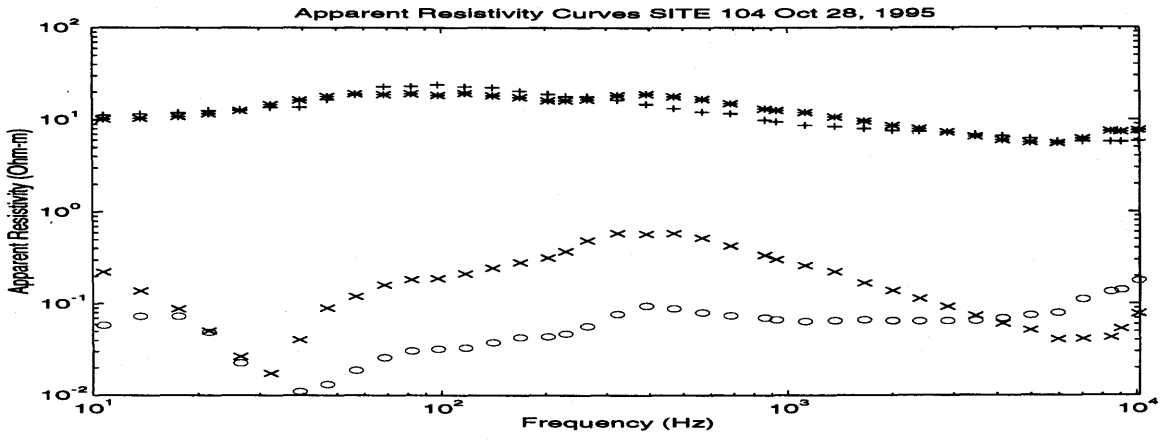

Figure 4.5: Edited Resistivity Curves. $\tilde{\rho}_{xy}$ (+), $\tilde{\rho}_{yx}$ (*), $\tilde{\rho}_{xx}$ (x) and $\tilde{\rho}_{yy}$ (o)

4.5 Bostick Transformation - A 1D inverse method

A very simple, yet surprisingly powerful inverse method was developed by Bostick (1977). With the Bostick Transform (Chapter 2), the approximate earth resistivity at a depth D is related to the value and slope (i.e., derivative) of the apparent resistivity curve at a frequency f. Shown below in Figure 4.6 is the Bostick transform of the $\tilde{\rho}_{xy}$, $\tilde{\phi}_{xy}$ pair at SITE 104. Note the resistive layer, centered at approximately 150 m.

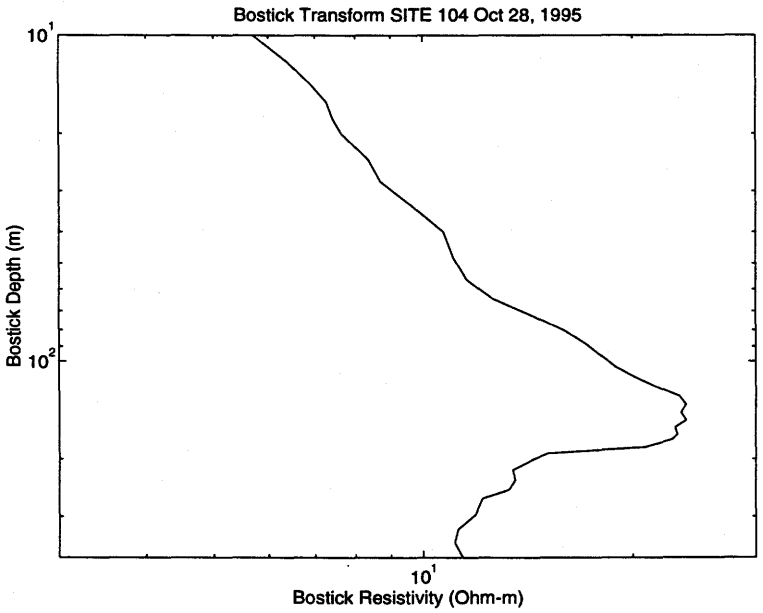

Figure 4.6: Bostick Transform of $\tilde{\rho}_{xy}$, $\tilde{\phi}_{xy}$ pair, SITE 104

Chapter 5

Analysis of the ELF/VLF Natural Source Field at Mid-High Latitude

5.1 Fall, Winter and Spring Field Operations

In the fourth week of October, 1995 six sites of MT data in the frequency band 10 Hz to 10 kHz were acquired at the Hepburn site, geographic co-ordinates approximately 52°N, 107°W. The author returned to the Hepburn site nearly two months later on December 22 and 23, 1995, at which time magnetic field transients were successfully recorded throughout the frequency band 10 Hz to 10 kHz.

Due to the success of the December, 1995 magnetic field recordings, it was proposed that a full MT data collection be attempted sometime in February, 1996, approximately the time of lowest signal levels and activity as it turned out. To avoid contact resistance problems on frozen ground, the sounding was performed at Rabbit Lake (geographic co-ordinates 52°N, 107°W) as the mud water-bottom of the lake is unfrozen perennially. On February 5, 1996 Rabbit lake was accessed with a snowmobile and a site was surveyed in with a compass and survey chain. As per the October ground-water survey, an electric dipole length of 100 m was used.

On February 11, 1996 Rabbit lake was again accessed with a snowmobile, but additionally with a canvas covered sled, heated for the benefit of both operator and recording instrument. Holes were drilled in the lake ice to allow placement of electrodes in the unfrozen mud water-bottom. It is interesting to note that Rabbit Lake is

quite saline, almost thirty percent as saline as the ocean (Hammer et al., 1978). This was seen firsthand in both the visible appearance and thickness of the ice on Rabbit Lake (very soft, speckled in appearance and approximately 70 cm thick). The February 11, 1996 MT data collection, employing porous pot $Pb - PbCl_2$ electrodes for electric field sensors, was unsuccessful due to poor electric field data. It is postulated that the light porous pot electrodes weren't firmly placed in the mud water-bottom resulting in poor electrical contact with the water-bottom. However, the recording of valid magnetic field transients was reassuring and prompted another attempt on February 18, 1996. The Rabbit Lake site is shown in Figure 5.1, during the initial recording on February 11, 1996. Note the square frame induction coil magnetometer in the foreground. The interior of the heated recording sled is shown in Figure 5.2. Note the recording instrument, GEOCOM-MT in the center of the picture. For the second data collection simple lead weights were used as electric field sensors. Their weight ensured good contact with the water-bottom, and as simple metal electrodes, lead is one of the best choices with respect to noise characteristics.

Figure 5.1: Rabbit Lake site, Feb 11, 1996

Figure 5.2: Interior of heated recording sled

The February 18, 1996 data collection was successful with simultaneous electric and magnetic field transients recorded over the frequency band 10 Hz to 10 kHz. However, due to instrumental problems with the E_x channel, only a scalar processing with the E_y and H_x channels of the Rabbit Lake data was possible.

On March 16, 1996 an experiment on frozen ground at the Hepburn site was initiated, at one of the locations occupied in the fall ground-water study. To investigate MT electric field measurements on frozen ground, stainless steel spikes approximately one meter long were driven into the frozen ground with a separation distance of 100 m, also, the possibility of making electric field measurements with a simple dipole antenna (non-contacting) was to be investigated. After allowing the stainless steel electrodes to stabilize for approximately 24 hrs, on March 17, 1996 the author returned and collected simultaneous magnetic and electric field data in the two fashions described above.

Approximately two months later on May 25, 1996, magnetic field transients were recorded in the frequency band 10 Hz to 10 kHz in order to compare spring signal and activity levels to that of the winter and fall recordings.

5.2 Variation in Natural Source Signal Amplitude

With the MT data collected throughout the fall, winter and spring of 1995/96, an analysis of the variation in natural source, $\vec{B}$ field signal amplitude at 52°N in the frequency band 10 Hz to 10 kHz was made possible.

Recall that GEOCOM-MT triggers on $\vec{B}$ field transients, which is accomplished by accepting the digitized output of the induction coil magnetometer into a flow-through buffer. When a user set trigger level is exceeded, data just before and just after the event on all four channels are used as input for polarization stacking (Kosteniuk and Paulson, 1988) or written to floppy disk as multiplexed time series which can be processed at a later date. The total window length for Low and Mid-Band is 512 points and 256 points for High-Band, with the triggered event located at the center of the window. Therefore, for every data file an average peak-to-peak signal amplitude was found for both the B_x and B_y components by summing the peak-to-peak signal amplitudes for each event and dividing by the total number of events, so calculating the arithmetic mean of the natural source signal amplitude at that time in a particular frequency band.

Tables 5.1 through 5.3 detail the number of recorded events in each frequency band over the fall, winter and spring of 1995/96. In some of the Low and Mid-Band files, intermittent connection problems with the induction coil magnetometer on the B_x channel resulted in B_y data being recorded only, in such cases the number of individual events on each channel is noted and the time reported is the time to collect the larger number of B_y events. Otherwise, the number of events refers to the number of simultaneous B_x, B_y recordings. Note that the data below were not all recorded at the same threshold or triggering level so a direct comparison of the activity, the number of events per second, between October 23-29, 1995 to February 18, 1996 for example is not warranted.

Shown in Figures 5.3 through 5.5 is the variation in average, natural source $\vec{B}$ field signal amplitude, at 52°N throughout the fall, winter and spring of 1995/96, in the frequency band 10 Hz to 10 kHz, with the data detailed in Tables 5.1 through 5.3.

Table 5.1: High-Band Data

Date(s)	Number of Events	Total Recording Time
Oct 23-29, 1995	550	114 min
Dec 22, 1995	90	60 min
Feb 11 and 18, 1996	100	62 min
Mar 17, 1996	50	43 min
May 25, 1996	70	2 min

Table 5.2: Mid-Band Data

Date(s)	Number of Events	Total Recording Time
Oct 23-29, 1995	275	110 min
Dec 23, 1995	16 B_x, 40 B_y	38 min
Feb 11 and 18, 1996	47 B_x, 80 B_y	78 min
Mar 17, 1996	50	66 min
May 25, 1996	60	4 min

Table 5.3 Low-Band Data

Date(s)	Number of Events	Total Recording Time
Oct 23-29, 1995	268	499 min
Dec 23, 1995	4 B_x, 30 B_y	78 min
Feb 11 and 18, 1996	18 B_x, 41 B_y	98 min
Mar 17, 1996	30	50 min
May 25, 1996	25 B_x, 45 B_y	15 min

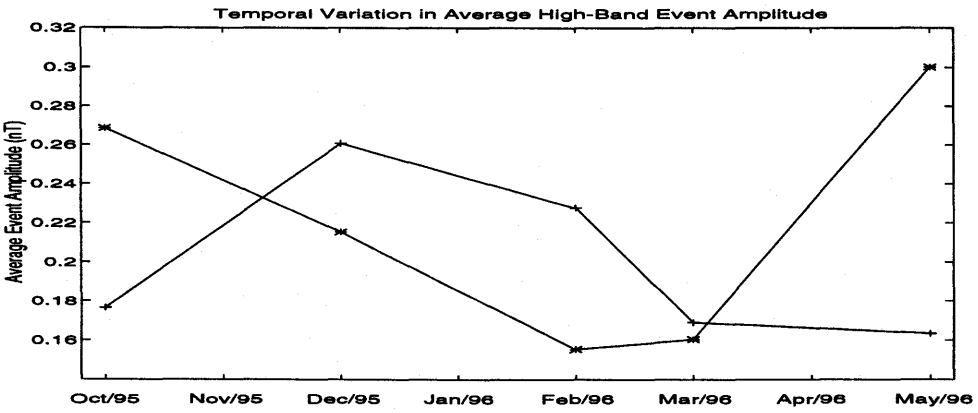

Figure 5.3: Average High-Band Event Amplitude B_x (+), B_y (*)

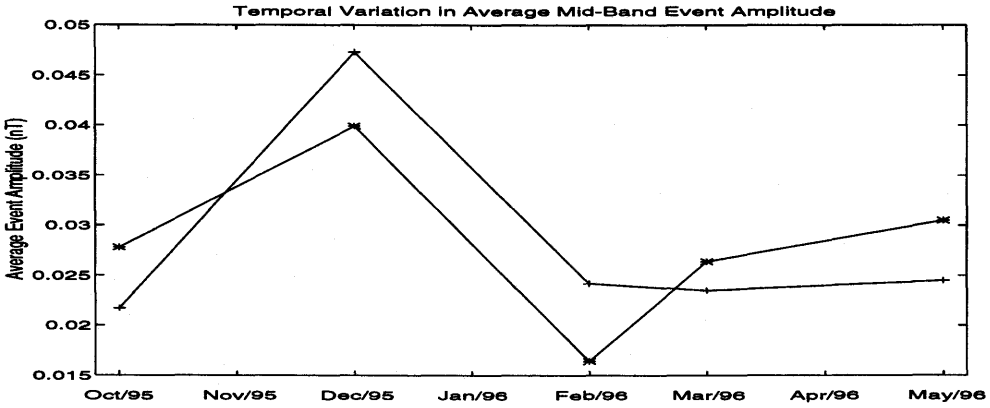

Figure 5.4: Average Mid-Band Event Amplitude B_x (+), B_y (*)

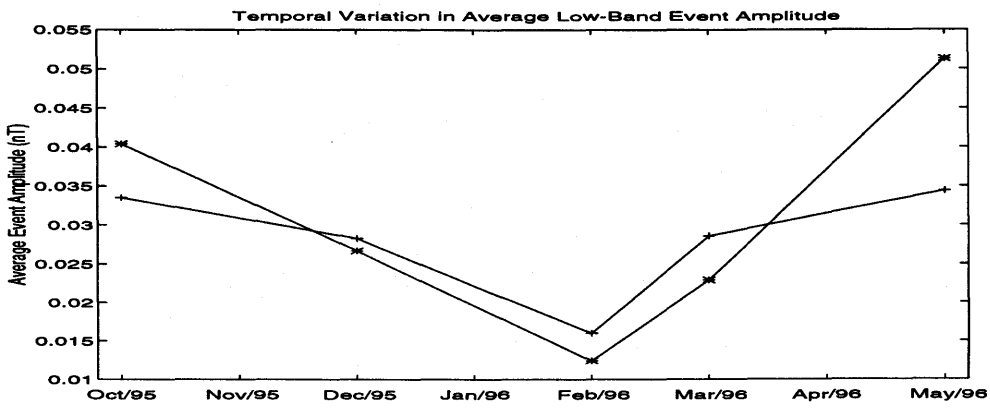

Figure 5.5: Average Low-Band Event Amplitude B_x (+), B_y (*)

Peak-to-peak signal amplitudes were plotted, in similar fashion to Campbell (1967), as opposed to spectral densities as the spectral density function depends not only on signal amplitude, but also on the signal's time localization or frequency bandwidth (pers. comm., P.R. Kosteniuk). This is reflected in the units of the spectral density function for $\vec{B}$, essentially normalized to a one Hz bandwidth with units of nT^2/Hz (Mean-Square) or $nT/Hz^{1/2}$ (Root-Mean-Square). This represents an overly large bandwidth at ELF and conversely, an overly small bandwidth at VLF. What would seem more appropriate would be a spectral density function with a constant percentage bandwidth (pers. comm., Dr. W.H. Pelton), note that constant bandwidth (or constant Q) analysis is a characteristic inherent to the wavelet transform. The one Hz bandwidth of the spectral density function results in spectral densities at ELF that are approximately two orders of magnitude *larger* than spectral densities at VLF, despite the fact that ELF signal amplitudes are usually an order of magnitude or more *smaller* than signal amplitudes at VLF. Furthermore, the trigger recording method used in the present study achieves a high degree of time localization, spectral densities so calculated are not directly comparable to those found from a continuous recording, as in Labson et al. (1985) and others (Vozoff, 1991. Macnae et al., 1984). With knowledge of the activity rate (section 5.4) it is possible to simulate what spectral density estimate would be obtained if the present study had employed a continuous recording. This would allow direct comparison to previous studies but is self defeating as we simply confirm that which is already known; namely that it is generally not possible to record valid MT data at ELF/VLF with the continuous recording technique in times of low source field activity. For these reasons, peak-to-peak signal amplitudes were plotted.

It is worthy to note that B_y displays a minimum in average signal amplitude in all three frequency bands in February, 1996. This is consistent with the study of Ward (1959) where measurements of the horizontal field strength at 500 Hz were made over 1957/58 at Orangeville, Ontario, although Ward never states which horizontal component of the $\vec{B}$ field was presented in his publication. Hoover et al. (1978) present electric field spectra in their study and found that signal decay above 200 Hz was most rapid in February although he too never states which signal component was presented.

We also note that B_x signal levels are higher than B_y signal levels from December,

1995 to March, 1996 in High and Low-Band and from December, 1995 to February, 1996 in Mid-Band, although this difference gets smaller as frequency decreases. This feature may not be statistically significant, as the winter time prevalence of the B_x component was mainly due to storms located on the west coast of the U.S.A. at the time of the winter recordings (section 5.5) and hence may not be repeatable from year to year. Note that the B_x component arises from east-west propagating signals and the B_y component arises from north-south propagating signals, with a co-ordinate system defined as ^+x pointing North, ^+y to the East and ^+z downward into the earth.

Another aspect that requires mention is the variation in width of the signal dead band from summer to winter. As mentioned previously, the width of the signal dead band is mainly a function of source-receiver separation although seasonal effects on the ionosphere and the surficial earth are also important. Even at relatively high latitude (Northern Saskatchewan, 55-60°N), summer MT recordings at ELF/VLF display quite a narrow signal dead band, approximately 1 to 3 kHz (pers. comm., P.R. Kosteniuk). However, high latitude winter MT recordings at ELF/VLF display a wider signal dead band due to increased source-receiver separation as any thunderstorms that occur, do so predominantly at lower latitudes during the winter. However, in disagreement with previous studies by Lakanen (1986), Labson et al. (1985), Herisson (1982), Hoover et al. (1978) and Ward et al. (1959), the present study found that the signal dead band was on average 500 Hz to 5 kHz for fall and winter recordings at 52°N, corresponding to storms on average, 2000 to 4000 km distant.

Lakanen (1986) states;"a lack of intensity in winter at frequencies from 100 to 5000 Hz". The measurements in the present study were made at 52°N, those of Lakanen's from 60 to 70°N in Finland. The trend of a wider dead band at higher latitude is most reasonable due to increased source-receiver separation, however the present study does not predict as wide a dead band at 60 to 70°N as stated by Lakanen (1986).

Labson et al. (1985) state that natural signal levels at 150 and 500 Hz (AFMAG) are "inadequate in high latitudes in winter". They go on to state: "The inherent noise level of the coils and their electronics is higher than the level of the weak signals originating in storms at the equator and southern temperate zones.". The present study contradicts both these statements as reliable tensor MT data was obtained up to 500 Hz at any time of the year, and signal levels were most certainly above noise

levels, also at any time of the year, throughout the complete band 10 Hz to 10 kHz with a maximum dead band of 500 Hz to 5 kHz (section 5.3).

Labson et al. (1985) make the above statements based in part on a "spectral study" of the horizontal components of the $\vec{B}$ field, carried out at approximately 38°N, 122°W (California) employing the induction coil magnetometers of Hoover et al. (1978) and Kennecott Copper Corp.. Note that the amplitude of the vertical component B_z, measured in AFMAG and some MT systems for determination of the tipper, is dependent not only on horizontal field strength but more importantly upon local geology. B_z is usually ten to fifty percent of the horizontal components at most (pers. comm., P.R. Kosteniuk. Vozoff, 1991), with this in mind, B_z may very well be below noise levels at 150 Hz in some cases (section 5.3), although this is also dependent on geology. The remote reference method (used by Labson et al. (1985)), has allowed MT surveys to be successfully carried out under conditions of signal-to-noise ratio ≤ 1, particularly around the signal minimum at one Hz (Vozoff, 1991).

Herisson (1982) of Geoconsult conducted a winter, scalar MT test survey in the frequency band .01 to 5000 Hz in Northern Saskatchewan ($\approx$ 57°N, 107°W), in February, 1982, for AGIP Canada. Herisson (1982) states: " a total lack of coherent signal" above 100 to 200 Hz. Again, the present study has found that good data up to 500 Hz are obtainable on a year round basis at 52°N.

Hoover et al. (1978) state that a winter dead band of 200 Hz to 5 kHz exists for measurements made at approximately 37°N in Nevada. Note that the present study employs an induction coil magnetometer based on the work of Hoover et al. (1978), although the induction coils in the two studies are not identical. The present study disagrees with that of Hoover et al. (1978), as valid magnetic field transients were recorded at ELF/VLF throughout the fall (October 23-29, 1995) and winter (December 22, 1995. February 18, 1996. March 17, 1996) with a dead band of 500 Hz to 5 kHz using a similar induction coil magnetometer. If Hoover et al. (1978) were completely accurate in his study, then the winter dead band at 52°N should be wider than that found at 37°N; in fact, the opposite was found.

Lastly, the study of Ward (1959) states that natural field exploration on the ground at 150 and 500 Hz (AFMAG) is limited to April 1 to November 1 in Northern Canada. Ward's statement regarding limitations of natural field exploration is based at least

partly on his measurements of horizontal field strength made throughout the year 1957/58 at Orangeville, Ontario ($\approx$ 44°N , 80°W). The present study found sufficient signal levels in the horizontal components at 150 and 500 Hz at any time of the year, at 52°N.

The reason for the dichotomy between the present and many previous studies is due to two factors, the first and most important being the recording method employed in the present study. GEOCOM-MT triggers on $\vec{B}$ field transients so that data is recorded only when signal is present. What the author calls the conventional recording method is to continuously (blindly) record analog or digital data over some time interval, perhaps several seconds to several minutes (EDA Instruments Inc., Strangway et al. 1973), implicitly assuming a high natural source activity level so that more signal than noise is recorded over this averaging or integration time. In times of low source field activity, this assumption is invalidated.

The scalar instrument (French built) employed by Lakanen (1986) used this recording method, at least partly contributing to his statements. It was found in the present study that even in the High-Band frequency range where activity is highest, the time between successive events at an optimum triggering level may be one minute or more in February (section 5.4). Therefore, in winter, or times of low activity, continuous recordings with averaging times of several minutes will very likely record more noise than signal. Conversely, shorter averaging times on the order of seconds are unlikely to contain any valid events giving rise to the poor results characteristic of the continuous recording method in times of low source field activity.

Similarly, the spectral study of Labson et al. (1985) employed the conventional recording technique. This appears to be the reason why no spectral density estimates were presented over the winter of 1979 in their study, perhaps partly explaining the reasoning behind their signal strength statements. In the second part of their paper, a field survey is conducted wherein the operator can view the output of the induction coil magnetometer on the screen of an oscilloscope and thus record data only when signal is present. In this fashion, Labson et al. (1985) collected repeatable tipper data year round in California, at 18 to 23 Hz and 130 to 150 Hz. Interestingly, every second station in their field program was an MT site with simultaneous electric field data collected also, although the authors never show any of the MT data collected in

their study.

The winter MT test survey of Geoconsult employed an analog instrument which also made continuous recordings of the $\vec{E}$ and $\vec{B}$ fields. This system recorded analog data in the field which was digitized and processed at the end of the day by a computer at the base camp. Here again, with the conventional recording method used and the low source field activity in winter, it is likely that more noise than signal was recorded throughout much of the frequency band giving rise to the poor results in their study.

The recording method employed by Ward (1959) was also the conventional method defined above. This explains the reason behind his statement of restricting ground operations to April 1 to November 1 in Northern Canada with the AFMAG method, although, as stated previously the vertical component may well be below noise levels at 150 Hz in some cases, but this is also dependent on local geology.

The conventional recording method is really a carry-over from low frequency MT surveys ($\leq 1Hz$) where the interaction of the solar wind with the earth's magnetosphere is the energy source. Of course the energy source for MT measurements at ELF/VLF is dominantly due to lightning activity at near and great distance. The largest signals from such a source arise from individual, particularly strong or equivalently, relatively nearby lightning strokes. As such, these signals arrive randomly and are well localized in time. These two energy sources are completely different making it unwise to employ the same recording method for both natural sources. The time localized, impulsive nature of the lightning generated MT signal at ELF/VLF has been recognized by practitioners of the TEM (Time-Domain-Electromagnetics) method (Spies and Frischneckt, 1991. Macnae et al., 1984. McCracken et al., 1984, 1986). This has allowed the development of appropriate algorithms for the reduction of sferic noise (MT signal) in ground and airborne TEM systems (Palacky and West, 1991). However, this has apparently gone unnoticed or has been ignored by many practitioners of the MT method as new commercial ELF/VLF MT instruments (fully digital) still employ the conventional recording technique which limits their practical use to times of high natural source field activity. The most notable example is the French scalar instrument SAMTEC1, built by IRIS Instruments. It has been shown in the present study that clear advantages exist for MT surveys at ELF/VLF which employ a "trigger" recording method. In particular reference to MT soundings at lower

ELF (10-100 Hz), Tzanis and Beamish (1987) similarly found that the best quality sounding curves are obtained when the large, individual, transient events that stand out above the background signal level (see below) are used for impedance estimation. Note that if the continuous recording technique has any chance of working for MT surveys at ELF/VLF, the highest probability of success exists at lower ELF where waveguide attenuation is less than 1 dB/Mm so that a low level, almost-continuous background signal is present due to the totality of global lightning activity. However, even at lower ELF, the trigger recording method was still found to be optimum for impedance estimation (Tzanis and Beamish, 1987). This clearly shows that the trigger recording method is the best approach for MT surveys at ELF/VLF.

The trigger recording method was arguably implemented first by Hoover et al. (1976) where a "human computer" visually located transient events on a strip-chart recorder and therefore processed data only when signal was present. More recently, Vozoff (1991) details the design of an ELF/VLF MT system built at Macquarie University in 1980 which also employed the "trigger" recording method, but saw little use. Of course, GEOCOM-MT, built by P.R. Kosteniuk at the Cybernetics Laboratory, University of Saskatchewan in 1982 also employs this recording method which permits the application of year round MT surveys at ELF/VLF.

The second reason for the success of the present study is due to the fact that GEOCOM-MT is a digital instrument. The analog equipment of Hoover et al. (1976, 1978) used an "envelope detection" scheme as mentioned above. With such a recording method, the present study predicts that Hoover et al. (1976, 1978) should have been able to obtain good MT data up to 500 Hz at any time of the year, and due to their location at lower latitudes, should have been able to get good data somewhat higher than 500 Hz. The reason for their statement of no signal above 200 Hz in winter appears to be due to coarse discretization of the ELF/VLF frequency band. Their instrument employed analog instrumentation tuned at discrete frequencies of 7.5, 10, 14, 27, 285, 685, 1200, 3300, 6700, 10200 and 18,600 Hz. GEOCOM-MT is a digital instrument, with which appropriate sampling and recording lengths discretizes the ELF/VLF frequency band much finer than the instrument of Hoover et al. (1976, 1978). The present study predicts that if the U.S.G.S. (United States Geological Survey) had tuned their analog instrument to a frequency of approximately 500 Hz

instead of 685 Hz, their statement of no signal above 200 Hz in winter may very well have changed to no signal above 500 Hz. This may also have played in as a factor in the study of Lakanen (1986), although it is not known whether the French built instrument used in his study was analog or digital.

5.3 Variation in Signal-to-noise Ratio

Knowledge of signal amplitude variations throughout the year is interesting, but perhaps a more relevant quantity for assessing the viability of year-round MT surveys at ELF/VLF is the signal-to-noise ratio (SNR), defined in equation 5.1 as the root-mean-square (RMS) ratio of signal to noise amplitude (Beckman, 1967);

$$SNR = \sqrt{\frac{{\sigma_s}^2}{{\sigma_n}^2}} \tag{5.1}$$

where ${\sigma_s}^2$ is the variance of the signal portion of the data and ${\sigma_n}^2$ is the variance of the noise portion of the data. To calculate ${\sigma_s}^2$ and ${\sigma_n}^2$, it is assumed that the signal contribution is comprised entirely of the triggered event at the center of each 256 or 512 point long data window, while all other data in the window is considered to be noise. It should be noted that this assumption is not valid when multiple events occur in a single data window, therefore, such cases were avoided in calculating the SNR. Furthermore, this assumption becomes increasingly less valid as frequency decreases into the ELF range, particularly less than 100 Hz, as global waveguide attenuation becomes very small ($\leq$ 1dB/Mm) giving rise to a low-level, generally-incoherent, almost-continuous signal background below 100 Hz (Tzanis and Beamish, 1987). Therefore, particularly in Low-Band, what is defined as noise in the present study most certainly contain some real signal. Therefore, the SNR calculated in the present study is lower than what would be obtained if the noise and signal components could be completely separated (i.e., the true SNR is higher than that found in the present study, particularly in Low-Band).

To separate signal and noise components just defined, modified boxcar windows (Chapter 4) were used to localize each triggered event at the center of every 256 or 512 point long record. Specifically, a 32 point window was used in High-Band, a 128 point window in Mid-Band and a 64 point window in Low-Band was formed around each

triggered event. From this, the variance of each signal event was calculated (usually 100 events for High-Band and 50 events for Mid and Low-Band). To calculate $\sigma_n{}^2$ the same boxcar windows as above were used, but this time the signal within the boxcar window was zeroed, removing the signal portion and assumed to leave behind only the integrated noise contribution due to cultural noise, instrument and sensor noise. This process is shown below in Figure 5.6. Having calculated $\sigma_s{}^2$ and $\sigma_n{}^2$ for every event, a SNR for every event could be calculated with equation 5.1. Lastly, an average SNR was obtained by averaging over SNR's for every valid event. SNR was calculated for all magnetic and electric field components when possible, but due to the different electrodes used to measure the electric field, only the magnetic field SNR was plotted.

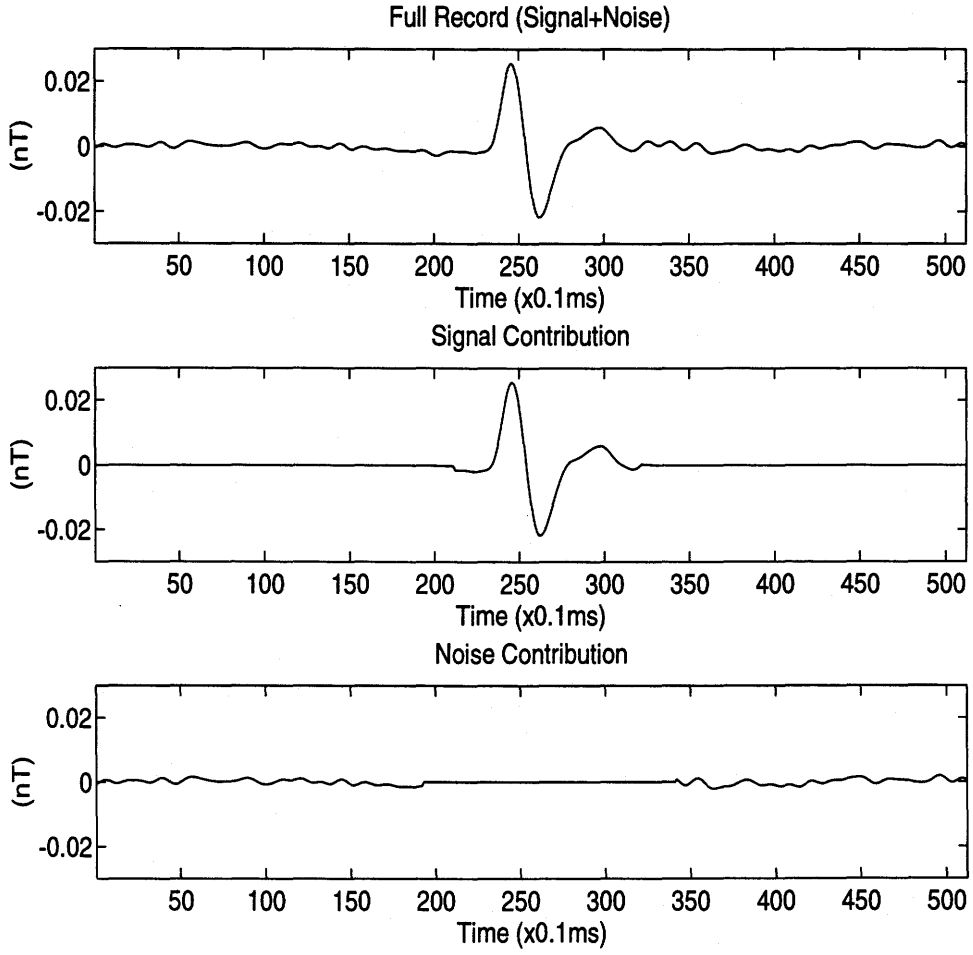

Figure 5.6: A B_y Mid-Band Event (100-1000 Hz, Oct 25, 1996)

Shown in Figures 5.7 through 5.9 is the SNR for the B_x and B_y components in all

three frequency bands, throughout the fall, winter and spring of 1995/96. SNR was found to generally decrease with frequency and was therefore lowest in High-Band and highest in Low-Band, although this may be partly due to the fact that the assumption made regarding noise and signal becomes less valid as frequency decreases. As stated previously, the ELF source field really consists of two parts; these being the low level, almost-continuous signal background caused by worldwide thunderstorm activity upon which is superimposed the response of the global waveguide to a particularly strong or relatively nearby lightning stroke (Tzanis and Beamish, 1987), where nearby at ELF could be considered as being $\leq$ 3000 km.

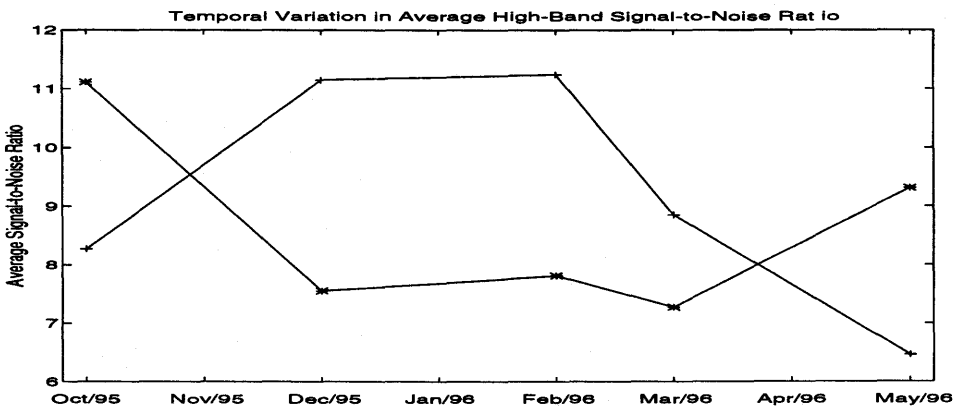

Figure 5.7: Average High-Band Signal-to-noise ratio B_x (+), B_y (*)

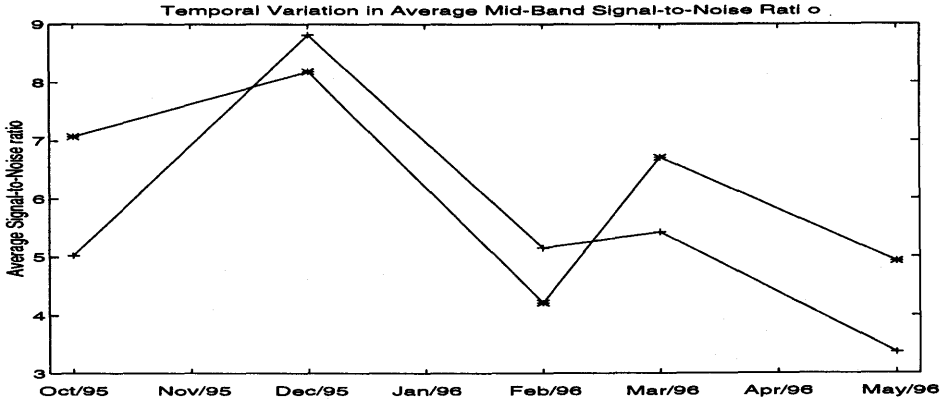

Figure 5.8: Average Mid-Band Signal-to-noise ratio B_x (+), B_y (*)

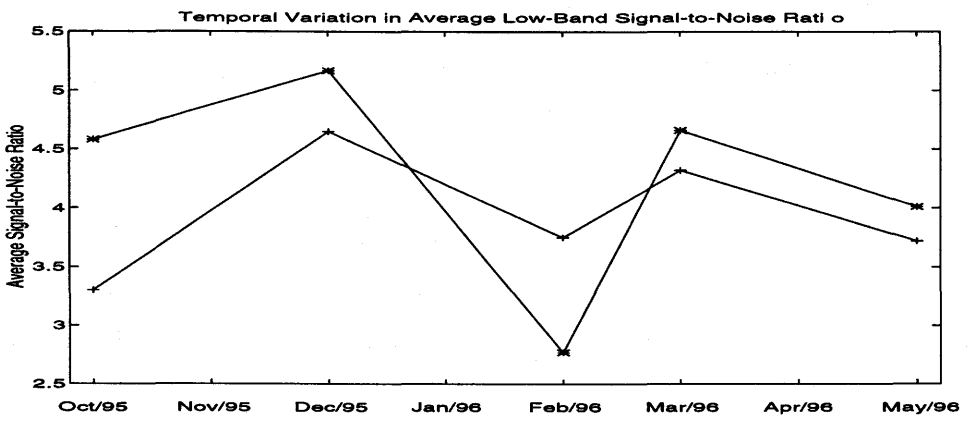

Figure 5.9: Average Low-Band Signal-to-noise ratio B_x (+), B_y (*)

The lowest SNR encountered was 2.77 which occurred for the B_y component in Low-Band on February 18, 1996. The highest SNR encountered was 11.24 which occurred for the B_x component in High-Band on February 18, 1996, mainly due to an active storm located off the coast of California at the time of the February 18, 1996 recording (section 5.5).

The SNR calculated for High-Band essentially reflects the shape of the average peak-to-peak signal amplitude graph in Figure 5.3. We see the enhanced signal levels of the B_x component in the higher SNR for B_x throughout the winter months. SNR for the B_y component was a maximum (11.11) for the October, 1995 recordings, due to storms located predominantly to the south of the recording site.

High-Band SNR for B_x displayed a minimum in May, 1996 (6.46) and B_y SNR displayed a minimum in March, 1996 (7.27). Also, average B_x signal amplitude decreased somewhat from December, 1995 to February, 1996 while SNR on B_x increased over this time period. Presumably, noise levels on the B_x channel at the Rabbit Lake site in February, 1996 were lower than those at the Hepburn site in December, 1995. Furthermore, B_x signal amplitudes change little between March, 1996 to May, 1996 yet the SNR on B_x decreases over this time period. Apparently noise levels in May were higher than those in March at the Hepburn site.

The Mid-Band SNR graph also reproduces the same general trend as the signal amplitude plot of Figure 5.4, with the exception of the May, 1996 data point where the SNR of both $\vec{B}$ components decrease relative to March, 1996, despite rising signal levels. Apparently, noise levels in Mid-Band were higher at the Hepburn site in May,

1996 than in March, 1996 or October, 1995. The B_x component displayed a minimum in SNR in May, 1996 (3.36) and B_y displayed a minimum in February, 1996 (4.21). SNR was a maximum for both components in December, 1995 (B_x 8.82, B_y 8.19), due to active storms located off the southern coast of Oregon and in the Gulf of Mexico off the coast of Louisiana (section 5.5).

The Low-Band SNR is the only one of the three frequency bands not to follow the same general trend as the signal amplitude plot. Low-Band signal amplitudes were found to decrease and rise out of a minimum in February, 1996. The SNR plot of Figure 5.9 is not so regular. It is interesting to note that even though signal amplitudes at the Hepburn site are decreased from October, 1995 to December, 1995, the SNR increases over this time period. Also, as was the case for Mid-Band, despite rising signal levels at the Hepburn site between March, 1996 to May, 1996, SNR in Low-Band decreased over this time period. Once again, noise levels at the Hepburn site were higher in May, 1996 than in March, 1996. This could be related to frozen ground conditions (higher resistivity) leading to higher attenuation of 60 Hz cultural noise in the ground return system employed by SaskPower, although studies in Finland found higher noise levels in winter due to electric heating (Lakanen, 1986). The signal amplitude minimum in February, 1996 is reflected in the SNR plot as well with a minimum SNR occuring for both $\vec{B}$ field components in February, 1996 (B_x 3.75, B_y 2.77). In contrast with High and Mid-Band SNR plots, with the exception of the February, 1996 data collection, the Low-Band B_x component was found to have a generally lower SNR than the B_y component despite the fact that B_x signal levels were slightly higher. This is explained in terms of cultural noise sources being coupled maximally to the B_x, E_y pair. This was found to be the case at the Hepburn site as the closest source of powerline noise was from two farmyards, both with above ground powerlines running approximately east-west, terminated or grounded to the earth (a single wire transmission line). With single wire transmission lines we have two kinds of 60 Hz noise contamination. Firstly we get 60 Hz noise in both $\vec{B}$ and $\vec{E}$ fields caused by currents flowing in the earth return path. The second source of contamination arises due to induced currents from the alternating current (AC) carried on the powerline itself. This type of powerline noise is less attenuated in resistive environments. In the latter case, with a one-dimensional earth, a powerline running east-west will possess

an azimuthal magnetic flux density (right-hand rule) and therefore currents induced through Faraday induction will be established perpendicular to the azimuthal magnetic flux density, or parallel to the powerline which in this case is east-west. Therefore, we would expect the B_x, E_y pair to be affected the most by powerline noise, as seems to be the case in the present study with generally lower SNR's on the B_x, E_y pair in Low-Band. The SNR at the Rabbit Lake site displays a SNR in direct relation to signal amplitude, perhaps due to lower cultural noise levels so that neither $\vec{B}$ nor $\vec{E}$ component was dominantly affected by 60 Hz noise.

Electric field SNR's were calculated when possible but not plotted due to the differing electrodes used throughout this study. Some comments are warranted however. The October groundwater study at the Hepburn site employed porous pot $Pb-PbCl_2$ electrodes. SNR in the electric field channels with the porous pot electrodes were approximately the same as the SNR in the magnetic field channels, except for Mid-Band where $\vec{E}$ field SNR was substantially lower than $\vec{B}$ field SNR. The highest SNR's on the electric field channels were obtained in High-Band, approximately 12, the lowest in Mid-Band, approximately 2.6, and Low-Band had SNR's of approximately 4, all in reference to the Hepburn site with porous pot electrodes.

The winter MT sounding on Rabbit Lake employed simple lead weights as electrodes. However, due to instrumental problems with the E_x channel, only the E_y channel was successfully recorded in all three frequency bands. E_y SNR with lead weight electrodes at the Rabbit Lake site gave lower SNR's than at the Hepburn site with porous pot electrodes. As per the October groundwater study, SNR on E_y was a minimum in Mid-Band at the Rabbit Lake site. Specifically, SNR in High-Band on the E_y component was approximately 10, 2.3 in Mid-Band and 2.6 in Low-Band. Although the lead weight electrodes and porous pot electrodes were never used simultaneously to collect $\vec{E}$ field data, it can be said that lower, but comparable, quality electric field data were obtained with simple lead weights in the frequency band 10 Hz to 10 kHz, as predicted by Petiau and Dupis (1980). However, it is difficult to compare $\vec{E}$ field SNR's at different sites as the $\vec{E}$ field SNR also depends on earth resistivity with larger amplitude $\vec{E}$ field signals induced in more resistive earth materials. Furthermore, the mud waterbottom of the lake allowed very good electrical contact to be made with the lead weights. Regardless, it was generally found that lead weight

electrodes performed nearly as well as porous pot $Pb - PbCl_2$ electrodes above 200 Hz, below 200 Hz porous pot electrodes are preferred with GEOCOM-MT. It should be noted that with new, lower noise amplifiers the frequency below which porous pots are preferred would increase also.

The frozen ground experiment at the Hepburn site on Mar 17, 1996 employed stainless steel stakes as electrodes. Due to the frozen ground and necessarily high contact resistances, this arrangement was found to have the lowest SNR on the electric field. High-Band SNR on the electric field was approximately 3.7, Mid-Band had no detectable signal on the electric field and Low-Band had a SNR of 1.6. A comparison with SNR's obtained on unfrozen ground with porous pot electrodes at the same site shows that we have a factor of 3 lower SNR in High-Band and about a factor of 2 lower SNR in Low-Band. The reason for not detecting any electric field signal in Mid-Band is unknown but appears to be equipment related.

The dipole antenna recommended by Thiel et al. (1989) was found to give very poor electric field data. The electric field measured in this fashion was amplitude/phase distorted as compared to that obtained with stainless steel stakes. Amplitude/phase distortion of the electric field measured with a dipole antenna has been noticed previously by Zonge et al. (1986). The signal with a 100 m dipole antenna was measurable at high frequencies (5 - 10 kHz), but was immeasurable at low frequencies (10 - 200 Hz). This is to be expected, as a dipole antenna displays a response proportional to $\omega^2 l$, where ω is the radial frequency and l is the length of the dipole antenna. Therefore, to obtain a measurable low frequency response (10 - 200 Hz) would require a dipole antenna on the order of kms in length. The frozen ground experiment is discussed further in Chapter 6.

5.4 Variation in Natural Source Activity

Variation in natural source activity is very important for MT surveys at ELF/VLF as this impacts on how long one needs to occupy a site to record enough events to get repeatable earth response curves. This aspect is interwoven with noise levels also, as lower noise levels at a site mean that lower thresholds can be used allowing for possibly faster data collection. Of course, if noise levels are higher than signal, then no data

collection can be reliably undertaken with this method. A new recording technique using the wavelet transform appears to hold substantial promise in this area (Zhang, 1997).

Different thresholds were used throughout the study, in accordance with the variation in signal amplitudes throughout the fall, winter and spring of 1995/96. Typical thresholds in High-Band were 60 to 100 ADU's (A/D units or bits) which corresponds to a signal amplitude with a positive or negative going amplitude attaining or exceeding 60 to 100 pT, 120 to 200 pT peak to peak if the signal is symmetrical about DC, at a frequency of 8 kHz with a programmable gain of 10. For Mid-Band, thresholds were in the range 130 to 200 ADU's which corresponds to a signal amplitude (positive or negative going) of 9 to 14 pT at a frequency of 200 Hz with a programmable gain of 100. In Low-Band, thresholds of 60-150 ADU's were used which corresponds to a signal amplitude (positive or negative going) of 7 to 18 pT at a frequency of 100 Hz with a programmable gain of 100.

The use of different thresholds complicates the analysis of activity variations because two datasets recorded at different triggering levels are not directly comparable in terms of activity. Therefore, activity variations were analyzed at the highest thresholds used in the study, namely those in October, 1995. This was accomplished by analyzing the winter data files whose recording times were accurately known and noting how many events exceeded the fall threshold levels, thereby obtaining the activity rate at a common threshold. This allows a direct comparison of activity rates between fall, winter and spring of 1995/96. Shown in Figures 5.10 through 5.12 is the activity rate in each frequency band at the fall trigger levels (positive or negative going) of approximately 100 pT in High-Band, 14 pT in Mid-Band and 18 pT in Low-Band. Due to the large change in activity between winter and spring in High and Mid-Band, the plots were made at as fine a scale as possible, therefore, the number in the upper right corner is the activity rate for the May 25, 1996 recording, which is off scale for both High and Mid-Band.

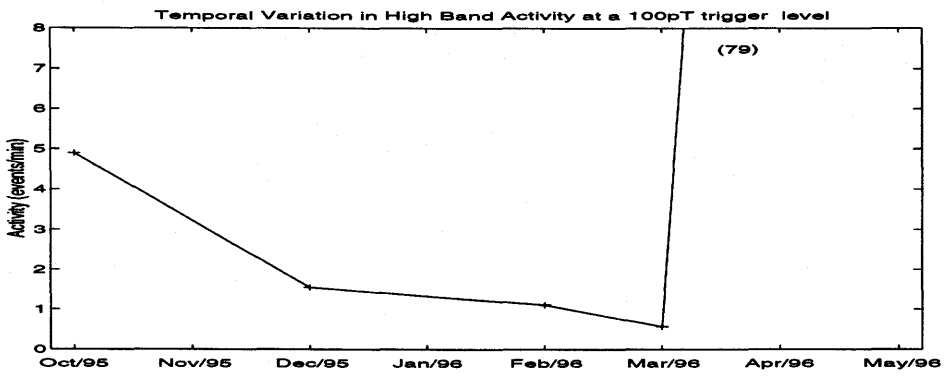

Figure 5.10: High-Band Activity Variation

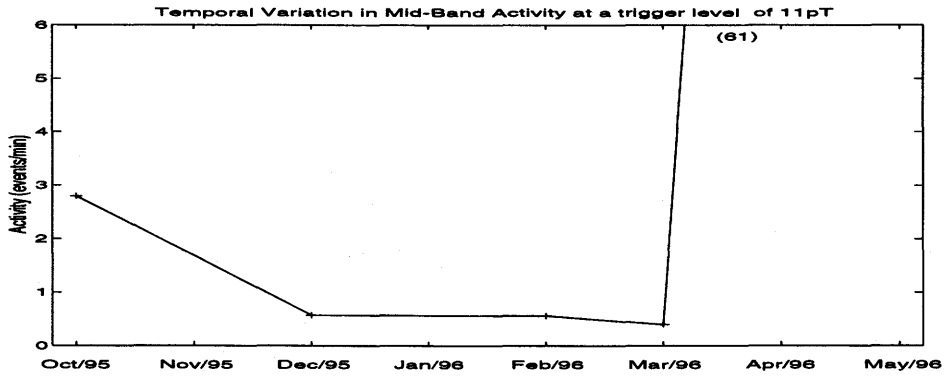

Figure 5.11: Mid-Band Activity Variation

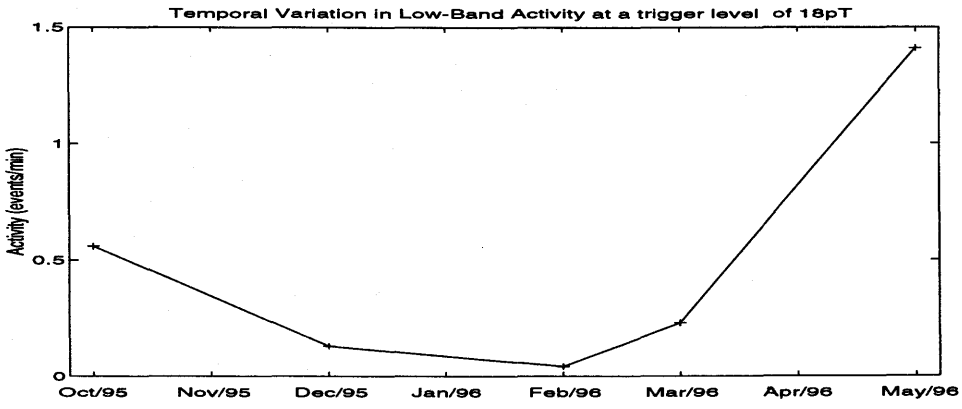

Figure 5.12: Low-Band Activity Variation

We see that both High and Mid-Band display a minimum in activity in March, 1996 and Low-Band in February, 1996. Also note that the largest difference in activity

between winter and spring is found in Mid-Band where we have approximately a factor of 150 difference. High-Band is approximately a factor of 130 different and Low-Band approximately a factor of 34 different.

This is consistent with global waveguide attenuation as the Mid-Band signals, with a dominant frequency component of about 200 Hz suffer an attenuation of approximately 4 dB/Mm under daytime conditions (Volland et al., 1982), High-Band signals with a dominant frequency component near 8 kHz suffer an attenuation of about 3 dB/Mm (daytime) and Low-Band signals with a dominant frequency component of about 100 Hz suffer less than 1.5 dB/Mm attenuation (day or night). Therefore, of all the *received* signals, those in the Mid and High-Band range are most sensitive to source-receiver separation as they are attenuated the most. Therefore the largest variation in activity between spring and winter is found in Mid and High-Band. Of course, the largest attenuation at ELF/VLF occurs at roughly 3 kHz where attenuation is on the order of 60 dB/Mm (Barr, 1971), but signals at 3 kHz are never received unless the recording site is within 200 to 500 km of an active thunderstorm (Vozoff, 1991) or very large induction coils specifically tuned to this frequency range are employed (Dinger et al., 1980). Conversely, the smallest change in activity was found in Low-Band, where global waveguide attenuation is on the order of 1 dB/Mm or less. Because of this, Low-Band signals can truly arise from global activity. Therefore, in Low-Band we are capable of receiving transients from any of the major storm centers of equatorial Indonesia ($\approx$ 13000 km distant), equatorial Africa ($\approx$ 12000 km distant), equatorial Brazil ($\approx$ 7500 km distant) and Central America ($\approx$ 5000 km distant). However, we will always be biased toward receiving signals in any frequency band, regardless of attenuation, from the nearest storm centers as these will produce the largest transients. In any case, the efficient propagation at lower ELF explains why the smallest change in activity is seen in Low-Band as we are the least sensitive to storm location in this frequency range.

Having analyzed the activity at a common trigger level for each frequency band, it must be noted that the above analysis is overly sceptical in terms of activity changes from fall to spring to winter. This follows because analyzing the activity variations at a common threshold required that we do so at the *highest* thresholds used throughout the study. At a lower threshold we can infer the activity at a higher threshold through

analysis of event amplitudes, but the opposite does not hold. Therefore, for winter field work in the present study, much lower thresholds were used than those in October, 1995. Of course the limiting factor in setting the threshold at a site is always dictated by noise levels.

With the winter data collections it was found that at least 1.5 events/min could be recorded in High-Band at a trigger level of 60 pT with a programmable gain of 10, approximately 1 event/min in Mid-Band at a trigger level of 8.1 pT with a gain of 100 and approximately .5 events/min in Low-Band at a trigger level of 7.8 pT. Therefore, it is estimated that a full data collection (100 High-Band events, 50 Mid-Band events and 50 Low-Band events) at a site in winter would take at the most, 180 min, the same data collection (same thresholds) in fall is estimated to take 60 min and 20 min or less in spring. We see that recording times at a site increase by at least a factor of three in winter as compared to fall and about a factor of ten in winter as compared to spring. This is seen to be the most important factor in assessing the viability of winter MT surveys at ELF/VLF, *not* signal strengths as one might intuitively assume. Labson et al. (1985) similarly found an increase in recording time (at ELF only) from 30 minutes in August, 1981 to 150 minutes in February, 1982 (in California) in order to obtain similar quality tipper data. However, it was found that with the data processing method used by the author, many fewer events need be recorded to get good quality resistivity and phase curves, mainly due to the suppression of noise. This is very important as fewer recorded events means faster data collections and hence increased productivity. A discussion on other ideas that can be implemented to improve the productivity of MT surveys at ELF/VLF in winter, and in general, is deferred to Chapter 7.

5.5 Approximate Signal Locating Methods

The analysis of the present section is carried out to show that thunderstorms appear to exist in sufficient number and intensity in the Northern Hemisphere throughout the fall and winter seasons allowing MT surveys at ELF/VLF to be carried out year round. Storm locating procedures carried out by the author have been independently verified by National Weather Service weather radar data, kindly provided by the Marshall

Space Flight Center, Hunstville, Alabama. In some cases, it was possible to infer the type of discharge (intra-cloud or cloud-to-ground) through coincident analysis of National Lightning Detection Network (NLDN) data, which detects only cloud-to-ground strokes, obtained from NASA by Dr. G. Davis, Institute of Space and Atmospheric Studies, University of Saskatchewan.

The bearing to the source of a particular transient (i.e., lightning stroke) may be obtained in the far field through measurement of horizontal, orthogonal components of the temporal changes of the magnetic flux density $\vec{B}$. Plotting the orthogonal components on a two dimensional cartesian co-ordinate system yields an approximately straight line with the bearing to the source at right angles to this line.

Firstly, the plot just mentioned forms an approximately straight line because the electromagnetic wave radiated from an individual lightning strike is nearly linearly polarized in the far field of the source (Tzanis and Beamish, 1987. Dinger et al., 1980. Pierce, 1977. Yamishita and Sao, 1974). The bearing to the source is obtained because the electromagnetic wave propagates to the far field with the magnetic field vector oscillating perpendicular to the direction of propagation. Note that we have a 180 degree ambiguity in the bearing as we can't tell with a single site measurement if a particular transient propagated from the NW or the SE for example. However, common sense would dictate that a thunderstorm in December, within the Arctic Circle would be highly unlikely. To illustrate typical source field polarization characteristics, a polarization plot with High-Band data, collected on December 22, 1995 at the Hepburn site is shown in Figure 5.13. Note the two dominant source bearings of 253 deg (270 deg being due west) and 143 deg (180 deg being due south), with a minor polarization at 213 deg.

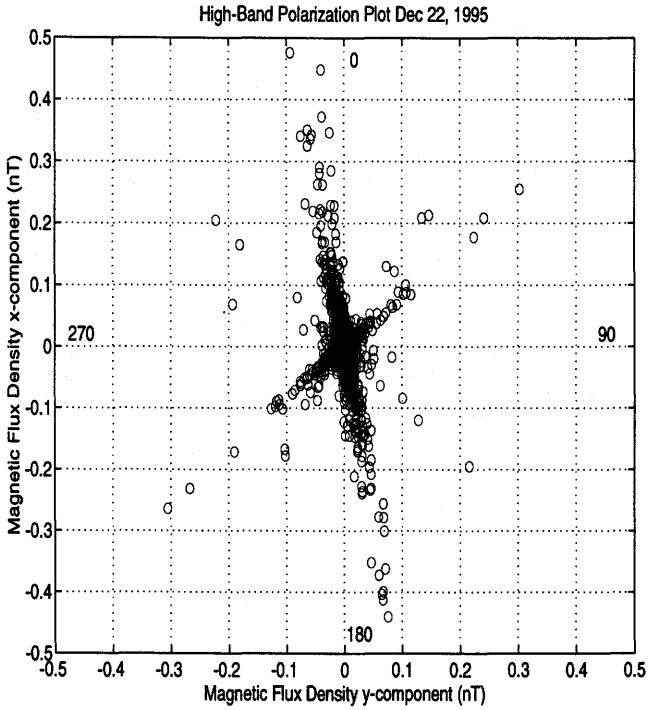

Figure 5.13: High-Band Polarization plot, Dec 22, 1995

Having found the bearings to the sources, we need to find the distance to each source in order to locate it. Intuitively, one might think that analysis of the auto-spectral density of the transient $\vec{B}$ field signal would yield the distance to the source quite easily through comparing spectral density estimates of the received signal with theoretical spectra obtained with modeling programs. In fact, this is quite a crude method to determine distance to the source (Pierce, 1977) as the received energy at various frequencies depends not only on propagation distance but also upon such variable source properties as the type and magnitude of the lightning current (Tzanis and Beamish, 1987. pers. comm., P.R. Kosteniuk).

A better way to find the approximate distance to the source is to make use of the dispersive, lossy properties of the global waveguide. By measuring the so called group time delay difference (GDD) between the VLF and ELF portions of the wavelet (the latter referred to as the "slow-tail"), we can estimate distance to the source. The two components arrive separated in time because the global waveguide is dispersive, therefore, propagation velocity depends on frequency. Furthermore, due to the attenuation properties of the global waveguide, sferic energy is propagated very efficiently at lower

ELF ($\leq$ 200 Hz) and mid to upper VLF ($\geq$ 8 kHz), therefore, this method may be used to locate storms at great distance. This technique has been used extensively for approximate storm location by Hepburn and Pierce (1953) who derived empirical formulas for both day and night time propagation, these are given below (Volland et al., 1982).

$$\delta = .15 + .56\rho \quad (day), \tag{5.2}$$

$$\delta = .36 + .21\rho \quad (night), \tag{5.3}$$

where δ is the time separation in ms between the start of the VLF portion and the first peak or quarter cycle of the slow tail or ELF portion of the wavelet and ρ is the approximate distance to the source in Mm's, or thousands of km. This GDD method is only applicable when the measuring station is sufficiently removed from the lightning transient that mode theory appropriately describes ELF/VLF propagation. In practice, mode theory describes ELF/VLF propagation at distances greater than approximately 1000 km (Volland et al., 1982) while systems to locate lightning strikes at relatively close range ($\leq$ 500 km) usually measure the separation in time between the direct arrival ground wave and the first hop sky wave. Note that between 500 and 1000 km neither method particularly holds, making storm locations in this range difficult (Volland et al., 1982). Fortunately, the present study was always removed at least 1000 km from the nearest thunderstorm; in fact, the closest thunderstorm located in this study was approximately 1500 km distant. Therefore, the empirical formula of Hepburn and Pierce (1953) is appropriate for the estimation of distance to MT signal centers (thunderstorms) at ELF/VLF in the present study.

A disadvantage of this method is that only VLF events with significant ELF energy (i.e., those with slow-tails) can be used for storm locating purposes. This is noted, as not all VLF events have slow tails associated with them. The characteristics of the current variation with time in the lightning stroke have to be of a certain form to generate slow tails or ELF energy. Specifically, slow tails are formed out of the "intermediate and/or continuing currents which sometimes, but not invariably, follow the initial current surge of the return stroke" (Pierce, 1977). This was seen first-hand in the present analysis as approximately 1/3 of the total number of received VLF transients had slow tail's associated with them. VLF events with significant ELF

energy, which were found to have originated off the coast of southern Oregon and off the coast of Louisiana, are shown in Figure 5.14, recorded on December 22, 1995 at the Hepburn site. Note the larger time lag between VLF and ELF portions of the wavelet originating off the coast of Louisiana ($\approx$ 3000 km) as compared to the wavelet originating off the coast of southern Oregon ($\approx$ 2200 km). Also, note the difference in polarity and amplitude between the two slow tail events. This polarity difference is due to opposite directions of current flow in the lightning strike. It is later shown that the sferic from the coast of Louisiana appears to have originated in an intra-cloud stroke. The event off the coast of Oregon was not in the range of coverage of independent data sources but the polarity of this event is of the usual type for cloud-to-ground strokes which dominantly lower negative charge to earth (Volland, 1982. Pierce, 1977. Hughes, 1966). The larger amplitude of the Oregon event (VLF and ELF portions) is also consistent with this hypothesis (Tepley, 1961. Hughes, 1970).

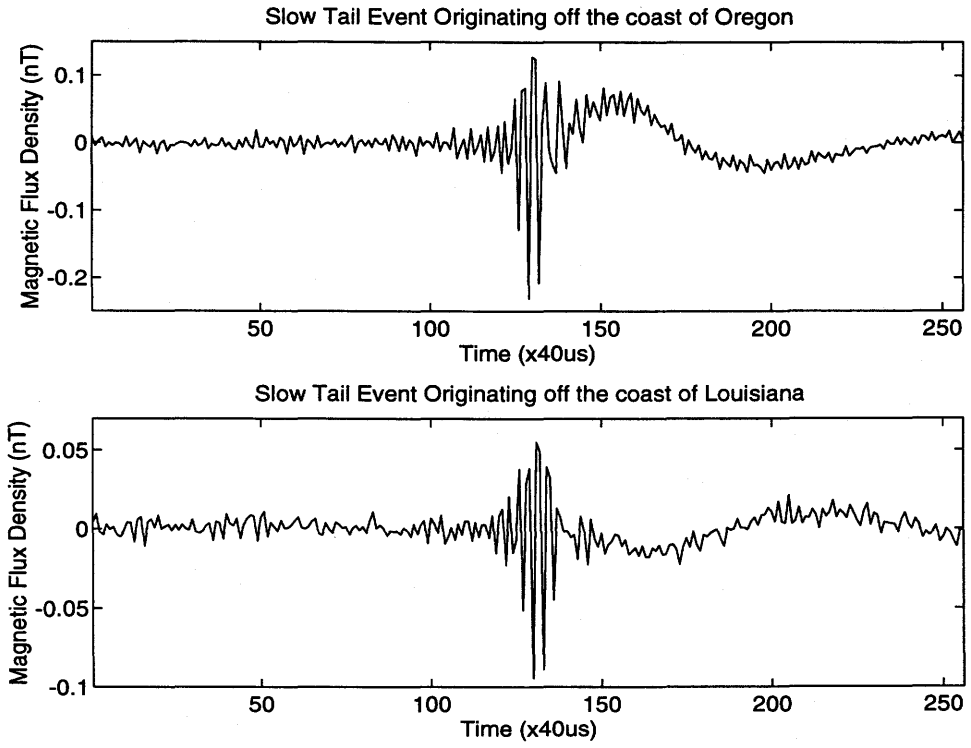

Figure 5.14: Slow Tail Events, B_x component, Dec 22, 1995

Fortunately for the present analysis, GEOCOM-MT doesn't remove (i.e., filter out) ELF energy when recording High-Band data. Unfiltered High-Band data is recorded

over the bandwidth 100 Hz to 10 kHz. The modifier "unfiltered" is added as the author band-passed filtered High-Band data from 1 to 10 kHz for impedance estimation. Therefore, with unfiltered High-Band data, both ELF and VLF energy is recorded. The recorded ELF slow tail usually had a dominant frequency component of about 200 Hz in the present study, although Taylor et al. (1970) found that slow tail energy was a maximum in the range 30-150 Hz. The maxima of slow tail energy around 200 Hz in the present study mainly reflects the recording parameters used in High-Band with GEOCOM-MT. A window 256 samples long is used to record High-Band transients, with a sample rate of 25 kHz. The lowest frequency that we can resolve with these parameters is approximately 98 Hz. Similarly, the recorded VLF component usually had a dominant frequency component of about 8 kHz in the present study. The dominance of the 8 kHz component recorded at VLF is really due to instrument anti-alias filtering more than anything, sferic energy continues to rise to a maximum at about 10 to 20 kHz and sferic's are easily received from many thousands of kilometers up to about 30 kHz as a window of low waveguide attenuation exists from about 10 kHz to 30 kHz. This is, coincidentally, the reason why European and North American countries designed their naval communication systems to operate at upper VLF, in the frequency range 15 to 30 kHz.

Therefore, to apply the empirical formula of Hepburn and Pierce (1953), unfiltered High-Band data was used. At each site usually 100 High-Band events were recorded, every event was examined, and each event with significant ELF energy was used for approximate distance calculations. Events with approximately the same bearing possessing slow tails were grouped together, an average time delay for all such events was found and from the average time delay an average source distance was obtained for each polarization.

With the bearing to the source and an average distance found with equation 5.1 we can solve for the approximate location of a thunderstorm with spherical trigonometry as follows. Consider the spherical triangle with angles A, B, C and spherical arc lengths a, b, c as shown in Figure 5.15.

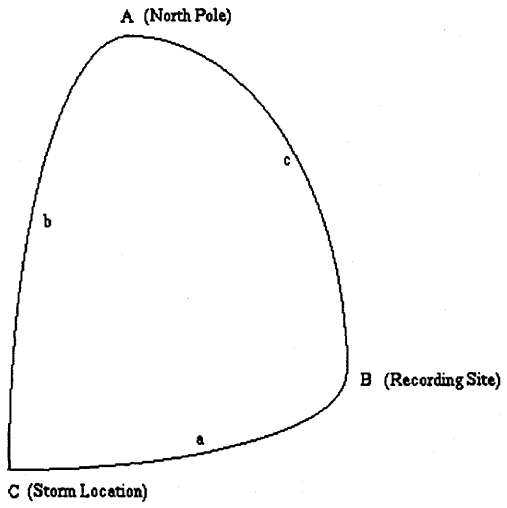

Figure 5.15: Spherical Triangle for solution of thunderstorm locations

If we locate the upper point of the spherical triangle at the North Pole, defined by geographic co-ordinates $(\pi/2, 0)$, and one of the lower points, where the angle B is defined, at the measurement site (whose co-ordinates are known), we immediately find the spherical arc length, c, between the North-Pole and the measurement site. We also know the angle B, the bearing to the unknown location of the thunderstorm, and the spherical distance a to that thunderstorm, estimated from equation 5.1. With this we have sufficient information to solve for the approximate location of the thunderstorm as follows:

- The spherical distance c is found as $\pi/2 - l_m$ radians, where l_m is the latitude of the measurement site, approximately $52(\pi/180)$ radians in the present study.
- The spherical distance a (in radians) is found as $a = d_s/r_E$ where d_s is the distance to the source found from equation 5.1, and r_E is the radius of the earth (6370 km).
- The spherical distance b is found with knowledge of a, c and B, where B is the bearing to the source. The bearing B is defined as 0 pointing North, $B = \pi/2$

corresponds to due east, $B = \pi$ due south and $B = 3\pi/2$ due west. Specifically, b is found with the Cosine law as

$$b^2 = a^2 + c^2 - 2ac\cos B \tag{5.4}$$

- The spherical angle A is found with the Sine law as

$$\frac{\sin B}{b} = \frac{\sin A}{a} \tag{5.5}$$

- Lastly, the geographic co-ordinates of the lightning transient are then found as $lat_s = \pi/2 - b$, and the longitude $long_s = long_m \pm A$ where $long_m$ is the longitude of the measurement site. The angle A is added to $long_m$ when the signal arrived from the west, and is subtracted from $long_m$ when arriving from the east.

On December 22, 1995, an MT source field recording in High-Band was made from 18:30 to 19:01 GMT (Greenwich Mean Time or Universal Time), two thunderstorms were located; one in the Gulf of Mexico off the coast of Louisiana at 29°N, 88°W and the second over the Pacific Ocean off the southern coast of Oregon at 42°N, 131°W. A fifteen minute weather radar image over the continental United States on December 22, 1995 from 18:30 to 18:45 GMT is shown in Figure 5.16 with the author's storm locations indicated with red crosses. The Louisiana location is coincident with a weather system possessing large precipitation echos, indicating high moisture content within the clouds at this location. Although the oceanic location off the coast of Oregon is out of range of the NWS weather radar, there is evidence of activity along the coast of northern California and southern Oregon which may have been related to lightning activity at the author's location.

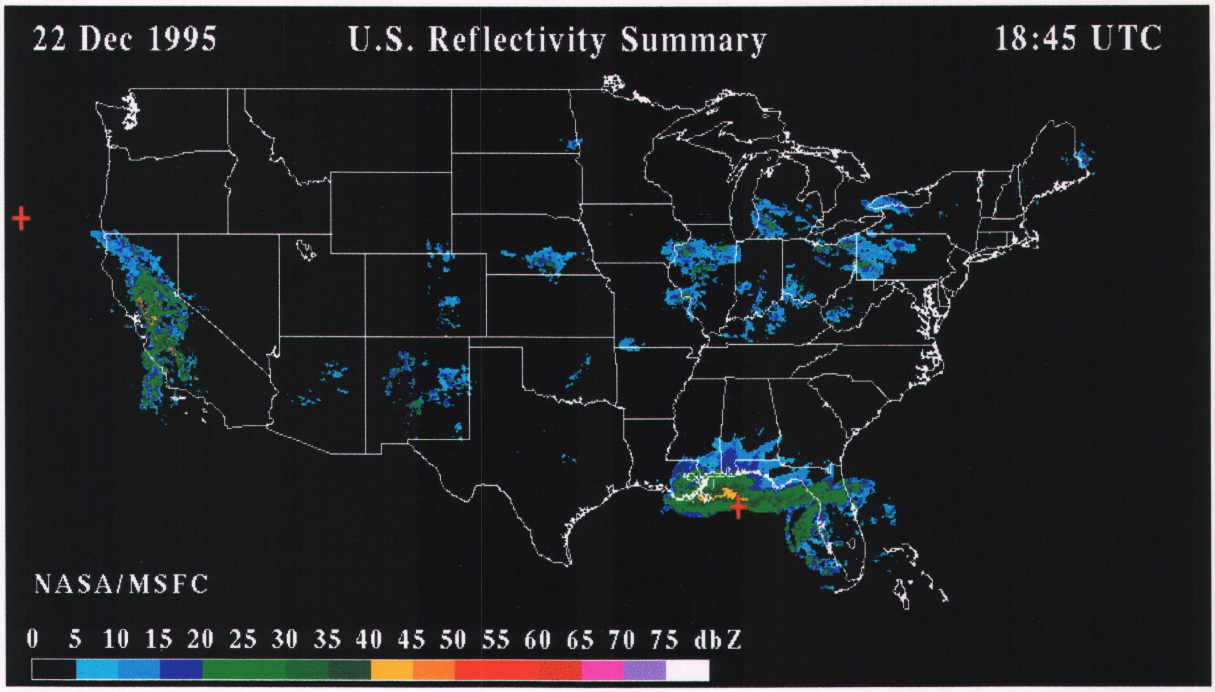

Figure 5.16: NWS Weather Radar Data, Dec 22, 1995 18:30-18:45 G.M.T

Verification of thunderstorm locations with NWS weather radar data, indicating high cloud moisture content has been carried out previously by McDonald et al. (1979), Krider et al. (1975) and Kinzer et al. (1974). In all of these studies, verified thunderstorm locations, achieved through various means, always occured within or very near NWS reflectivity patterns as;"In clouds where the electrification has developed sufficiently to cause lightning, precipitation is almost invariably present" (Vonnegut, 1982).

On October 23, 1995 thunderstorm locations over Iowa (43°N, 92°W) and Mexico (20°N, 90°W) were found. Shown in Figure 5.17 is the daily composite, total rainfall over the continental United States. Fifteen minute updates as shown in Figure 5.16 were not available for this day. Nevertheless we note the intense rainfall activity over Iowa, near one of the locations specified by the author with a red cross. The second location at 20°N, 90°W (Mexico) is out of range of the NWS weather radar and off the map shown in Figure 5.17.

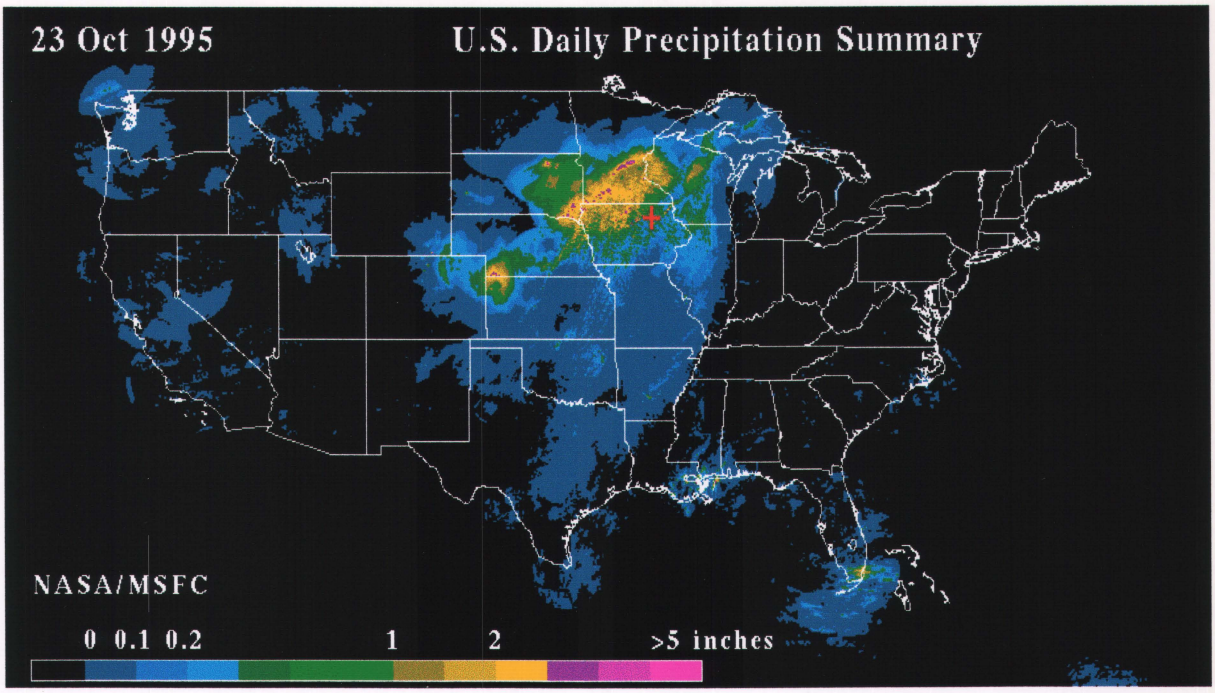

Figure 5.17: Total Rainfall, Oct 23, 1995

On February 18, 1996 High-Band data was recorded over the time period 21:30 to 22:07 GMT, thunderstorms off the northern coast of California (40°N, 124°W) and over the Atlantic Ocean off the coast of Florida (31°N, 68°W) were located. Shown in Figure 5.18 is the fifteen minute, NWS weather radar reflectivity pattern over the continental United States on February 18, 1996, from 21:30 to 21:45 GMT, with the author's storm locations indicated with red crosses. Large precipitation echos are again evident at the author's California location, the location over the Atlantic ocean is out of the coverage area of the NWS weather radar. It should be noted that for the February 18, 1996 recording, a thunderstorm location was also found at 43°N, 84°W near Detroit, Michigan. This location did not coincide with any observable weather system as indicated by the NWS weather radar, as such, the validity of this location is suspect. The other possibility lies in the 180 degree ambiguity, if the signal had propagated to the author's location from the north-west instead of the assumed south-east, this would yield a storm location over the Pacific Ocean, near the southern coast of Alaska, which is unlikely in February (WMO, 1956). The reason for the apparent failure of the locating method in this instance is not known.

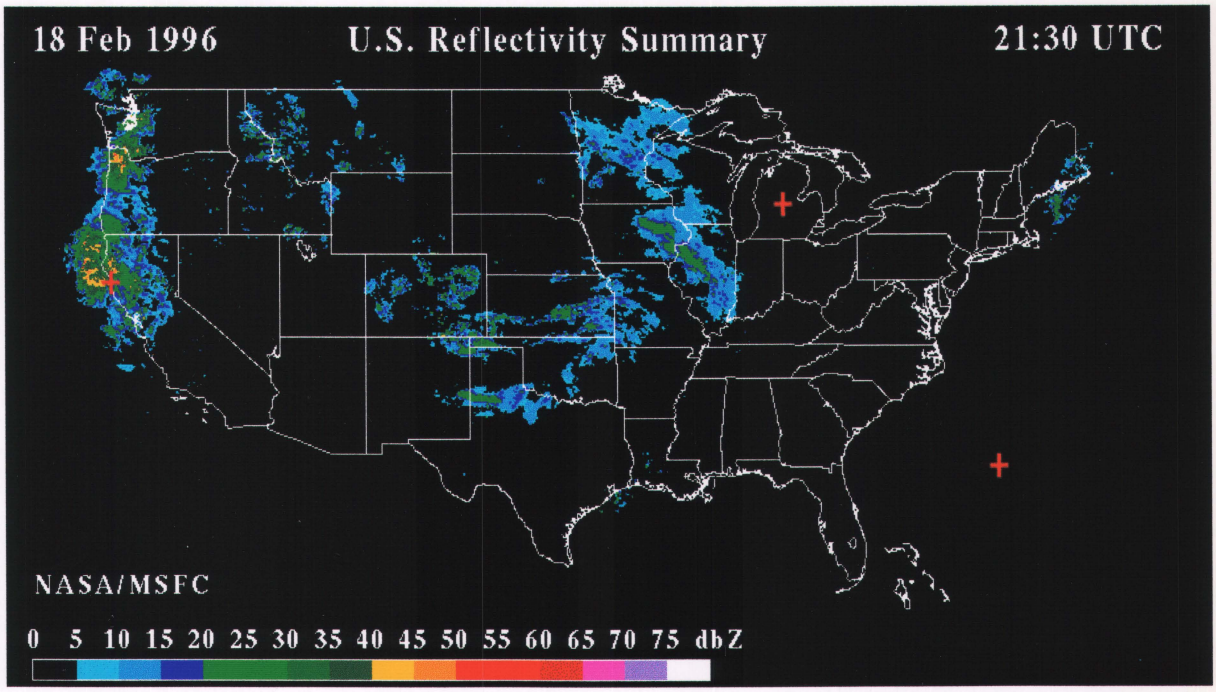

Figure 5.18: NWS Reflectivity Data, Feb 18, 1996 21:30-21:45 GMT

The present method of storm locating has been verified with NWS weather radar data. National Lightning Detection Network (NLDN) data (Idone et. al, 1993. Orville, 1994), which maps very accurately the location of cloud-to-ground strokes only, was obtained for the days of December 22, 1995 and February 18, 1996. Similar to the NWS weather radar data, the NLDN has limited areal coverage. However, the locations specified by the author within the NLDN coverage area on December 22, 1995 and February 18, 1996 were strictly not verified by the NLDN data. Specifically, the NLDN detected no cloud-to-ground strokes at the Louisiana location (29°N, 88°W) on December 22, 1995 from 18:30 to 19:01 GMT. On February 18, 1996 the author's California storm location (40°N, 124°W) over the time period 21:30 to 22:07 GMT also did not coincide with any cloud-to-ground activity as detected by the NLDN. However, the NLDN did detect cloud-to-ground lightning activity within 200 km of the author's California location over the time interval 21:00 to 21:15 GMT on February 18, 1996. Therefore, lightning activity was indeed present in this weather system on February 18, 1996, although apparently not cloud-to-ground lightning over the recording time 21:30 to 22:07 GMT when High-Band data was collected in the present study.

Although the storm locations in the present study were not quantitatively verified with NLDN data, the present analysis is not necessarily invalidated as the NLDN detects cloud-to-ground lightning strokes only. Larger current moments and near optimum orientation (usually near vertical) means that cloud-to-ground strokes are the dominant source of sferics (Pierce, 1977). However, intra-cloud strokes occur much more frequently (Christian et. al, 1996. Ogawa, 1977. Prentice, 1977) and over a much wider range of current moments (Pierce, 1977) and orientations, although generally tilted with horizontal extension commonly three times the vertical extension (Teer and Few, 1974). Therefore, intra-cloud strokes do indeed radiate sferics, although they are relatively "richer" in high frequency content than typical return strokes. Malan (1958) found that for frequencies less than 10 kHz, sferics radiated by intra-cloud strokes were approximately an order of magnitude smaller in amplitude than those radiated by cloud-to-ground strokes. Also, 50 kHz intra-cloud generated sferics are comparable in amplitude with return stroke generated sferics. It is hypothesized that the two locations which do not agree with the NLDN data are locations where intra-cloud lightning occured predominantly and hence were not detected by the NLDN.

This hypothesis could be confirmed with satellite based, Optical Transient Detector (OTD) data, available free of charge from the Marshall Space Flight Center (MSFC). The OTD locates both intra-cloud and cloud-to-ground strokes by detecting the visible flashes of light associated with both lightning types. Unfortunately, the satellite carrying the OTD sensor was never in the right location at the right time to confirm the author's hypothesis, but shown in Figure 5.19 is coincident OTD and NLDN data as available on the MSFC home page (wwwdaac.msfc.nasa.gov) on the Internet. As is generally the case, we see that many more intra-cloud strokes occur than do cloud-to-ground strokes and in some cases, as hypothesized in the present study, intra-cloud lightning is produced exclusively.

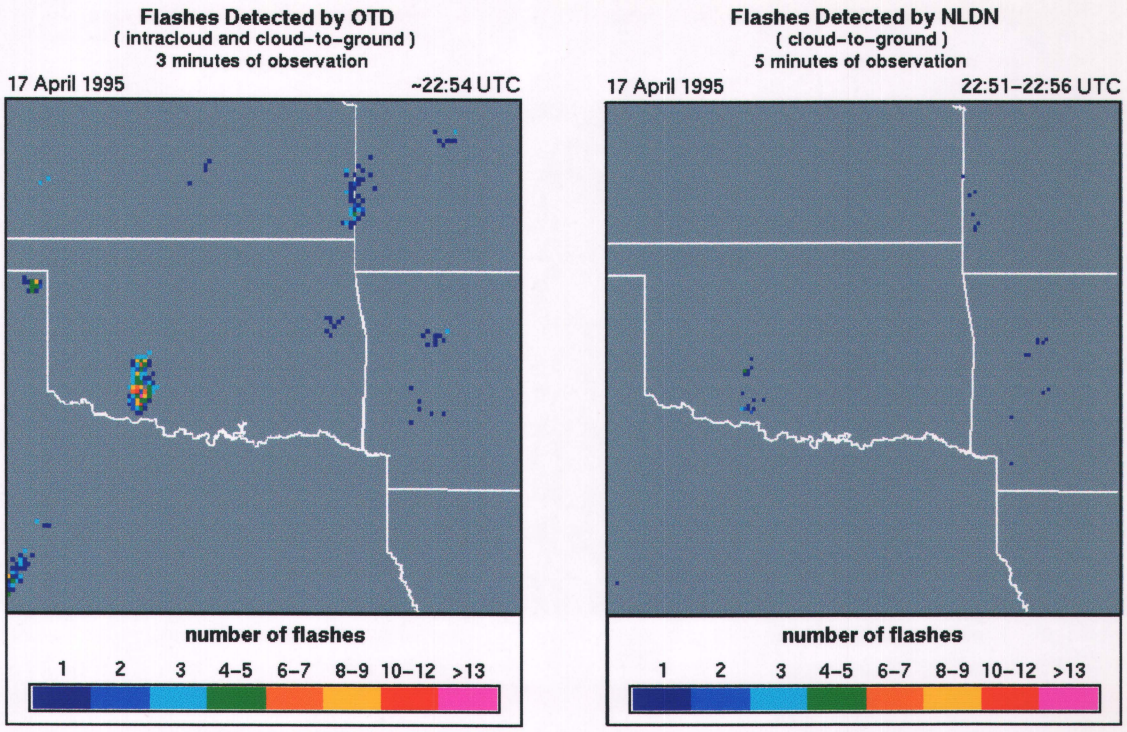

Figure 5.19: Coincident OTD and NLDN data

The ratio of intra-cloud to cloud-to-ground lightning varies significantly with latitude with intra-cloud lightning becoming more frequent as latitude decreases. This is believed to be due to variation in parameters such as cloud base height and humidity (Pierce, 1970). Specifically, the ratio of intra-cloud to cloud-to-ground lightning is seen to vary from three at temperate latitudes to six at tropical latitudes (Prentice, 1977). Furthermore, the polarity of the slow tail indicates the direction of current flow in the lightning strike (Hughes, 1966). At one time, it appeared that clear distinction could be made between intra-cloud generated ELF/VLF events and return stroke generated ELF/VLF events based on the polarity of the slow tail. This is seen because intra-cloud lightning usually involves the transfer of positive charge between layers in a cloud (Ogawa, 1977) and cloud-to-ground strikes dominantly lower negative charge to earth (Volland, 1982. Pierce, 1977). However, this distinction does not always hold as the characteristic current changes which occur dominantly in intra-cloud strikes can also occur in cloud-to-ground strikes (Pierce, 1977). However, in the present study it was found that 78 percent of all slow tails had the polarity indicative of origin in typical intra-cloud strokes. This agrees with the findings of Tepley (1961)

who similarly found 69 percent and Jones and Kemp (1971) who obtained 66 percent. Therefore, based on the author's storm location analysis, NWS weather radar data and NLDN data, it appears that intra-cloud strokes can be of importance for MT surveys at ELF/VLF.

This information might be considered extraneous for the practitioner of the MT method at ELF/VLF. However, it is important to recognize that not only return stroke generated sferics can be propagated to great distance; in some cases it appears that intra-cloud generated sferics can also be propagated to distances of 3000 km or more, and that intra-cloud lightning can generate significant ELF energy, as hypothesized by Pierce (1977), Jones and Kemp (1971) but discounted by Volland (1982). Intra-cloud lightning strokes are generally tilted with a smaller vertical extension than horizontal (Teer and Few, 1974). As such, intra-cloud strokes do not radiate as much energy to the far field as do return strokes. This being so as horizontal dipoles are not optimum for the radiation of TM mode waves (Ogawa, 1977. pers. comm., P.R. Kosteniuk) and only TM mode waves can be propagated to great distance within the global waveguide. Presumably, the present study received only the largest current moment intra-cloud strokes and/or those with a significant vertical current component. Furthermore, because only the energy radiated by the vertical current component of any discharge is propagated efficiently to the far field, no significant bearing error due to radiation by horizontal components appears to have been encountered (Yamashita and Sao, 1974). The radiated TE components (due to horizontal currents in the discharge) are damped severely with distance from the source (Polk, 1982) and are therefore present only at relatively small distances from the lightning channel.

The analysis of the present section was verified by NWS weather radar data. Discrepancies between NWS weather radar data and NLDN data on December 22, 1995 and February 18, 1996 are hypothesized to be due to the natural source signals origin in intra-cloud strokes. Therefore, due to good agreement with NWS weather radar data, the storm location analysis was thus extended to include the complete dataset. It was found that signal centers could be grouped into geographical bins as three major storm centers were consistently found in the present study. This is shown in Figure 5.20 with the number of storms located in that bin indicated above the top right or left corner of a particular bin. The author's approximate recording

location is indicated with a star and single storm locations over Iowa, Michigan and Brazil are indicated with a black cross. We see that the dominant signal center in the present study was due to thunderstorms in the south to south-eastern United States (Florida, Georgia, Alabama, Louisiana, Texas), also notable were oceanic/coastal storms on the west coast of the United States (Oregon, California). Several storms were also located in the Caribbean, Central America and southern Mexico, the most spectacular example in the present study was the location of a storm over 8000 km away in central Brazil (4°S, 51°W), one of the three major storm centers of the world. Although this was indeed a rarity as most storms were located within 2000 to 4000 km of the recording site. The storm locations in the present study are also in good agreement with the well known publication of the World Meteorological Organization (WMO) (1956), detailing the global distribution of thunderstorms as a function of month throughout the year.

Figure 5.20: Signal centers for the present study

Albeit very interesting, this information is also quite important as for tensor MT surveys we require at least two different storms to be present. That is we need at least two different polarizations for estimation of the impedance tensor. If only one polarization is present, solution of the impedance tensor is meaningless and only a scalar processing can be reliably done. In this respect the present study found no difficulties in estimating the impedance tensor. At a given site, usually three or at most four different polarizations were present, with two dominant polarizations possessing bearing differences of at least 30 degrees and one or two relatively minor polarizations with bearing differences of ninety degrees or more. This was sufficient for estimation of the impedance tensor in the present study.

Note that the storm locating procedure carried out, was done only with the one third of High-Band data having significant energy at ELF. Surprisingly, this procedure was found to identify the dominant storm centers in all but two cases. This was found by examining the similarity between polarization plots of High-Band data with all the recorded events and polarization plots of those events with ELF energy only.

Polarization plots in Mid-Band, and less so in Low-Band had approximately the same polarization characteristics as the High-Band data. As mentioned previously, waveguide attenuation at 200 Hz is on the same order as that at 8 kHz, so it is highly likely that High-Band signal centers were also Mid-Band signal centers. This was verified in the high degree of similarity between Mid and High-Band polarization plots. This was seen to a lesser degree in the Low-Band data, but even here some commonality existed in polarization characteristics between High and Low-Band. Therefore, it appears that in Low-Band we most likely derived at least some signal from the storm centers identified with the High-Band data, although owing to the very low attenuation less than 100 Hz we are capable of receiving Low-Band transients from just about anywhere on the earth. This was qualitatively confirmed as although there were some similarities between Low and High-Band polarizations, the Low-Band polarization plots usually had at least one completely different polarization not seen in either the High or Mid-Band polarization plots.

The two cases in which slow tail analysis did not identify the dominant polarizations will now be discussed. At SITE 104 (Chapter 1), occupied on October 28, 1995 a total of four High-Band polarizations were evident, with two dominant polar-

izations with bearings of 167° and 125°. The polarization at 167° was not identified with slow tail analysis but is consistent with previous locations identified in Texas and Southern Mexico. On May 25, 1996 at SITE 110 activity was roughly equally divided between three different polarizations at 144°, 170° and 211°. The storm centers for polarizations of 170° and 211° were not identified but are consistent with previous locations in Texas or Southern Mexico and southern California or oceanic over the Pacific respectively.

Also of interest in the present study is the high occurrence of oceanic and/or coastal thunderstorms throughout the fall and most notably the winter of 1995/96. Meteorologists distinguish between two types of thunderstorms, so called "air mass" thunderstorms, created by daytime heating which cause buoyant parcels of air to rise creating the necessary updrafts and downdrafts giving rise to charge separation. The second type, more common in winter, is that of a "frontal storm" where relatively warm, moist air mixes with cooler, dense air creating a system of updrafts and downdrafts. Such winter thunderstorms are notable over the Sea of Japan where cold dry air from Siberia flows over the warmer waters of the Sea of Japan giving rise to frontal storms (Takeuti et al., 1978). Winter thunderstorms are also prevalent over the North Atlantic where cold polar air flows over warmer ocean waters, thunderstorms being more frequent here in winter than in summer (Vonnegut, 1982. Orville et al., 1979. World Meteorological Organization, 1956). The higher occurrence of oceanic thunderstorms in winter also agrees with the findings of Lugeon et al. (1959) who made lightning activity and storm location analyses for almost three years continuously.

It is also interesting to see that at all sites, small amounts of data from two polarizations not identified with slow tail analysis consistently arose, namely one polarization with bearings between 89° and 139° and another with bearings between 167° and 234°. The bearings between 89° and 139° could come about from storms over the North Atlantic, and bearings of 167° to 234° could arise from storms in the southwestern U.S.A., Mexico or the Pacific Ocean.

Lastly, we should note that GEOCOM-MT records a fairly narrow window around each VLF event so we are limited in range determinations as the width of the recording window places an upper limit on the size of the group time delay difference we can measure. Therefore, during the day we have a maximum possible range determination

of about 9000 km, at night this increases to over 20,000 km due to changes in the ionosphere, namely the disappearance of the weakly ionized D layer. However, the finite width of the recording window does not seem to have been a prevalent factor, as most times we were limited in receiving signals in the frequency band 200 Hz - 10 kHz from storms less than 4000 km away, although several instances of 5000 km occured and one of 8000 km occured. This agrees with the studies of Lugeon et al. (1959) who found that receival of VLF energy at 27 kHz under daytime conditions was usually limited to about 2000 km, with rare instances of 5000 km with his equipment. Due to lower waveguide attenuation at night, the range of VLF reception increased to over 10,000 km in Lugeon's study.

Chapter 6

Results

6.1 Fall Groundwater Survey

This section deals with the presentation and interpretation of the processed magnetotelluric data, collected over the assumed edge of the Dalmeny and Tyner valley aquifer systems in the fourth week of October, 1995. Shown in Figures 6.1 and 6.2 are the raw resistivity and phase data for both the xy and yx polarizations respectively. Note that the three intermediate sites on the northern MT line were not occupied (Fig 1.4b) because of equipment problems, hence the horizontal gap in the figures. The vertical gap from approximately 500 Hz to 5 kHz reflects the "dead band" in the data caused by the very large global waveguide attenuation centered roughly at 3 kHz. Because of this we have no reliable signal over this frequency band in the present study, and therefore, the figures are left blank over this frequency range. As mentioned previously, the increased width of the "dead band" in the present study is simply a result of increased source-receiver separation in fall/winter recordings at mid-high latitude. Equipment problems precluded the acquisition of Low-Band data at the northern-most site, hence there is a vertical gap in the bottom right corner of all figures. Note the distortion around the powerline frequency of 60 Hz in the raw data. This is due to slight imbalances of the Twin-T notch filters on respective $\vec{E}$ and $\vec{B}$ channels. Recall that the author was forced to 60 Hz notch filter the E_x channel with a digital approximation of the analog Twin-T notch filters inside GEOCOM-MT.

Shown in Figures 6.3 and 6.4 are the edited resistivity and phase pseodosections

for both polarizations, the result of graphical interpolation over the "dead band" in the data. Recall that the graphical interpolation step is justified by noting that the impedance tensor, and therefore apparent resistivity and phase, must be smoothly varying functions of frequency. The most evident feature on the edited plots is the imaging of a resistive layer centered at approximately 100 Hz, indications of the resistive layer are also seen in the phase data. Note the high degree of similarity between the two polarizations, indicative of an approximately one-dimensional, isotropic earth at the Hepburn site.

Shown in Figures 6.5 and 6.6 are the Bostick transforms of the edited data for each polarization. Once again, we see the high degree of similarity between the two polarizations.

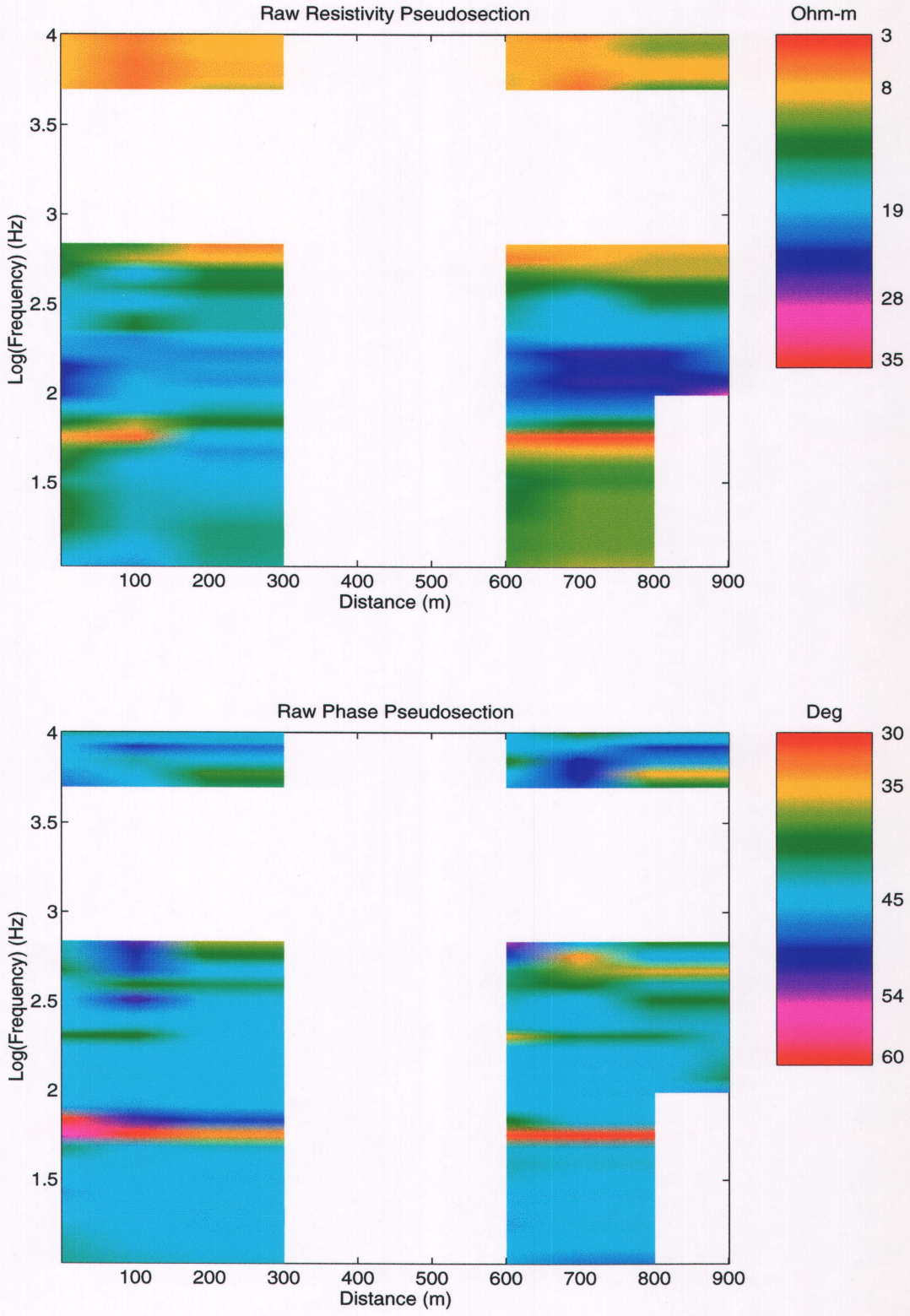

Figure 6.1: Raw $\tilde{\rho}_{xy}$ and $\tilde{\phi}_{xy}$, Hepburn Site

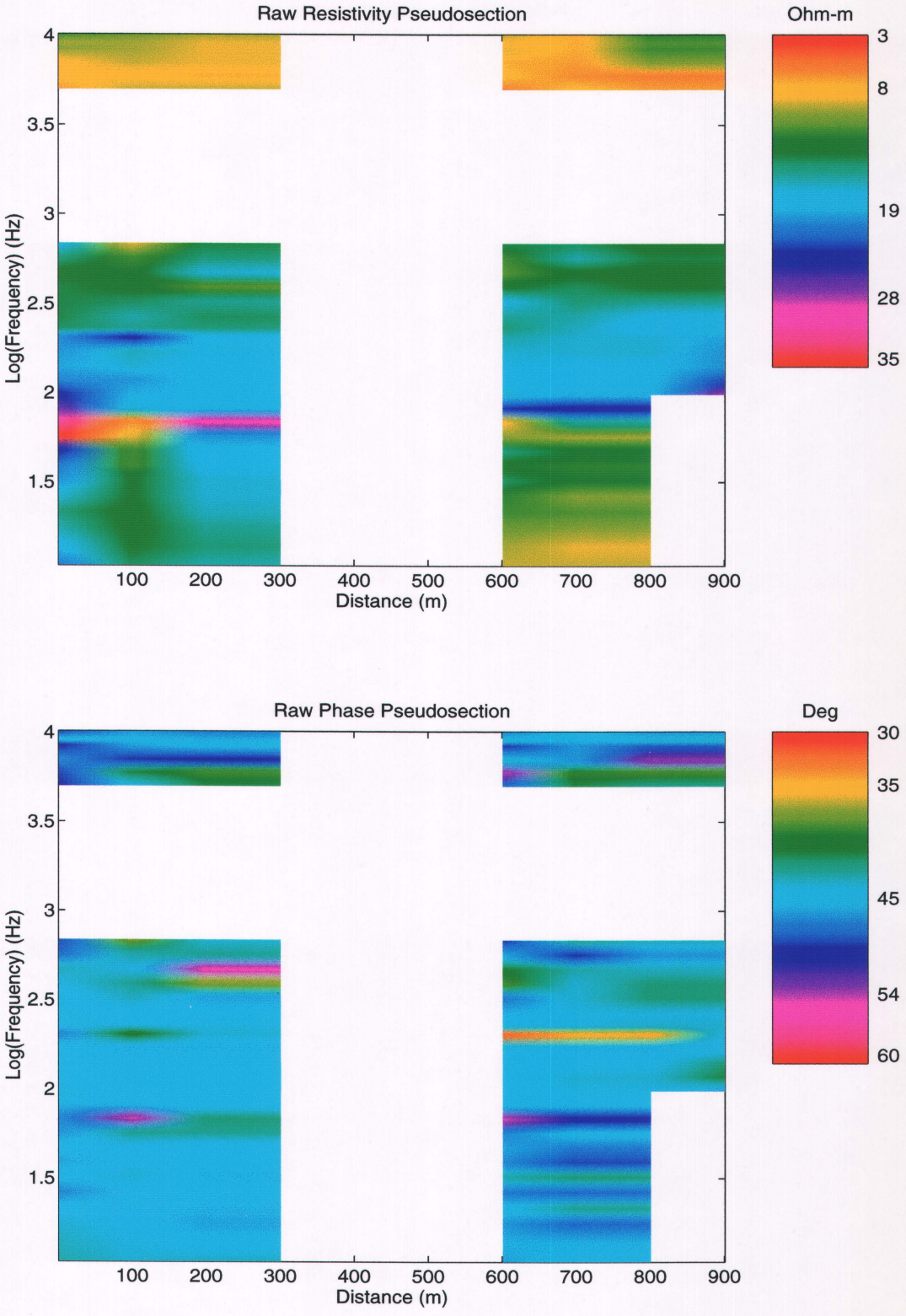

Figure 6.2: Raw $\tilde{\rho}_{yx}$ and $\tilde{\phi}_{yx}$, Hepburn Site

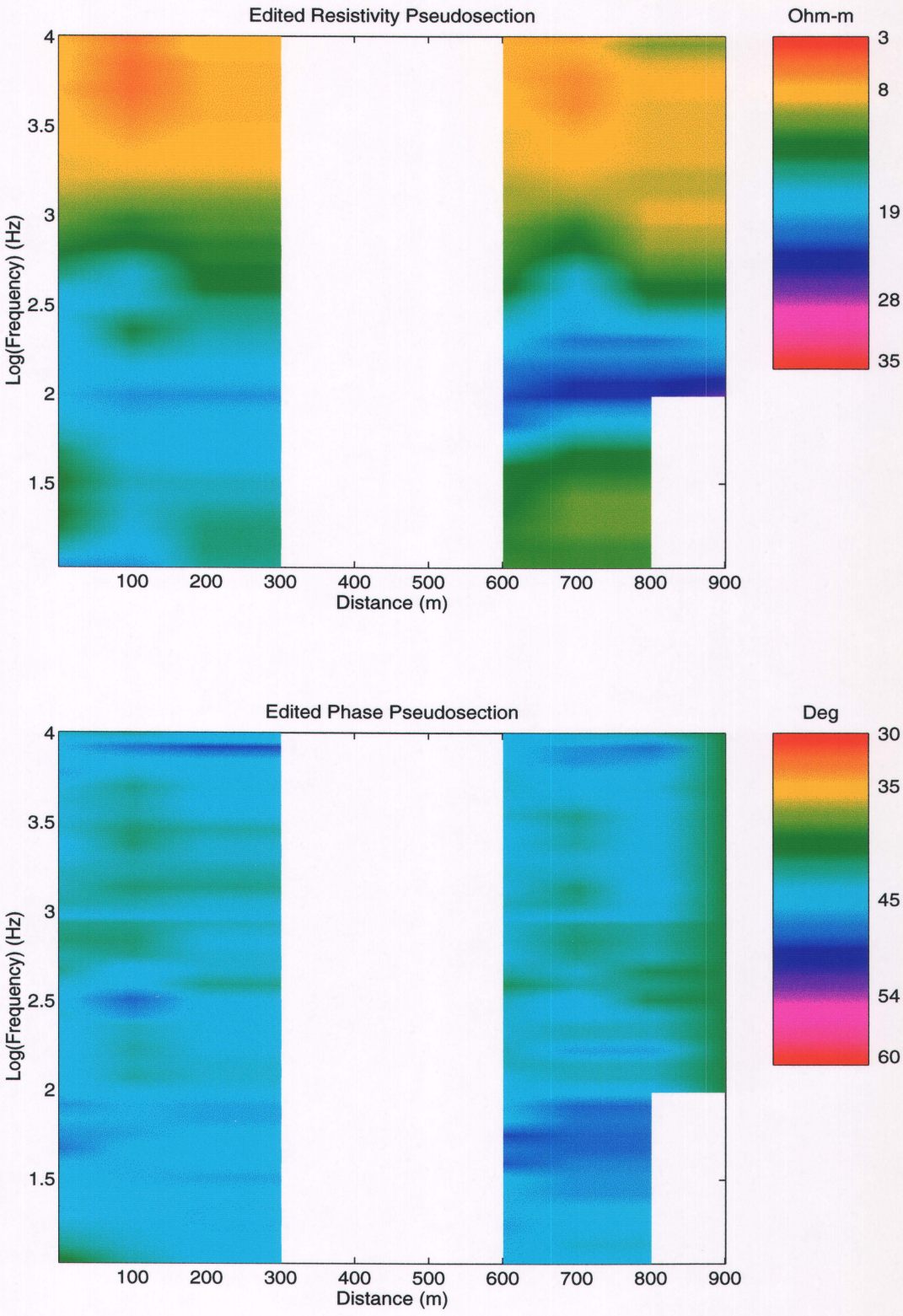

Figure 6.3: Edited $\tilde{\rho}_{xy}$ and $\tilde{\phi}_{xy}$, Hepburn Site

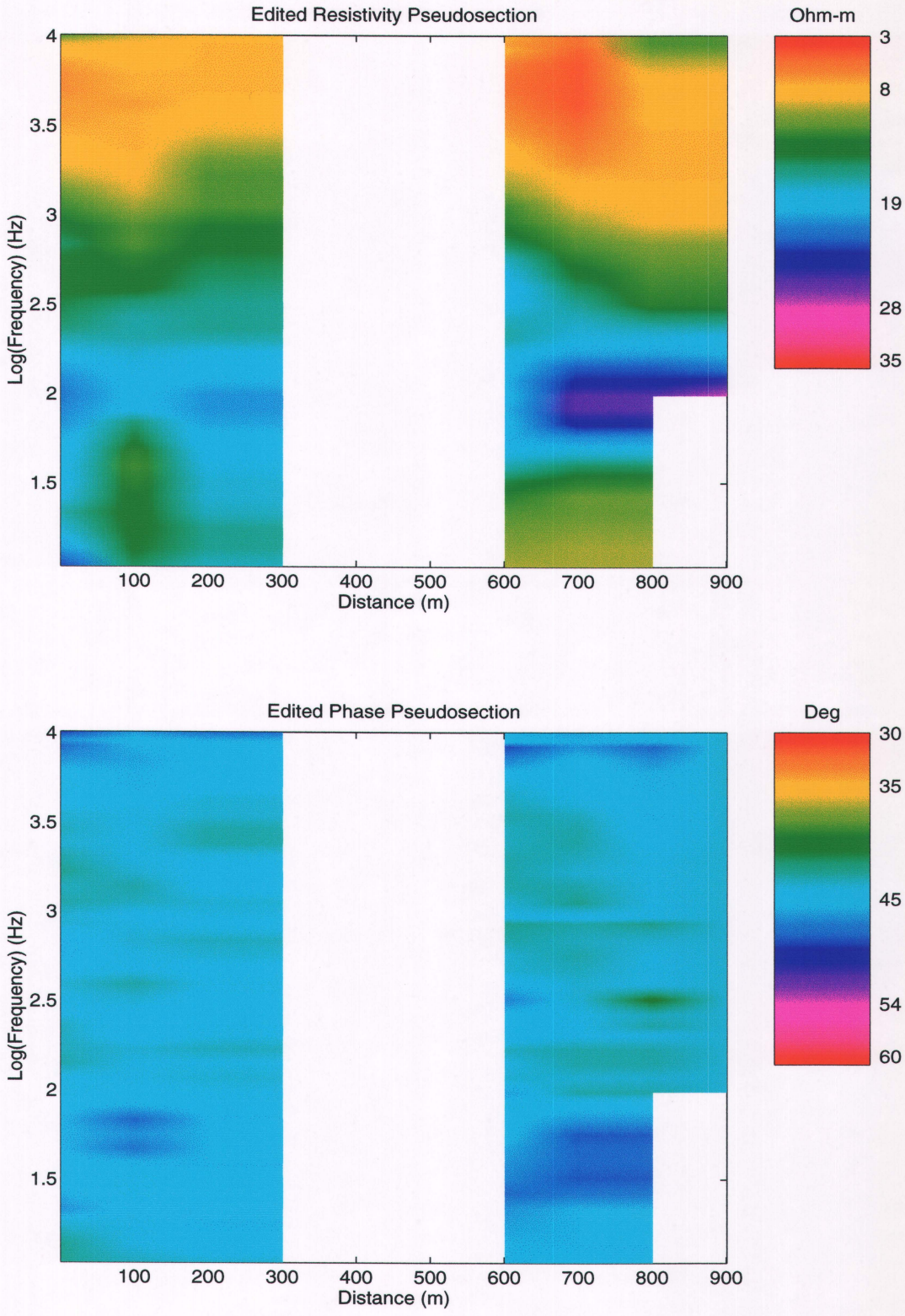

Figure 6.4: Edited $\tilde{\rho}_{yx}$ and $\tilde{\phi}_{yx}$, Hepburn Site

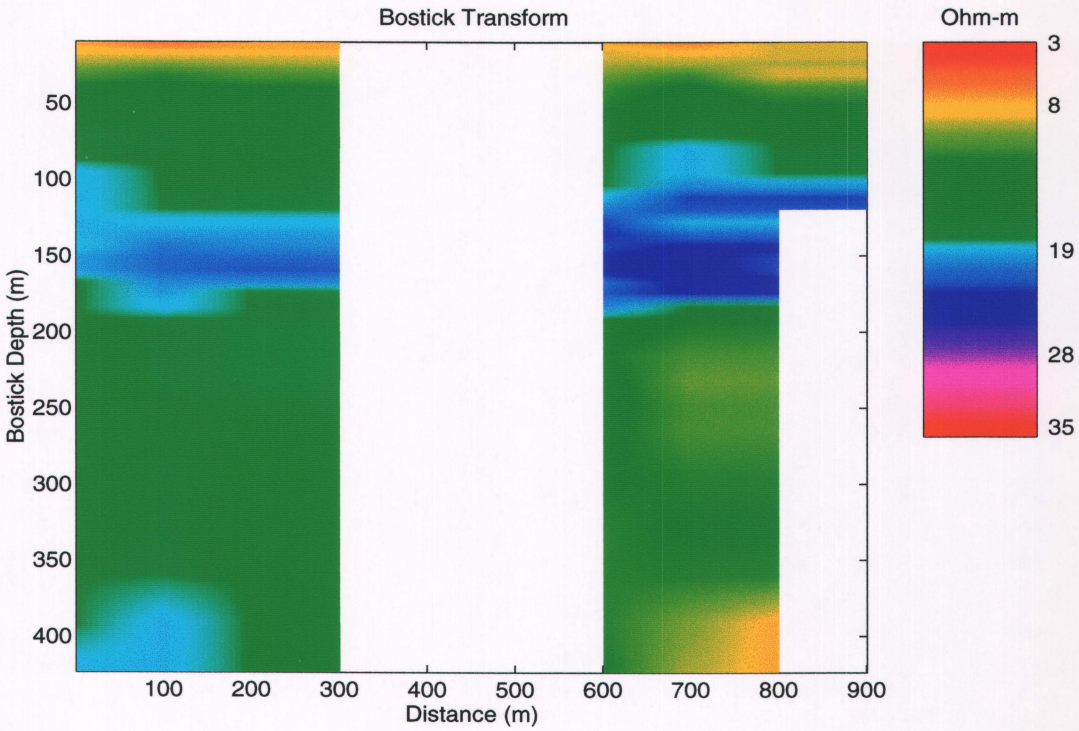

Figure 6.5: Bostick Transform of $\tilde{\rho}_{xy}$, $\tilde{\phi}_{xy}$ pair, Hepburn Site

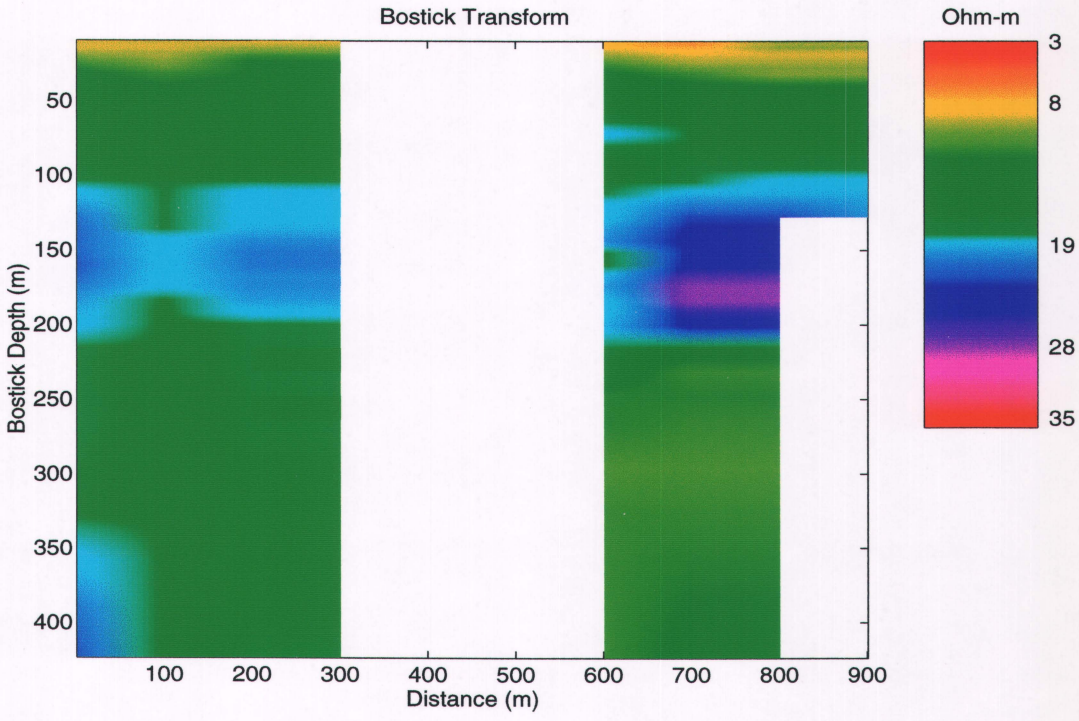

Figure 6.6: Bostick Transform of $\tilde{\rho}_{yx}$, $\tilde{\phi}_{yx}$ pair, Hepburn Site

The well logs that will be subsequently presented are termed single point resistance logs. Such well logs are "one of the most widely used in ground-water hydrology" (Keys, 1989). Despite the fact that quantitative interpretation cannot be carried out with such electrical logs, they are more useful in providing lithologic information (Keys, 1989). As its name implies, a single point resistance log measures resistance, as opposed to resistivity. This is accomplished by having two electrodes, one down-hole, and the other at surface. By maintaining a constant current as the down-hole electrode is lowered, the resistance between the down-hole and surface electrode can be measured simply through the ratio of voltage over current. However, quantitative information is not obtained as resistance is not a fundamental property of a medium. The measured resistance will depend on cross-sectional area and the length of material through which the current must flow. Therefore, resistance changes in single point resistance logs can be due both to changes in earth material properties and/or path length increase, etc. Another disadvantage of single point resistance logs is that the radial depth of investigation is quite small, approximately five to ten times the diameter of the down-hole electrode. A common drill diameter is five and one eighth inches, giving a radial depth of investigation of about six feet, or almost two meters at best.

Conversely, single point resistance logging equipment is simple and can be operated to provide simultaneous S.P. (Self-Potential) and resistance information. Moreover, the vertical resolution of single point resistance logs is quite good making it a good tool for lithologic mapping (Keys, 1989). Therefore, it should be emphasized that the lithologic information accompanying the single point resistance logs be given the most importance; the resistance log itself is only a qualitative indicator of earth resistivity. Also, recall that with MT, and electromagnetic methods in general, the apparent resistivity can be thought of as the average resistivity of some field absorbing volume. Even at the highest frequencies, and in the most conductive environments, the averaging volume for electromagnetic methods will be much larger than that obtained with a single point resistance log. This should be kept in mind when interpreting MT data, and electromagnetic data in general, when using single point resistance logs as a reference. Once again, it should be stressed that the lithologic information with the single point resistance log be given the most importance for interpretation.

The results of the one-dimensional inversions shown in Figures 6.5 and 6.6 will

now be discussed in more detail. A near surface conductive layer from approximately 10 to 20 m depth is noted, below which, a less conductive layer of uniform resistivity is present from about 20 to 110 m depth. Below 110 m, the inverted results begin to show indications of a resistive layer which becomes clearly present at approximately 130 m and extends to about 160 m at the southern most MT site (the origin in Figures 6.1 through 6.6). The resistive layer was found to increase in thickness to the north, extending over the depth range of approximately 100 to 170 m at the northern most MT site (at 900 m in Figures 6.1 through 6.6). Below the resistive layer centered at about 150 m, an electrically uniform layer was found to extend to the greatest depth imageable, which because of the rather conductive nature of the earth at the Hepburn site, was only slightly more than 420 m. In more resistive environments, such as northern Saskatchewan, depths of investigation on the order of 1000 m are easily attainable.

In terms of a geological interpretation, a thick till layer, of largely uniform resistivity, was present from the near surface to approximately 110 m. This depth range encompasses both the Saskatoon and Sutherland groups. The Dalmeny aquifer, which occurs in the Sutherland group, was absent at the Hepburn site meaning that the edge of the Dalmeny aquifer as outlined by the SRC is verified. The resistive layer centered at approximately 150 m is at the correct depth and is of the right thickness to be the Judith River or Oldman formation, comprised of sand and silt. At the southern-most MT sites the Oldman formation occurs solely, with very minor indications of Empress group sands near 110 m. The thickening of the resistive unit to the north is interpreted to be due to the increasing presence of Empress group sands overlying the Oldman formation. The stacking together of Empress and Oldman sands is seen to occur near or over top of the edges of glacial valleys (Christiansen et al., 1970). The Bearpaw formation, comprised of silt and clay shale, usually lies between the Empress and Oldman sands. However, the Bearpaw formation was not clearly imaged at the Hepburn site meaning that it was either absent or perhaps too thin to be resolved. The very thin, or perhaps absent, Bearpaw formation allowed Empress group sands to be essentially stacked on top of Oldman sands, yielding a thick resistive layer.

In order to verify this interpretation, a single point resistance and self potential log, collected and provided by the Saskatchewan Research Council (SRC), is shown in

Figure 6.7. Fortunately for the present study, a wealth of such well logs are available from the SRC. This particular well log was collected within 50 m of the southern-most MT site, although because it was acquired 33 years ago (1964), the exact location of the drill hole was not found. The depth scale of the well log is in increments of 20 ft, the resistance scale is ten Ohms per inch. Similarly, the S.P. log has a horizontal scale of 10 mV per inch. The lithologic log indicates a very thick till layer, extending from the surface to approximately 100 m, below which two very thin sand layers were noted, in between which is a thin till layer. Unfortunately, the well log does not extend below about 120 m. The inverted results at the southern-most MT site (the origin in Figures 6.5 through 6.6) agree very well with the single point resistance log of Figure 6.7. Specifically, a uniform layer was found to extend from about 20 to 110 m depth, however, the imaging of a somewhat more conductive layer from approximately 10 to 20 m depth does not agree with the well log. Differences here could be due to the inherently small averaging volume of the well log, contrasted with the comparatively large averaging volume with MT. At the greatest depth extent of the well log, slightly more resistive, very thin sand/gravel layers were found, there are minor indications of this in the inverted results, but the dominant resistive feature centered at about 150 m is unfortunately out of the depth range of the well log. Note that the Bearpaw formation was interpreted to be the approximately 3 m thick, calcareous till layer lying between the two thin sand layers near the bottom of the well log. As interpreted above, the Bearpaw formation, 3 m thick at the Hepburn site, would be much too thin to image electromagnetically. Essentially then, the single point resistance log indicates, as far as MT is concerned, uniform electrical properties over the entire depth scale of the well log, which is approximately 3 to 120 m. This agrees very well with the inverted results at the origin in Figures 6.5 and 6.6, especially from 20 to 120 m depth.

Shown in Figure 6.8 is a single point resistance log collected approximately 2.4 km north of the northern-most MT site (900 m from the origin in Figures 6.1 through 6.6). The most significant difference in the lithology between the well log of Figure 6.7 and that of Figure 6.8 is the more definitive presence of Empress group sands between approximately 80 to 100 m depth in the latter. This agrees with the interpretation above where the northward thickening of the resistive layer centered at about 150 m is interpreted to be due to the increasing presence Empress group sands. Also note

that the Bearpaw formation is clearly evident below the Empress sands, occurring in its usual composition of silt and clay shale.

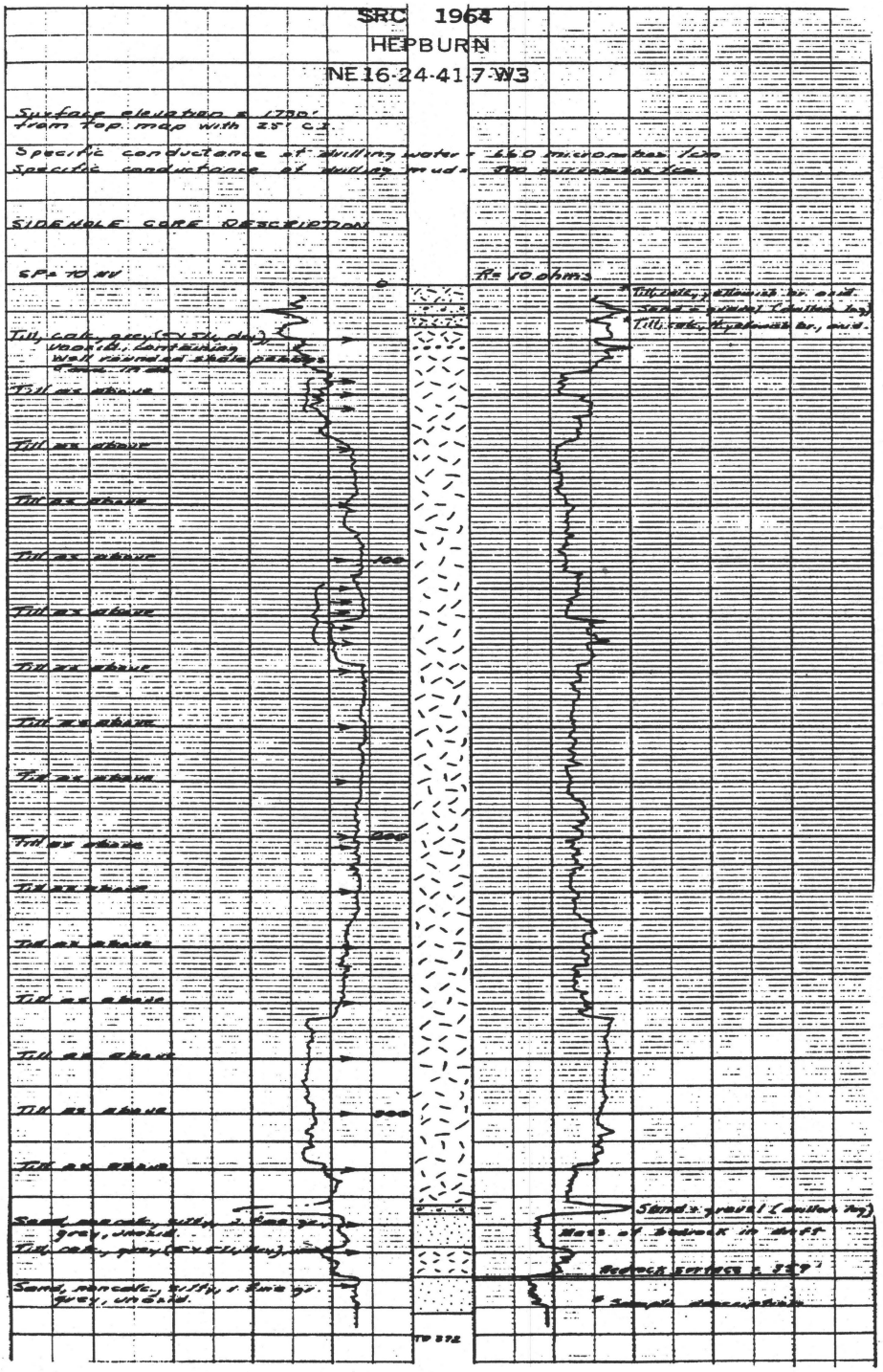

Figure 6.7: Simultaneous Self-Potential and Single Point Resistance Log

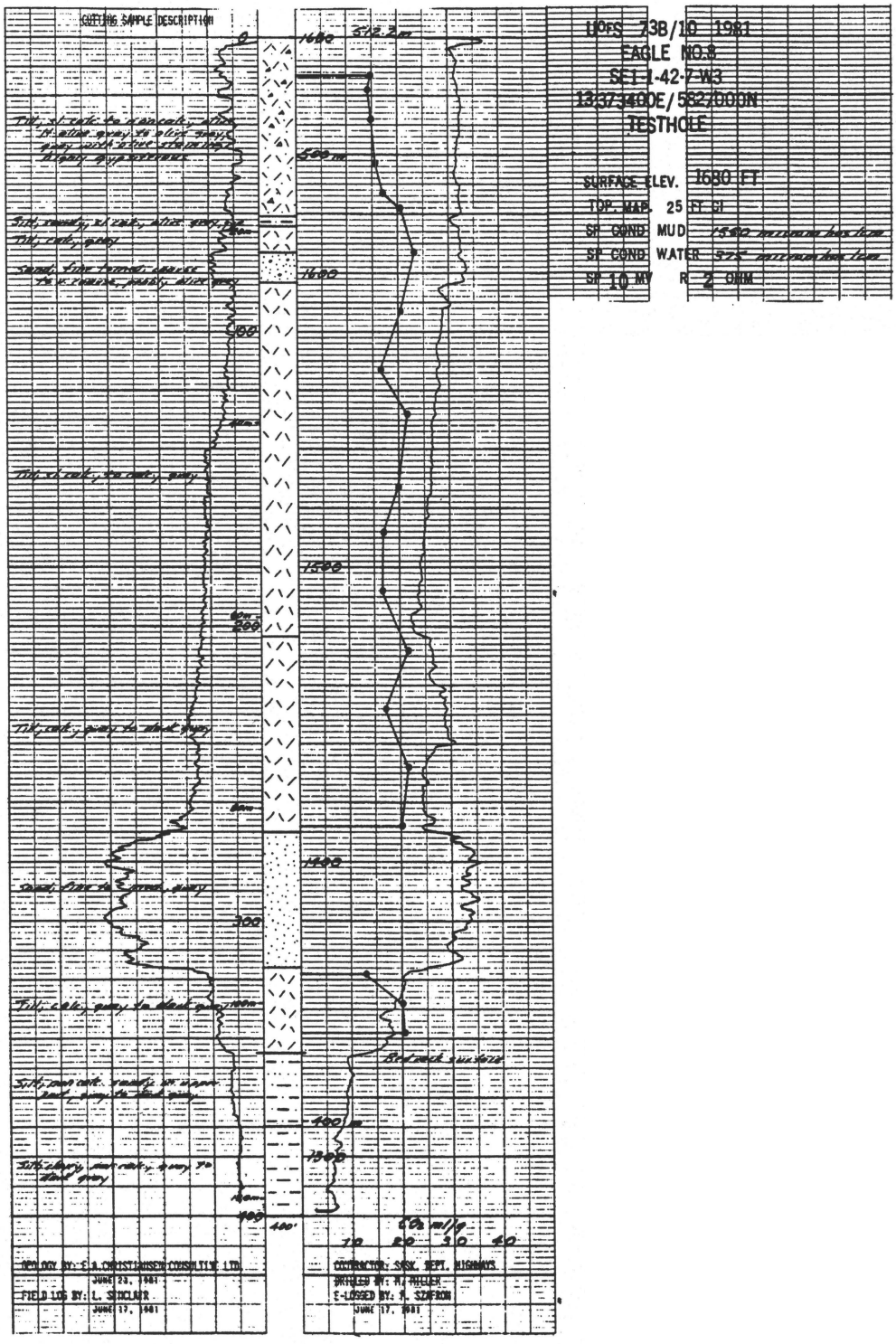

Figure 6.8: Simultaneous Self-Potential and Single Point Resistance Log

Due to the lack of deep well control in the present study, verification of the interpretation for depths exceeding 120 m is best accomplished with a reconnaissance oil well log, collected approximately 19 km south-west of the Hepburn site (the well log of Figure 1.3 was collected over 60 km south of the Hepburn site). However, because no lithology accompanies the oil well log (i.e., horizons have not been picked), it will not be shown. In any case, a resistive feature is noted on the well log between 125 and 150 m, this appears to be the Oldman formation, comprised of sand and silt. This agrees very well with the inverted results in the present study with the Oldman formation interpreted to occur from 130 to 160 m depth and 130 to 175 m depth, for the southern and northern MT sites respectively. Note that this well log was collected near the opposite edge of the Tyner valley than is the Hepburn site. Therefore, its proximity to the edge of the Tyner valley explains the presence of Oldman sands (see below).

The upper margin of the Lea Park formation or Upper Colorado group is interpreted to lie at approximately 160 - 175 m, however, its lower margin was not clearly imaged as a layer of uniform resistivity was found to extend to 420 m. The top of Lea Park determined in the present study compares quite well with the deep well log where the top of Lea Park occured at 150 m, below which a layer of approximately uniform resistivity extended to 365 m depth. At 365 m depth, a transition between the more resistive, calcareous base of Lea Park (Figure 1.3), to the more conductive non-calcareous Lower Colorado group is seen. This feature is absent at the Hepburn site with a layer of approximately uniform resistivity extending from 160 - 175 m, to 420 m depth. This shows that the calcareous base of Lea Park was not resolved as it constitutes a fairly thin electrical layer. Specifically, the calcareous base of Lea Park is indicated on the deep well log to have approximately the same resistivity as a shallow sand/gravel layer and is about 45 m thick, spanning the depth range of 315 to 360 m depth. This depth range is near the depth limit of the present study where skin depths are largest and therefore resolution the lowest; it is not unreasonable that this relatively thin resistive layer not be resolved.

Therefore, it appears that the deepest layer imaged in the present study was most likely the Lower Colorado group. However, because there is no appreciable resistivity contrast between the Lea Park formation and the Lower Colorado group, this statement

is based purely upon the deep well log. Therefore, we see that the bottom of Lea Park and top of Upper Colorado group appears to be unresolvable with an electromagnetic sounding. It is not until about 650 m depth, where the top of the Duperow formation occurs, comprised of limestone and dolomite, that a substantial resistivity contrast is seen. Therefore, an electromagnetic sounding would expect to see rather uniform resistivity from approximately 160 - 175 m to 650 m depth.

It is well known that the Oldman formation comprises the walls of the the Tyner valley aquifer system (Meneley, 1970). Most of the recharge to the Tyner valley aquifer results from lateral groundwater flow from the Oldman formation, comprising the walls of the aquifer, into the Empress group sands (Meneley, 1970) located mainly in the center of the buried valley. Therefore, it appears that at the southern-most MT sites, we are near the edge of a buried preglacial river valley. This is as expected (Figures 1.4a and b), and is evidenced by the presence of Oldman sands, which as stated above, comprise the walls of buried preglacial river valleys. However, as we move north we appear to be moving closer to the center of a buried valley, as opposed to farther away as initially expected. This is evidenced by the increasing presence of Empress group sands which are seen mainly near or over top of the center of buried preglacial river valleys. However, Oldman sands are still present at the northern-most MT sites which indicates that we are still, at least partially, on the edge of a buried valley and have not yet reached the center.

If the existence of a buried valley, perhaps a tributary valley, to the north were correct, then at additional MT sites collected further to the north, at or near the center of the valley, we would expect to see only Empress group sands lying between roughly 90 to perhaps 120 m depth. This is seen in the well log of Figure 6.8, collected approximately 2.4 km north of the northern-most MT site. Here, Empress group sands occur between approximately 80 and 100 m depth. However, because the well log extends to about 120 m only, it is not known whether Oldman sands are present at depth. As we hypothetically move further north still, we may expect to see the recurrence of the Oldman formation as we approach and cross the opposite side of the buried valley.

The presence of a buried preglacial river valley, or perhaps more likely, a tributary valley, the center of which may lie approximately 2 km to the north of the

northern-most MT site, has been hypothesized. This does not agree with a map of preglacial river valleys compiled by Christiansen (1967), which was based on well log information. In any case, with the small amount of MT data collected in the present study, only the presence of a tributary valley can be hypothesized with any degree of confidence. It would require many more MT sites to establish both the presence and orientation of the inferred tributary valley.

Lastly, note that a rule of thumb for accuracy of depth estimates to a layer with MT is ±10-30 percent (Zonge et al., 1991). However, based on good agreement with well logs, it appears that the present study is on the small side of this error range. Also, recall that one-dimensional inversions with the Bostick transform gives inherently smooth resistivity-depth profiles. This can make it difficult to decide where true layer boundaries are, particularly for resistive layers. Therefore, if the geology of an area is truly layered, and therefore the resistivity-depth profile sharply changing, a layered earth inversion may give more accurate results than that obtained with the Bostick transform. However, the Bostick transform gave very good results in the present study. This is evident in the good agreement between the inverted results and both nearby and regional well logs.

6.2 Winter MT Results

6.2.1 The Rabbit Lake Sounding

Shown in Figure 6.9 are the edited and raw, scalar resistivity and phase curves, collected at Rabbit Lake on February 18, 1996. Shown in Figure 6.10 is the Bostick transform of the Rabbit Lake data and shown in Figure 6.11 is a single point resistance well log, collected approximately 3 km away from the Rabbit Lake site. Recall that the purpose of the Rabbit Lake sounding was to demonstrate that valid MT data at ELF/VLF could be collected in the dead of winter at mid-high latitude. Consequently, only one site of data was collected and therefore, only a brief geological interpretation is included.

The inverted results indicate a near surface conductive layer which is consistent with the saline, and therefore conductive, mud waterbottom at Rabbit Lake. Such a

near surface conductive layer is not noted on the well log of Figure 6.11. However, the well log was collected over 3 km away from the Rabbit Lake site, hence near surface disagreement is not unreasonable. By 20 m depth, the inverted results show evidence of a uniform layer of resistivity, extending to about 50 m depth, below which a small resistive feature is present between about 50 to 65 m depth. From 65 to about 150 m depth, a more conductive layer is noted, below which a uniform, more resistive layer is present to the depth limit attained at the Rabbit Lake site, which was approximately 500 m.

Despite the rather large separation between the well log and the Rabbit Lake site, the inverted results agree reasonably well with the well log of Figure 6.11. Particularly, the well log indicates a relatively conductive till/silt layer from 8 to approximately 40 m depth. From 40 to 50 m depth, a resistive sand/gravel layer is noted, below which, more conductive till is seen to the depth limit of the well log, which is only 70 m. Note that depth estimates to the sand/gravel layer obtained with the Bostick transform are greater than that indicated on the well log. Differences here could be due both to the approximate nature of the Bostick transform and/or the occurrence of real geologic change over the more than 3 km separation between the well log and the measurement site.

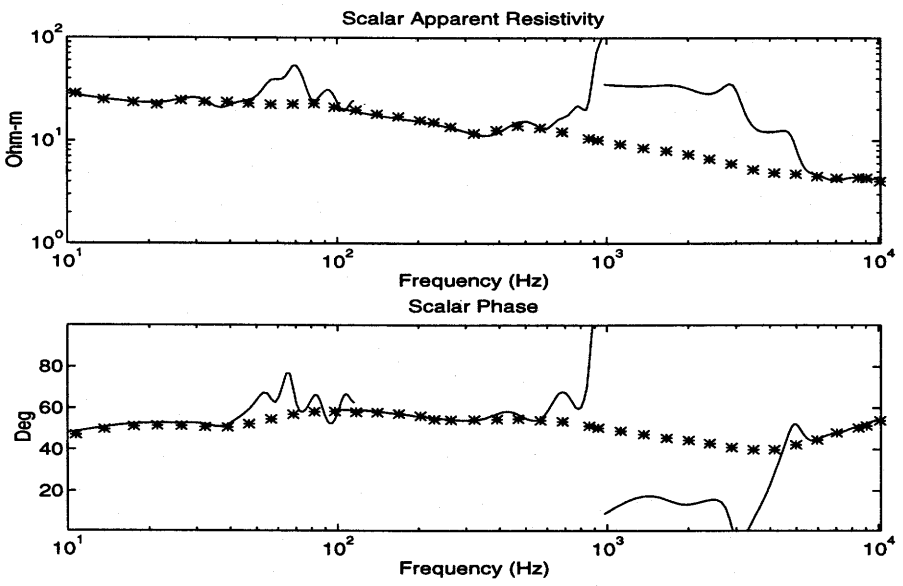

Figure 6.9: Scalar $\tilde{\rho}_{yx}$, $\tilde{\phi}_{yx}$, Rabbit Lake

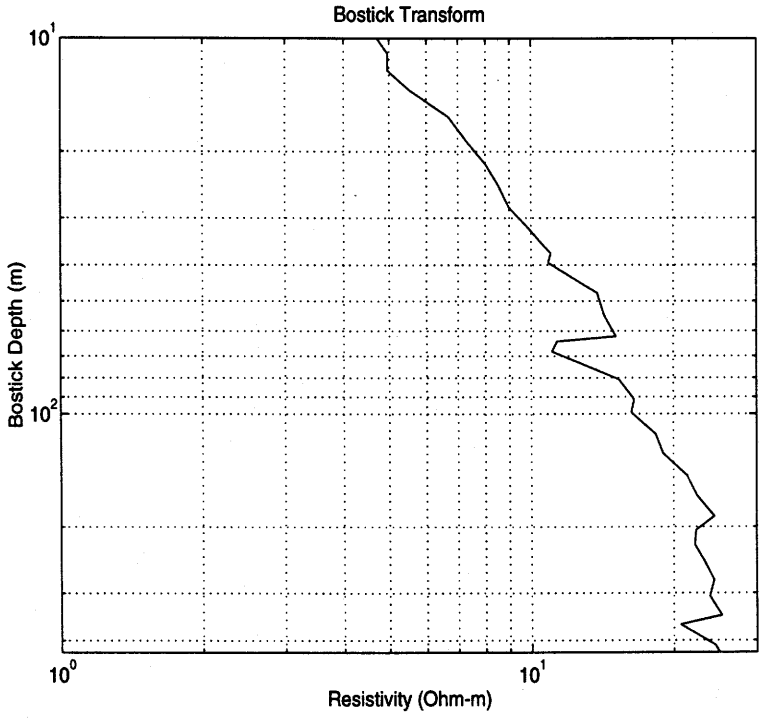

Figure 6.10: Bostick Transform of $\tilde{\rho}_{yx}$, $\tilde{\phi}_{yx}$ pair, Rabbit Lake

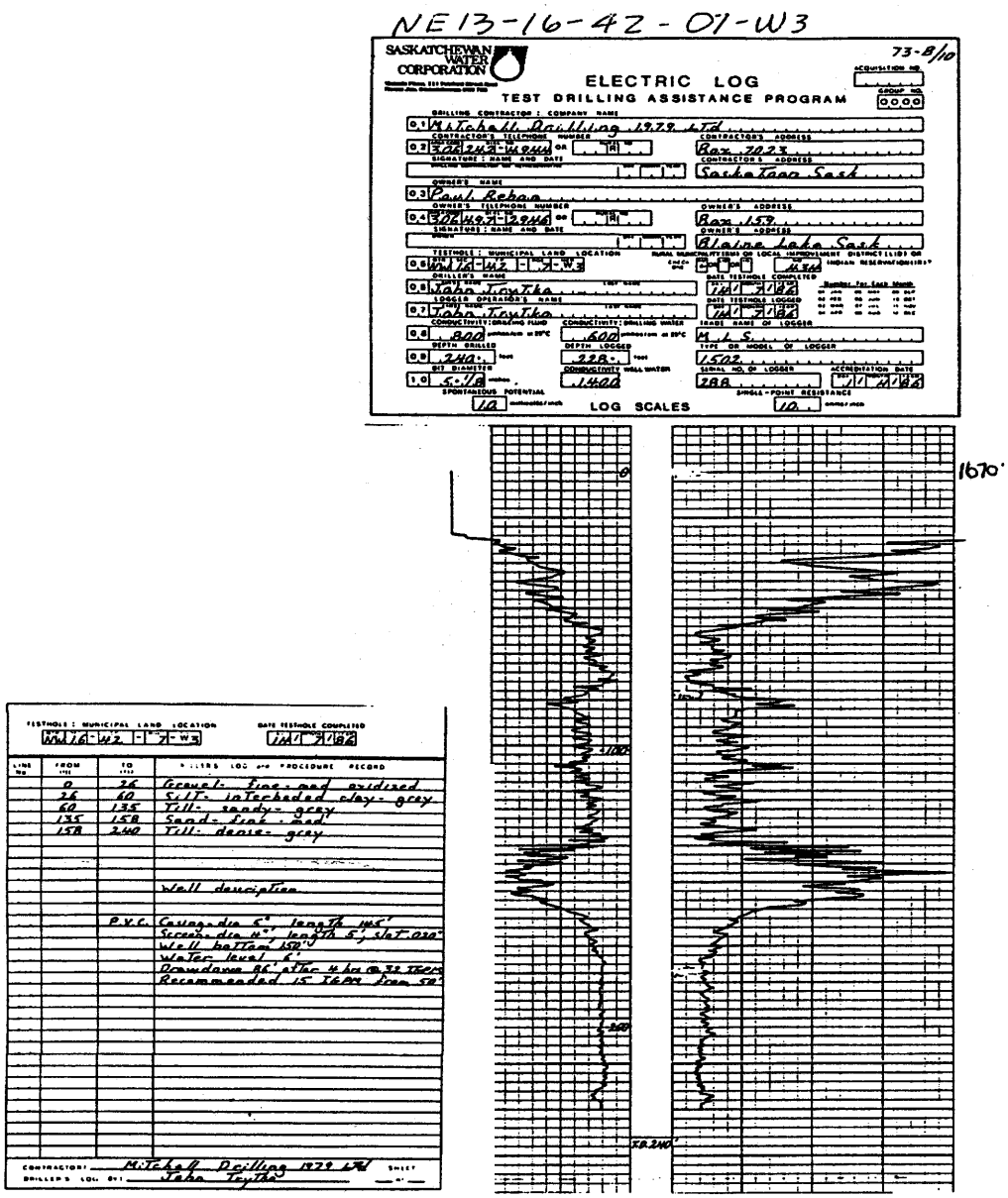

FROM	TO	DRILLER'S LOG AND PROCEDURE RECORD
0	26	Gravel - fine - rust oxidized
26	60	Silt - interbedded clay - grey
60	135	Till - sandy - grey
135	158	Sand - fine - wet
158	240	Till - dense - grey

Figure 6.11: Regional Single-Point Resistance and S.P. log, Rabbit Lake

6.2.2 The Frozen Ground Experiment

Shown in Figure 6.12 are the results of the winter MT data collection at the Hepburn site on March 17, 1996. This experiment investigated electric field measurements on frozen ground. Two methods were employed; stainless steel stakes were driven into the frozen ground and a non-contacting dipole antenna 100 m long was evaluated. The electric field data measured with the stainless steel stakes was found to be very noisy due to the extremely large contact resistance on frozen ground. Without the author's time localized data processing method, the March data on frozen ground with stainless steel stakes would be unusable due to the high levels of noise in the electric field data. The 100 m dipole antenna yielded measurable electric field data in High-Band only but was amplitude and phase distorted.

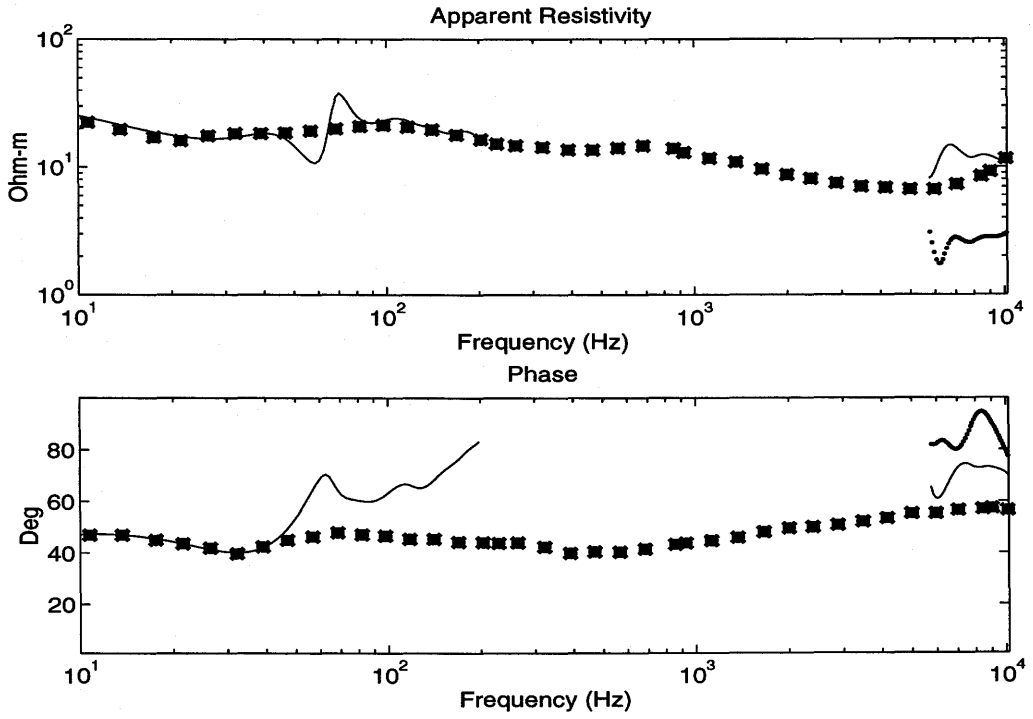

Figure 6.12: $\tilde{\rho}_{yx}$, $\tilde{\phi}_{yx}$ plots: From October, 1995, data using porous pot electrodes: "$*$". From March, 1996, data using stainless steel electrodes in frozen ground: "solid line". March, 1996, data using dipole antenna over frozen ground: "o".

Note that only the Low-Band portion of the resistivity curve, and less so the phase, was repeatable on frozen ground with the stainless steel electrodes. The High-Band

data collected with the stainless steel electrodes gave resistivity values that were biased upwards, presumably due to the high noise levels on the electric field channels. The dipole antenna yielded measurable electric field data in High-Band only, but gave resistivity values that were too small by about a factor of five. The very fact that we were able to measure electric field transients with the dipole antenna in High-Band gives insight into why the resistivity values with the stainless steel electrodes were too large in High-Band, it is hypothesized that they were too large because we were in fact detecting electric field transients in two fashions. Firstly, we detected the "conductive" electric field transient induced in the ground, albeit in a rather noisy fashion, and secondly we must also have been partly detecting the electric field in the air associated with the propagated transient. The efficiency with which the electric field associated with the propagated transient (in the air) is detected depends on contact resistance. As contact resistance increases we become more susceptible to having signals induced directly into the wires connecting the electrodes. Because the contact resistance on frozen ground is so large, this appears to be why the High-Band electric field data with stainless steel electrodes were biased upward, as we were in fact detecting two components of the electric field, one associated with the propagated transient and the other with the electric field induced in the earth.

Furthermore, for a given length, a dipole antenna becomes more efficient as frequency increases, which is why this problem appeared in High-Band only. The Low-Band signals were not distorted in this fashion, a 100 m dipole antenna was seemingly transparent to picking up signals out of the air at lower ELF. Therefore, with the author's time localized data processing method, repeatable resistivity and less so phase data were obtained on frozen ground with stainless steel stakes in Low-Band.

Also, because some small but finite capacitance exists between the wire laying on the earth's surface, and the earth itself, as contact resistance becomes large we can in effect create an RC, low pass filter which can further distort the high frequency electric field signal by draining a portion of it to ground (pers.comm., P.R. Kosteniuk). However, because high frequency electric fields in the present study were too large, this doesn't seem to have been a factor. It has also been stated that a horizontal wire lying on the earth's surface responds more to variations in the extremely intense vertical field across the previously mentioned capacitance (Polk, 1982). Whether or

not this was a factor in the present study is not known.

This quantitatively shows why it is imperative to minimize contact resistance when making electric field measurements with electrodes coupled galvanically to the earth. Furthermore, it is most important at high frequencies as this is where the connection wires laying on the ground have the most potential for picking up signals out of the air. The horizontal electric field is continuous across the air-earth interface, so theoretically, it should be possible to measure the same electric field above the surface of the earth as that measured within it by electrodes in galvanic contact with the earth. However, as clearly shown in the present study, measurement of the correct electric field in the air would require prohibitively large antennae for most, if not all, of the frequency band of interest for MT at ELF/VLF. Recall that even at 10 kHz, the correct electric field was not measured with a 100 m dipole antenna. Therefore, the best results are obtained for MT surveys at ELF/VLF when the electric field is measured with electrodes coupled either galvanically, or perhaps capacitively, with the earth.

Similar tests were carried out by Zonge (1986) in Arizona. In agreement with the present study, it was found that an ungrounded dipole antenna gave amplitude/phase distorted results, with artificially low electric fields measured. He obtained apparent resistivities too low by a factor of six at 2048 Hz. He also noticed that as contact resistance increased, high frequency electric field measurements are prone to error. To avoid this error as much as possible, particularly with high frequency electric field measurements, a differential measurement with three pots for each component is imperative. This is the configuration employed in the present study, the use of three pots for each component is desired as common mode noise picked up in the wires themselves, or otherwise, can be cancelled. Furthermore, for the October groundwater survey, shielded cables were also used, with the shields connected to ground. This was found to substantially decrease the amount of noise picked up in the lines themselves, especially at high frequencies. However, the shielded cables are quite delicate, therefore, more durable stainless steel wire was used for all the winter work.

To summarize, due to the high contact resistance on frozen ground, and therefore the vulnerability of picking up signals out of the air, High-Band electric field data were not recorded successfully with the stainless steel electrodes on frozen ground. In Mid-

Band, absolutely no signal was detected. This appears to be equipment related. In Low-Band the correct electric field was obtained with stainless steel stakes in frozen ground. With the time localized data processing method of the author, repeatable earth response curves were obtained in Low-Band. A 100 m dipole antenna was found to be completely ineffective as a horizontal electric field sensor in the frequency band 10 Hz to 10 kHz.

The use of so called active-pots or buffered probes (Zonge et al., 1991. Powell et al., 1981. Lafleche et al., 1981. Hoekstra et al., 1975) and capacitive electrodes (Macnae et al., 1991) to obtain reliable electric field data when working on frozen ground will be discussed further in Chapter 7.

Chapter 7

Conclusions and Recommendations for Future Work

7.1 Discussion

It has been shown in the present study that magnetotelluric measurements at ELF/VLF are of practical use for groundwater exploration in the sedimentary environment of southern Saskatchewan. Due to the location of the measurement sites, the Dalmeny aquifer was not imaged. However, because the deeper sand/gravel layers comprising the Tyner valley aquifer were imaged, there is no reason why the shallower Dalmeny aquifer may not also be imaged if present, as; due to its shallower depth and comparable thickness to the Tyner valley aquifer, it poses somewhat of an easier target. Therefore, magnetotelluric measurements are of use in groundwater studies in southern Saskatchewan, both for shallow and deep exploration.

It has further been shown that MT measurements at ELF/VLF can be carried out year round at mid-high latitude. Signal strengths are not inadequate in winter, as has been commonly stated. What is required however, is a recording method which exploits the time localized nature of the largest natural source signals present in the ELF/VLF bands of the geoelectromagnetic field. Such signals originate in electromagnetic radiation from *individual* lightning discharges, occurring usually within 5000 km of the measurement site for daytime recordings, although at lower ELF, electromagnetic radiation from lightning discharges can be truly received on a global scale. In

any case, a time localized recording method, denoted as the trigger recording method in the present study, allows MT measurements at ELF/VLF to be carried out year round at mid-high latitude, reducing the problem of winter MT surveys to one of time. That is, due to decreased thunderstorm activity in the northern hemisphere during the winter months, MT surveys at ELF/VLF simply require more time to collect data during the winter. This is seen to be the most important factor in assessing the viability of winter MT surveys at ELF/VLF, not signal strengths as has been commonly stated (Lakanen, 1986, Labson et al., 1985, Herisson, 1982, Hoover et al., 1978, Ward, 1959). Another problem for winter MT surveys at ELF/VLF, although certainly not insurmountable, is the increased width of the dead band caused by increased source-receiver separation in winter. A common dead band for summer MT measurements at ELF/VLF in Saskatchewan is 1-3 kHz (pers. comm., P.R.Kosteniuk), for winter measurements the dead band was found to increase in width to approximately 500 Hz to 5 kHz in the present study. Recommendations to counteract the lower activity and increased width of the dead band in winter MT recordings at ELF/VLF will be subsequently given. The interested reader is also referred to the recent work of Zhang (1997), wherein substantial advantages are shown to exist when MT data at ELF/VLF are processed with the wavelet transform.

7.2 Recommendations for Future Work

7.2.1 Groundwater Surveys

The search for groundwater contained in sand/gravel layers of a sedimentary basin is a challenging task for any geophysical method (Lennox and Carlson, 1967). Electromagnetic methods are no exception due both to the resistive nature of the targets and their usually small thickness relative to their depth of burial. For these reasons, high quality data are needed to image these difficult targets. In particular, results of one-dimensional forward modeling indicate that the phase is a much more sensitive indicator of resistive layering than is the apparent resistivity. Therefore, for groundwater exploration in a sedimentary environment, where resistivity contrasts may be three to five, accurate phase information is extremely important. Towards this end,

if a new instrument were built, a dedicated analog to digital (A/D) converter for each channel may be desired. This would achieve simultaneous sampling across all channels, thus removing the necessity of an A/D skew error correction and possibly resulting in more precise phase data. Also, careful selection of notch filter components is required so that phase drifts with temperature are minimized. Ideally, if notch filter components are truly identical, the phase drift with temperature will be the same on all channels so that the effect is negated when the impedance tensor, essentially the ratio of $\vec{E}$ over $\vec{B}$, is calculated. However, notch filter components are never truly identical and therefore phase drifts with temperature are invariably present. Instrumentation developed by EMI (Electromagnetic Instruments Inc.) incorporates a notch filter phase compensation routine in their data processing software to remove notch filter phase drift due to temperature variations. For Twin-T notch filters (Chapter 3), the complex transfer function is available in closed form. Therefore, a notch filter phase compensation program could be easily implemented if the variation in notch filter components (resistance, capacitance) as a function of temperature are known.

7.2.2 Decreasing the width of the Dead Band

Although approximately fifteen years old, GEOCOM-MT is arguably the best instrument in the world for MT measurements at ELF/VLF. However, because substantial improvements in electronics and computing power have occurred over this time, improvements in MT data quality and survey productivity could be realized in the construction of a new instrument with accompanying sensors.

One of the most significant improvements could be obtained in the use of a higher resolution analog to digital (A/D) converter. In chip form, single channel, successive approximation type, 16 bit A/D converters are available with maximum sample rates exceeding 500 kHz. Higher quality, delta-sigma type, single channel, 16, 18 and 20 bit A/D converters are available in chip form with maximum sample rates of 50 kHz per channel. Unfortunately, 24 bit A/D converters are presently available with maximum sample rates on the order of only 5 kHz per channel. However, use of all these A/D converters would require the construction of necessary analog front end circuitry and the coding of associated software for control of the A/D converters. Data acquisition boards designed for use inside field computers with delta-sigma type,

16 bit A/D converters for each channel, along with associated analog circuitry and control software are available with maximum sample rates of 52 kHz per channel. As mentioned previously, although more expensive, A/D boards with a dedicated A/D converter for each channel permits truly simultaneous sampling and would perhaps result in more precise phase data.

In any case, even a 16 bit A/D converter would offer a substantial increase in resolution and dynamic range over a 12 bit A/D converter, as is used with GEOCOM-MT. Note that the increase in dynamic range with higher resolution A/D converters is achieved through being able to digitize smaller amplitude signals. This is reflected in the fact that a single digitization level with a 12 bit A/D converter corresponds to 16 digitization levels with a 16 bit A/D converter, 64 levels with an 18 bit and 256 levels with a 20 bit A/D converter. The higher resolution offered by a 20, 18 or 16 bit A/D converter would help decrease the width of the dead band by being able to more accurately digitize the small signals around the edges of the dead band, assuming induction coils and electric field sensors of sufficient sensitivity are used. Whether or not one would expend the additional effort, and most likely cost, to custom build an A/D board using an 18 or 20 bit A/D converter would be contingent upon a decrease in dead band width obtained through their use.

Another area where significant progress could be made in decreasing the width of the dead band is through the use of more sensitive induction coil magnetometers. In particular, the BF-6 induction coil, manufactured by EMI, is advertised as having a sensitivity of .3 V/nT from 10 Hz to 40 kHz. Induction coils manufactured by Metronix have similar sensitivities. These sensitivities are much higher than the induction coil used in the present study which has a maximum sensitivity of about .055 V/nT at 1300 Hz, which subsequently falls to approximately .035 V/nT at 10 kHz. We see that induction coils commercially available at this time have sensitivities on the order of six times that of the induction coil used in the present study. This is perhaps not surprising considering that the original design of the induction coil used in the present study is approximately twenty years old. Both EMI and Metronix manufacture their coils with a magnetic feedback design and therefore sense the current in the induction coil, as opposed to the voltage, as is done with the coil used in the present study (Chapter 3). Induction coils designed by Metronix additionally have the option of

being able to tailor the amplitude response of the induction coil to expected signal amplitudes as a function of frequency. In this case, it would be desirable to obtain maximum sensitivity over the range 500 Hz to 5 kHz, where spectral content is reduced on average. Induction coils manufactured by EMI have a very simple response, which is extremely flat over the operating range of the coils (Chapter 3). Regardless, commercially available induction coils would offer much increased sensitivity over that used in the present study and would therefore help decrease the width of the dead band.

In particular reference to winter MT surveys, if logistically possible, night-time recordings would be advantageous because of enhanced propagation conditions at night and therefore, richer spectral content in received transients (i.e., narrower dead band). Herisson (1982) found that higher quality MT data were obtained in night-time recordings in his winter MT test survey in northern Saskatchewan. Specifically, better quality data were obtained across a wider bandwidth than what was obtained during daytime recordings. The study of Dinger et al. (1980) also found enhanced levels of 3 kHz atmospheric noise (MT signal) during night-time recordings, once again, this comes about as a result of enhanced propagation conditions. Similarly, Ward (1959) found that nocturnal signal amplitudes at 500 Hz were much increased over those present during the daytime. However, due to the difficulty of working at night, night-time MT recordings are probably only practical on a frozen lake, as done by Herisson (1982), where less obstructions are present.

7.2.3 Improving the Productivity of MT surveys at ELF/VLF

In the absence of geological inhomogeneities, the horizontal magnetic field associated with a propagated transient is uniform over distances of the order of a free space wavelength (pers. comm., K.V. Paulson, Labson et al., 1985). Studies by Dinger et al. (1980) in the lower ELF range have confirmed the homogeneity of the magnetotelluric source field over distances of tens of kilometers, thus giving further evidence of the correctness of the plane wave assumption. A new instrument could be constructed to exploit the uniformity of the magnetotelluric source field by collecting electric field data at three sites simultaneously and using either a single induction coil magnetometer, or perhaps a pair, if remote reference techniques were incorporated.

Multi-site recording of the electric field was in fact presented in the original design of GEOCOM-MT but was not incorporated due to financial constraints (pers. comm., Dr. K.V. Paulson). In the context of multi-site electric field recordings, one advantage of remote reference is that any nonhomogeneity of the source field, due to the distortion of sub-surface currents by geologic structure, could be directly measured (see below). As stated above, the assumption of source field homogeneity holds in simple geological environments. In more complex environments, as is generally the case in mining oriented surveys, this assumption can break down. Zonge et al. (1991) have found that substantial errors in apparent resistivity and phase data can result in some cases. However, this is generally more of a problem for controlled-source surveys where electric field data is collected simultaneously at as many as six scalar sites while using only one induction coil magnetometer. Zonge et al. (1991) have found that a good compromise between speed and data accuracy is to measure two or three sites simultaneously. If remote reference data processing was incorporated into the design of a new instrument, each one of the magnetometers could be placed at the outer sites, thus obtaining the correct magnetic field input at the extremities of the three site array, if any differences are present between the two outer measurements, simple linear interpolation could be done to obtain the approximate magnetic field input at the centrally located site. In this fashion, we obtain a three-fold increase in productivity over GEOCOM-MT, and are in effect, measuring any departure from source field homogeneity over the extent of our electric field array.

Another benefit of measuring the electric field at three sites simultaneously is obtained through increased averaging of any near surface irregularities and therefore much decreased risk of what is commonly called "static shift". Note that because most controlled-source surveys are scalar, small dipole lengths of 30 m are commonly used in an attempt to compensate for the shortcomings of a scalar measurement in mapping geologic structure. Therefore, the so called static shift problem is much worse for controlled-source surveys than for natural-source tensor surveys.

Furthermore, with a 20, 18 or 16 bit A/D converter, due to the much increased dynamic range over a 12 bit A/D converter, it should be possible to record the entire bandwidth 10 Hz to 10 kHz, or higher, simultaneously. The very fact that the present study was able to record slow tails or ELF energy, which sometimes accompany VLF

transients, with a 12 bit A/D converter, clearly shows that this is possible. However, a larger dynamic range than that afforded by a 12 bit A/D converter is probably generally required so that the smaller ELF component of the transient can be accurately tracked in the presence of the relatively large VLF component of the transient. Recall that Taylor and Sao (1970) found that slow tail energy was a maximum in the range 30-150 Hz. Therefore, every slow tail found to accompany VLF transients in the present study most likely possessed significant energy over this frequency range as well. It was simply not observed as the lowest frequency that could be resolved with GEOCOM-MT in High-Band, as used in the present study, was approximately 100 Hz. Therefore, instead of dividing the bandwidth 10 Hz to 10 kHz, or higher, into narrow overlapping frequency bands, adjusting gain levels appropriately and subsequently recording these frequency bands separately, the entire bandwidth could be recorded at once as there would be less of a requirement to pre-whiten the instrument bandwidth with a higher resolution A/D converter. This would also reduce the recording time necessary to obtain high quality earth response curves. However, recall that not every lightning discharge radiates significant ELF energy (i.e., not all events have slow tails), therefore, impedance calculations with individual events would be carried out only over the frequency bands where substantial signal energy is present. This could probably be best determined through visual inspection of every triggered event, or perhaps automatically through a coherency based calculation, although with the latter approach we are susceptible to erroneous results when noise is coherent between $\vec{E}$ and $\vec{B}$ channels.

Another benefit of recording the entire bandwidth at once is that by triggering off of the large VLF transient, successful data collection may be possible in noisier environments. This is noted as the threshold required for triggering off of a VLF transient is easily an order of magnitude higher than that required for triggering off of a typical ELF transient. Therefore, by triggering off of the larger VLF component, we are less susceptible to triggering off of noise, and any ELF energy that may accompany the large VLF transient will be successfully recorded also. Therefore, even if the ELF signal level is at or below the noise level at a site, by triggering off of the VLF component, any ELF signal energy, if present, is also recorded. The problem then becomes how to extract the ELF signal from the noisy time domain recordings, the

wavelet transform may be of help in cases such as these (Zhang, 1997).

Once again, in particular reference to winter MT surveys, it may be advantageous to work at night because of enhanced activity levels at night, which arise at least partly due to enhanced propagation conditions at night. Note that changes in activity can arise solely out of enhanced propagation conditions, or to increased thunderstorm activity, or a combination of both factors. In the study of Lugeon et al. (1959) (Chapter 1), at both mid latitude and polar sites, activity was consistently highest during local night in the fall and winter months. Lugeon et al. (1959) interpreted this to be due to a combination of enhanced propagation conditions and peaked oceanic thunderstorm activity in winter. The hypothesis of enhanced oceanic thunderstorm activity in winter agrees with the studies of Vonnegut (1982), Orville et al. (1979), Wallace (1974) and the World Meteorological Association (1956) (Chapter 5). It should be noted that at mid latitude sites the nocturnal maximum is present year round, however, in summer time, a second maximum is also present giving rise to what lightning researchers call a double humped activity curve. That is, one activity peak caused by near-distant thunderstorms, which tends to occur at local mid to late afternoon, and a second nocturnal peak arising due to enhanced propagation conditions at night and perhaps also peaked oceanic thunderstorm activity in winter. However, because of the absence of local thunderstorm activity during the winter months, the daytime hump is not seen and only the nocturnal maximum survives.

7.2.4 General Improvements

Remote reference has been a very successful addition to MT data processing but has been mainly used at the lower micropulsation range of frequencies, less than approximately 1 Hz. As signal levels are generally weaker in the winter months (Chapter 5), remote reference would most likely be a valuable addition for winter MT surveys at ELF/VLF, and in general. Vozoff (1991) has stated that remote reference data processing has routinely allowed usable data to be extracted under the conditions of signal-to-noise ratio ≤ 1. Therefore, remote reference may also be valuable for decreasing the width of the of the ELF/VLF dead band. Furthermore, due to the reduction of noise in impedance tensor estimation, high quality earth response curves should be obtainable with fewer events and therefore also lead to better productivity. The disad-

vantage of remote reference is the extra cost required in the purchase or construction of twice as many induction coil magnetometers. Also, it is of no help in cases when coherent noise exists between the two induction coil magnetometers.

The incorporation of the tipper, which requires measurement of the vertical component of the magnetic field, would also be desired for a new system. For measurement of the vertical magnetic field component, a large air-core loop, perhaps similar to the one used in the study of Dinger et al. (1980) may be desired. The advantage of this approach is that the long, slender induction coils used for measurement of the horizontal components can be housed in a separate, low profile enclosure, as per the induction coil magnetometer used in the present study. This would allow both the horizontal component induction coils and the vertical component coil to be more easily shielded from the wind. As mentioned previously, in simple one-dimensional environments, no vertical component of the magnetic field exists, however, in more complex areas, the tipper is a useful aid in delineating faults and shear zones and is therefore particularly useful for mining oriented surveys (Vozoff, 1991., Labson et al., 1985. Ward, 1959).

A new instrument could also be designed to acquire MT data to frequencies much higher than the 10 kHz limit of the present study, this would of course depend on the A/D converter used. However, it is apparently not worthwhile, on average, to extend the highest frequency of investigation above about 50 to 70 kHz as greater than this frequency range signal reception is heavily dependent on source-receiver separation. Therefore, data above 70 kHz would probably not be consistently obtained year round at mid-high latitude. According to Spaulding (1982), the amount of energy at 50 kHz is on average, approximately the same as that at 5 kHz, which is of course, approximately the upper edge of the winter ELF/VLF dead band in the present study. Pierce (1977) shows a calculated amplitude distribution of a sferic with a source-receiver separation of 3000 km. Here the amplitude at about 70 kHz is approximately the same as that at 5 kHz. Therefore, it appears that we could expect to receive energy from sferics, on a year round basis at mid-high latitude to about 50 to 70 kHz, but perhaps not higher. This follows as storms located in the present study were found to be approximately 2000-4000 km distant at mid-high latitude during the fall/winter months.

The use of higher frequencies is attractive because it allows shallower depths of investigation and thus provides more sub-surface resistivity information. This par-

ticularly impacts on the so called static shift problem, which essentially arises due to undersampling in time and space (Vozoff, 1991). As a result, this effect is much reduced through the use of higher frequencies which enables one to image the near surface more effectively. This phenomenon is a major problem for surveys conducted with commercial instruments as many times high frequency information is lacking (Chouteau et al., 1997, Livelybrooks et al., 1996), most likely due to the poor recording technique employed (Chapter 5). As a result, some MT contractors have additionally hired TEM contractors to obtain the near surface resistivity information lacking in the original MT sounding (Sternberg et al., 1988). However, this would not be required for a new instrument built in the tradition of GEOCOM-MT as excellent quality data could be obtained easily as high as 24 kHz thus obtaining the required near surface resistivity information. Therefore, the major concern then becomes correcting the data for topographic variations (pers. comm., Dr. K.V. Paulson).

Note also that as we move to higher frequencies in the VLF range, we run the risk of triggering off of the man made, naval communication signals. The danger in so doing is that these signals are essentially single frequency and possess a single polarization, therefore they are not desired for estimation of the impedance tensor. However, it appears as though these signals are usually quite small, on the order of 10 pT or less, when the observation site is at moderate distance from the VLF antenna ($\geq$ 1000 km). This is to be compared with the natural source signal amplitude in this frequency range, usually greater than 500 pT. Therefore, the man made VLF signals would constitute a small background signal under most circumstances.

7.2.5 Electric Field Sensors

More field work needs to be carried out in determining the most effective method for making electric field measurements on frozen or highly resistive ground. Due to the success at lower ELF of the March experiment on frozen ground, using stainless steel stakes, it appears that the active pot configuration should be able to provide usable quality electric field data in such cases. This is perhaps not surprising as successful electric field measurements at upper VLF have been reported with VLF-R (Chapter 1) instruments working on frozen ground with the active pot design (Powell et al., 1981., Lafleche et al., 1981., Hoekstra et al., 1975., Collet and Becker, 1968.). With the active

pot design, the connecting wire running back to the recording instrument is driven at the output impedance of the op-amp. This effectively removes the possibility of the connecting wire acting as an antenna, detecting unwanted signals out of the air. This prevents high frequency signal distortion and has been used extensively for making valid electric field measurements at upper VLF and above on highly resistive ground. Zonge et al. (1991) has also used this configuration successfully for controlled-source measurements on highly resistive ground.

The possibility of using capacitive electrodes for MT electric field measurements also needs to be investigated. Their successful use over the bandwidth 5 Hz to 50 kHz in the UTEM system (Chapter 1), on frozen ground, has been published by Macnae et al. (1991). No design information was given in their paper, hence research would need to be done in their application to MT measurements at ELF/VLF. If they could be used effectively, they would significantly enhance the productivity of winter MT surveys due to their ease of use.

Also, as originally presented by Schmucker and Weidelt (1975), the possibility of measuring the horizontal electric field through the vertical gradient of the horizontal $\vec{B}$ field could also be investigated. Such a configuration has been patented by Vozoff (1982), although one in which SQUID magnetometers are used which therefore limits its use to low frequencies. However, one should note that VLF signal amplitudes are comparable with micropulsation signal amplitudes. Therefore, if signal amplitudes alone are any indication, this method may also work at VLF. The critical frequency range would most likely be from 10-1000 Hz.

Bibliography

[1] Barr, R. , 1970, The propagation of ELF and VLF radio waves beneath an inhomogeneous anisotropic ionosphere, *Journal of Atmospheric and Terrestrial Physics*, **33**, 343–353.

[2] Becker, A., 1967, Design formulas for electromagnetic sensing coils, *Geoexploration*, **5**, 81–88.

[3] Beckman, P., 1967, *Probability in communication engineering*, Harcourt, Brace and World Inc.

[4] Bernard, J., C. Vachette and P. Valla, 1990, Deep groundwater survey with audiomagnetotelluric soundings, *60'th Annual International Meeting of the Society of Exploration Geophysicists, Expanded Abstracts*, 528–531.

[5] Boehl, J.E., F.X. Bostick and H.W. Smith, 1977, An application of the Hilbert transform to the magnetotelluric method, *Electrical Geophysics Research Laboratory, The Univerisity of Texas at Austin*, Naval Research Contract N00014-76-C-0484.

[6] Bostick, F.X., 1977, A simple almost exact method of MT analysis, *Workshop on electrical methods in geothermal exploration*, Snowbird, Utah.

[7] Bostick, F.X., 1985, Z-Axis Exploration Inc., EMAP, *Z-Axis Inc.*, unpublished brochure.

[8] Bourgeois, B., F. Mathieu, C. Vachette and P. Vaubourg, 1994, AMT measurements compared with gravimetry and magnetometry for structural study of a sedimentary basin: Letlhakeng-Botlhapatlou groundwater project, Botswana, *Journal of Applied Geophysics*, **31**, 7–25.

[9] Brook, M. and T. Ogawa, 1977, The cloud discharge, in Golde, R.E., ed., *Lightning.*, **1**, Academic Press.

[10] Brooks, C.E.P., 1925, The distribution of thunderstorms over the globe, *Geophysical Memo. 3.*, **24**, 147–164 (Air Ministry, Meteorological Office, London, England).

[11] Cagniard, L., 1953, Basic theory of the magneto-telluric method of geophysical prospecting, *Geophysics*, **18**, 605–635.

[12] Campbell, W.H., 1967, Geomagnetic Pulsations, in Matsushita S. and W.H. Campbell, eds., *Physics of Geomagnetic Phenomena*, Academic Press.

[13] Cantwell, T., 1960, Detection and analysis of low frequency magnetotelluric signals, *Mass. Inst. Tech.*, Ph.D. thesis.

[14] Challinor, R.A., 1967, The phase velocity and attenuation of of audio-frequency electromagnetic waves from simultaneous obsrvations of atmospherics at two spaced stations, *Journal of Atmospheric and Terrestrial Physics*, **29**, 803.

[15] Chapman, F.W., D.L. Jones, S.D.W. Todd and R.A. Challinor, 1966, Observations on the propagation constant of the earth-ionosphere waveguide in the frequency band 8 c/s to 16 kc/s, *Radio Science*, **1**, 1273.

[16] Chen, K., 1991, A magnetotelluric survey near Creston, British Columbia, unpublished M. Sc. thesis, University of Saskatchewan. Saskatoon.

[17] Chouteau, M., P. Zhang, D.J. Dion, B. Giroux, R. Morin and S. Krivochieva, 1997, Delineating mineralization and imaging the regional structure with magnetotellurics in the region of Chibougamou (Canada), *Geophysics*, **162**, no.3, 730–748.

[18] Christian, H.J. and M.A. McCook, 1996, Lightning detection from space, *NASA*, http://www.msfc.nasa.gov.

[19] Christiansen, E.A., 1970, *Physical environment of Saskatoon, Canada*, National Research Council of Canada, **11378**.

[20] Collett, L.S. and A. Becker, 1968, Radiohm method for earth resistivity surveying, *Canadian patent*, **795919**.

[21] Dennis, A.S., 1965, Lightning observations from satellites, *Stanford Research Institute*, Project **4877**.

[22] Dinger, R.J., W.D. Meyers and J.R. Davis, 1980, Experimental measurements of ambient electromagnetic noise from 1.0 to 4.0 kHz, *Naval Research Laboratory*, Report **8413**.

[23] Dinger, R.J. and J.A. Goldstein, 1980 Spatial coherence measurements and evaluation of a noise reduction technique for ambient noise from 0.3 to 40 Hz, *Naval Research Laboratory*, Report **8430**.

[24] E.D.A. Instruments, SAGAX, Scalar audiomagnetotelluric system, *EDA Instruments*, promotional brochure.

[25] Fischer, G. and P.A. Schnegg, 1979, The dispersion relations of the magnetotelluric response and their incidence on the inversion problem, *Geophysical Journal, Royal Astronomical Society*, **53**, 599–616 .

[26] Fortin, G., G. van der Kamp and J.A. Cherry, 1990, Hydrogeology and hydrochemistry of an aquifer-aquitard system within glacial deposits, Saskatchewan, Canada, *Journal of Hydrology*, **126**, 265–292.

[27] Gamble, T.D., W.M. Goubau and J. Clarke, 1979, Magnetotellurics with a remote reference, *Geophysics*, **44**, 53–68.

[28] Grant, F.S. and G.F. West, 1965, *Interpretation theory in applied geophysics*, Mcgraw-Hill.

[29] Griffiths, D.J., 1989, *Introduction to electrodynamics*, Prentice Hall.

[30] Groom, R.W. and R.C. Bailey, 1989, Decomposition of magnetotelluric impedance tensors in the presence of three dimensional galvanic distortion, *Journal of Geophysical Research*, **94B**, 1913–1926.

[31] Hammer, U.T., 1978, The saline lakes of Saskatchewan, a chemical characterization, Part 3 *Int. Revue. Ges. Hydrobiol.*, **63**, 311–335.

[32] Hepburn, F. and E.T. Pierce, 1953 Atmospherics with very low frequency components, *Nature (London)*, **171**, 837.

[33] Herisson, P., 1982, *Winter MT test survey in Northern Saskatchewan*, AGIP Canada, Internal report.

[34] Hessler, V.P. and A.R. Franzke, 1958, Earth potential electrodes in permafrost and tundra, *Arctic*, **1**, 211–217.

[35] Hoekstra, P., P.V. Sellman and A. Delaney, 1975, Ground and airborne resistivity surveys of permafrost near Fairbanks, Alaska, *Geophysics*, **40**, no. 4, 641–656.

[36] Hoover, D.B., F.C. Frischknecht and C.L. Tippens, 1976, Audiomagnetotelluric sounding as a reconnaissance technique in Long Valley, California, *Journal of Geophysical Research*, **81**, no. 5, 801–809.

[37] Hoover, D.B., C.L. Long and R.M. Senterfit, 1978, Some results from audiomagnetotelluric investigations in geothermal areas, *Geophysics*, **43**, no. 7, 1501–1514.

[38] Hughes, H.G., 1967, On the directional properties of slow tail atmospherics waveforms, *Journal of Atmospheric and Terrestrial Physics*, **29**, 545–552.

[39] Idone, V.P., A.B. Saljoughy, R.W. Henderson, P.K. Moore and R.B. Pyle, 1993, A re-examination of the peak current calibration of the National Lightning Detection Network,*Journal of Geophysical Research*, **98**, no. 10, 18323–18332.

[40] Jones, D.L. and D.T. Kemp, 1971 The nature and average magnitude of the sources of transient excitation of Schumann resonances, *Journal of Atmospheric and Terrestrial Physics*, **33**, 557–566.

[41] Kalantzis, F., 1990, Magnetotelluric experiment in Southeast Turkey: Data acquisition and imaging with electromagnetic reflectivity sections, unpublished M. Sc. thesis, University of Saskatchewan, Saskatoon.

[42] Keller, G.V. and F.C. Frischknecht, 1966, *Electrical Methods in Geophysical Prospecting*, Pergamon Press.

[43] Keys, W.S., 1989, *Borehole geophysics applied to groundwater investigations*, National Water Well Association.

[44] Kinzer, G.D., 1974, Cloud-to-ground lightning versus radar reflectivity in Oklahoma thunderstorms, *Journal of Atmospheric Science*, **31**, 787.

[45] Kitigawa, N. and M. Brook, 1960, A comparison of intracloud and cloud-to-ground lightning discharges, *Journal of Geophysical Research*, **65**, no. 4, 1189–1201.

[46] Kosteniuk, P.R. and K.V. Paulson, 1988, The application of polarization stacking to natural-source magnetotellurics, presented at, *Annual meeting of the Canadian Geophysical Union.*

[47] Kosteniuk, P.R., Topographic corrections of magnetotelluric responses, *Cybernetics Laboratory Research Memorandum* **CL-90-1**, University of Saskatchewan, Saskatoon.

[48] Krider, E.P., R.C. Noggle and M.A. Uman, 1976, A gated wideband magnetic direction finder for lightning return strokes, *Journal of Applied Meteorology*, **15**, 301.

[49] Kunetz, G., 1972, Processing and interpretation of magnetotelluric soundings, *Geophysics*, **37**, 1005–1021.

[50] Labson, V.F., A. Becker, H.F. Morrison and U. Conti, 1985, Geophysical exploration with audiofrequency natural magnetic fields, *Geophysics*, **50**, no. 4, 656–664.

[51] Lafleche, P.T.and O.G. Jensen, 1981, Wave impedance measurements at 60 kHz, in Jensen, O.G. and L.S. Collett, eds., 1981, *Geophysical applications of surface wave impedance measurements*, Geological Survey of Canada, **81-15**.

[52] Lakanen, E., 1986, Scalar audiomagnetotellurics applied to base- metal exploration in Finland, *Geophysics*, **51**, no. 8, 1628–1646.

[53] Lennox, D.H. and V. Carlson, 1967, Integration of geophysical methods for groundwater exploration in the prairie provinces, Canada, in Morley, L.W., ed., *Mining and groundwater geophysics*, Geological Survey of Canada, report **26**.

[54] Livelybrooks, D., M. Mareschal, E. Blais and J.T. Smith, 1996, Magnetotelluric definition of the Trillabelle massive sulfide body in Sudbury Ontario, *Geophysics*, **61**, no. 4, 971–986.

[55] Lugeon, J., A. Junod, P. Wasserfallen and J. Reiker, 1959, Mesures de parasites atmospheriques d'electricite atmospherique et de radioactivite de l'air a Murchison Bay (Spitzberg), *Payerne et Zurich*, Zurich.

[56] Lukoschus, D.G., 1979, Optimization theory for induction coil magnetometers at higher frequencies, *IEEE Transactions on GeoScience Electronics*, **GE-17**, no. 3, 56–63.

[57] Macnae, J.C., Y. Lamontagne and G.F. West, 1984, Noise processing techniques for time-domain EM systems, *Geophysics*, **49**, 934–948.

[58] Macnae, J.C. and P. McGowan, 1991, Quantitative resistance and capacitive electrodes: new developments in inductive source resistivity, *Exploration Geophysics* (Australian), **22**, 251–256.

[59] Madden, T. and P. Nelson, 1964, A defense of Cagniard's magnetotelluric method, in Vozoff, K., ed., 1986, *Magnetotelluric methods*, Society of Exploration Geophysicists.

[60] Malan, D.J., 1958, Radiation from lightning discharges and its relation to the discharge process, in Smith, L.G., ed., *Recent advances in atmospheric electricity*, Pergamon Press.

[61] Marriot, W., 1908, Brontometer records at west Norwood, June 4, 1908, *Quarterly Journal of the Royal Meteorological Society*, **34**, 210–212.

[62] McDonald, T.B., M.A. Uman, J.A. Tiller and W.H. Beasely, 1979, Lightning location and lower ionospheric height determination from two station magnetic field measurements, *Journal of Geophysical Research*, **84**, 1727.

[63] McCracken, K.G., J.P. Pik and R.W. Harris, 1984, Noise in EM exploration systems, *Exploration Geophysics* (Australian), **15**, 169–174.

[64] McCracken, K.G., M.L. Oristaglio and G.W. Hohmann, 1986, Minimization of noise in electromagnetic exploration systems, *Geophysics*, **51**, 819–832.

[65] Meneley, W.A., 1970, Groundwater resources, in Christiansen, E.A., ed., *Physical environment of Saskatoon, Canada*, National Research Council of Canada, **11378**.

[66] Nabighian, M.N. and J.C. Macnae, 1991, Time domain electromagnetic prospecting methods, in Nabighian, M.N., ed., *Electromagnetic methods in applied geophysics*, **2**, part A, Society of Exploration Geophysicists.

[67] Netzer, Y., 1981, The design of low-noise amplifiers, *Proceedings of the IEEE*, **69**, no. 6, 728–741.

[68] Nichols, E.A., H.F. Morrison and L. Seunghee, 1994, Controlled source magnetotellurics for groundwater, *64'th Annual International Meeting, Society of Exploration Geophysicists*, Expanded Abstracts, 553–554.

[69] Orville, R.E. and D.W. Spencer, 1979, Global lightning flash frequency, *Monthly Weather Review*, **107**, 934–943.

[70] Orville, R.E., 1994, Cloud-to-ground lightning flash characteristics in the contiguous United States: 1989-1991, *Journal of Geophysical Research*, **99**, no. D5, 10833–10841.

[71] Padilha, A.L., N.B. Trivedi, J.M. da Costa, I. Vitorello, A. Dupis and C. Cavoit, 1989, Audiomagnetotelluric study in northeast region of Parana basin, South America, *Geophysics*, **54**, 824–831.

[72] Palacky, G.J. and G.F. West, Airborne electromagnetic methods, in Nabighian, M.N., ed., *Electromagnetic methods in applied geophysics*, **2**, part B, Society of Exploration Geophysicists.

[73] Paulson, K.V., 1987, A "diamond-necklace" array for magnetotelluric sounding, *Cybernetics Laboratory Research Memorandum* **87-05**, University of Saskatchewan, Saskatoon.

[74] Pierce, E.T., 1970, Latitudinal variation of lightning parameters, *Journal of Applied Meteorology*, **9**, 194–195.

[75] Pierce, E.T., 1977, Atmospherics and radio noise, in Golde, R.H., ed., *Lightning*, **1**, Academic Press.

[76] Petiau, G. and A. Dupis, 1980, Noise, temperature coefficient and long term stability of electrodes for telluric observations, *Geophysical Prospecting*, **28**, 792–804.

[77] Polk, C., 1982, Schumann resonances, in Volland, H., ed., *CRC Handbook of Atmospherics*, **1**, CRC Press Inc..

[78] Powell, B.W. and O.G. Jensen, 1981, Radiohm mapping of permafrost, in Collett, L.S. and O.G. Jensen, eds., *Geophysical applications of surface wave impedance measurements*, Geological Survey of Canada, **81-15**.

[79] Prentice, S.A., 1977, Frequency of lightning discharges, in Golde, R.H., ed., *Lightning*, **1**, Academic Press.

[80] Press, W.H., S.A. Teukolsky, W.T. Vetterling and B.P. Flannery, 1988, *Numerical Recipes in C*, Cambridge University Press.

[81] Robin, G., 1984, Etude structurale par geophysique dans la bassin hydrogeologique du Nohain (Nievre), *University of Paris VI*, These 3eme Cycle.

[82] Schmucker, U. and P. Weidelt, Electromagnetic induction in the earth, *Aarhus University*, unpublished lecture notes.

[83] Sims, W.E., F.X. Bostick and H.W. Smith, 1971, The estimation of magnetotelluric impedance tensor elements from measured data, *Geophysics*, **36**, 938–942.

[84] Spaulding, A.D., 1982, Atmospheric noise and its effects on telecommunication systems performance, in Volland, H., ed., *CRC Handbook of Atmospherics*, **1**, CRC Press Inc.

[85] Spies, B.R. and F.C. Frischknecht, 1991, Electromagnetic sounding, in Nabighian, M.N., ed., *Electromagnetic methods in applied geophysics*, **2**, part A, Society of Exploration Geophysicists.

[86] Sternberg, B.K., J.C. Washburne and L. Pellerin, Correction for the static shift in magnetotellurics using transient electromagnetic soundings, *Geophysics*, **53**, no. 11, 1459–1468.

[87] Strangway, D.E., C.M. Swift and R.C. Holmer, 1973, The application of audio-frequency magnetotellurics to mineral exploration, *Geophysics*, **38**, 1159–1175.

[88] Sutarno, D. and K. Vozoff, 1991. An application of regression-M estimation with the Hilbert transform to magnetotelluric data processing, *Geophysics*, **56**, no. 12, 1999-2007.

[89] Swift, C.M., 1967, A magnetotelluric investigation of an electrical conductivity anomaly in the south-western United States, *Mass. Inst. Tech.*, Ph.D. thesis.

[90] Takeuti, T., M. Nakano, M. Brook, D.J. Raymond and P. Krehbiel, 1978, The anomalous winter thunderstorms of the Hokuriku Coast, *Journal of Geophysical Research*, **83**, 2385–2394.

[91] Taylor, W.L. and K. Sao, 1974, ELF attenuation rates and phase velocities observed from slow tail components of atmospherics, *Radio Science*, **5**, 1453.

[92] Teer, T.L. and A.A. Few, 1974, Horizontal lightning, *Journal of Geophysical Research*, **79**, 3436.

[93] Telford, W.M., L.P. Geldart and R.E. Sheriff, 1990, *Applied Geophysics*, second edition, Cambridge University Press.

[94] Tepley, L.R., 1961, Sferics from intracloud lightning strokes, *Journal of Geophysical Research*, **66**, no. 1, 111–123.

[95] Thiel, D.V. and X.W. Wu, 1989, Electric field sensors in electromagnetic sounding, *IEEE Transactions on GeoScience and Remote Sensing*, **27**, no. 1, 24–27.

[96] Tikhonov, A.V., 1950, Determination of the electrical characteristics of the deep strata of the earth's crust, *Dokl. Akad. Nauk.*, **73**, 295.

[97] Tzanis, A. and D. Beamish, 1987, Audiomagnetotelluric sounding using the Schumann resonances, *Journal of Geophysics*, **61**, 97–109.

[98] Volland, H., 1982, Low frequency radio noise, in Volland, H., ed., *CRC Handbook of Atmospherics*, **1**, CRC Press Inc.

[99] Vonnegutt, B., 1982, The physics of thunderclouds, in Volland, H., ed., *CRC Handbook of Atmospherics*, **1**, CRC Press Inc.

[100] Vozoff, K., 1972, The magnetotelluric method in the exploration of sedimentary basins, *Geophysics*, **37**, no. 1, 98–141.

[101] Vozoff, K., 1982, Superconducting gradiometer-magnetometer array for magnetotelluric logging, U.S. Patent no. 4,349,781.

[102] Vozoff, K., 1991, The magnetotelluric method, in Nabighian, M.N., ed., *Electromagnetic methods in applied geophysics*, **2**, part B, Society of Exploration Geophysicists.

[103] Wait, J.R., 1954, On the relation between telluric currents and the earth's magnetic field, *Geophysics*, **19**, 281–286.

[104] Wallace, J.M., 1974, Diurnal variations in precipitation and thunderstorm frequency over the conterminous United States, *Monthly Weather Review*, **103**, 406–419.

[105] Wannamaker, P.E., 1983, Interpretation of magnetotelluric data, *Electrical methods in oil and gas exploration*, workshop notes, University of Utah.

[106] Ward, S.H., 1959, AFMAG-Airborne and ground, *Geophysics*, **24**, no. 4, 761–789.

[107] Ward, S.H. and G.W. Hohmann, 1988, Electromagnetic theory for geophysical applications, in Nabighian, M.N., ed., *Electromagnetic methods in applied geophysics*, **1**, Society of Exploration Geophysicists.

[108] Weidelt, P., 1972, The inverse problem of geomagnetic induction, *Journal of Geophysics*, **38**, 257–289.

[109] World Meteorological Organization, 1956, Atmospheric electricity, in Smith, L.G., ed., *Handbook of Geophysics.*

[110] Yamashita, M. and K. Sao, 1974, Some considerations of the polarization error in direction finding of atmospherics-I. Effect of the earth's magnetic field, *Journal of Atmospheric and Terrestrial Research*, **36**, 1623–1632.

[111] Yee, E. and K.V. Paulson, 1987, The canonical decomposition and its relationship to other forms of magnetotelluric impedance tensor analysis, *Journal of Geophysics*, **61**, 173–189.

[112] Yee, E. and K.V. Paulson, 1988, Concerning dispersion relations for the magnetotelluric impedance tensor, *Journal of Geophysics*, **95**, 549–559.

[113] Zhang, Y., 1997, Wavelet transforms, neural networks and migration applied to magnetotellurics, unpublished Ph. D. thesis, University of Saskatchewan, Saskatoon.

[114] Zonge, K.L., A.G. Ostrander and D.F. Emer, 1986, Controlled-source audio-frequency magnetotelluric measurements, in Vozoff, K., ed., *Magnetotelluric methods*, Society of Exploration Geophysicists.

[115] Zonge, K.L. and L.J. Hughes, 1991, Controlled-source audio-frequency magnetotellurics, in Nabighian, M.N., ed., *Electromagnetic methods in applied geophysics*, **2**, part B, Society of Exploration Geophysicists.